Shared Autonomous Electric Vehicles: Potential for Power Grid Integration

Riccardo Iacobucci

Shared Autonomous Electric Vehicles: Potential for Power Grid Integration

Riccardo Iacobucci

A thesis submitted in partial fulfillment of the requirements for the degree of
Doctor of Philosophy in Energy Science

supervised by
Prof. Tetsuo Tezuka

Graduate School of Energy Science
Kyoto University
September 2018

Abstract

Shared autonomous electric vehicles (SAEVs), also known as autonomous mobility on demand systems, are expected to become commercially available by the next decade. The introduction of SAEVs can transform the car into a service, accelerate electrification of the transport sector, and allow for large scale control of electric vehicle charging. It would also alter the availability of controllable storage from electrified transportation when compared to private vehicles. Although literature exists on the operation of SAEVs, there has been no investigation of their potential for grid integration.

This thesis aims at exploring the integration of SAEVs with the electric grid. Several aspects of this problem are investigated, using the Tokyo transport survey as a case study. A novel model of SAEV operation with scheduled charging based on dynamic electricity price is firstly proposed. The potential for the system to supply operating reserve is investigated by formulating an optimization problem for the optimal deployment of vehicles during a grid operator request. The influence of fleet size is studied in terms of transport service quality and break-even prices for the system. The results of the simulations for the case study show that a fleet of SAEVs would only need to be about 10%-14% of a fleet of private cars providing a comparable level of transport service, with low break-even prices. The system can also provide operating reserve under several operational conditions even at peak transport demand without significant disruption to transport service.

The integration of SAEVs with renewable energy is then investigated. A simulation methodology is developed for the optimization of vehicle charging in the context of a virtual power plant (VPP) or microgrid, with and without grid connection or

distributed dispatchable generators. The model considers aggregate storage availability from vehicles based on transport patterns taking into account the necessary vehicle redistribution. The case of a grid-connected VPP with rooftop solar and the case of an isolated microgrid with solar, wind, and dispatchable generation were investigated. A comprehensive sensitivity analysis is conducted to study the effect of several parameters on the results for both cases.

Finally, the problem of charging optimization and vehicle relocation is considered. A methodology for the optimization of SAEV charging with vehicle-to-grid in parallel with optimized routing and rebalancing is presented. The challenge of the different time frames for the optimization of transport service and charging is overcome by running two model-predictive control optimization algorithms in parallel. Charging is optimized over longer time scales to minimize both approximate waiting times and electricity costs. Routing and rebalancing is optimized at shorter time scales to minimize waiting times, with the results of the long-time-scale optimization as charging constraints. This approach allows efficient optimization of both aspects of system operation. The problem is solved as a mixed-integer linear program. Results for the case study show that the system can substantially reduce charging costs without significantly affecting waiting times, with cost reduction dependent on electricity price variability. Vehicle-to-grid is shown to be unsuitable for current electricity and battery prices, however offering substantial savings with price profiles with higher variability.

Aknowledgements

Firstly I would like to thank the Ministry of Education, Culture, Sports, Science and Technology of Japan (MEXT) for the opportunity and the trust they gave me in funding my PhD. I would also like to thank the Ministry of Land, Infrastructure, Transport and Tourism of Japan for the access to the transport survey data.

I feel deeply indebted to Professor Tetsuo Tezuka, who gave me the chance and the trust to join his research group and constantly supported me during my studies. As my supervisor, he guided me to understand what it means to do research, and what are the questions I should be making, always with kindness and integrity. I am extremely grateful for his guidance, help and support. I am also exceptionally grateful for the support and patience of my co-supervisor Professor Benjamin McLellan, who also gave me precious and crucial guidance throughout my PhD. I would also like to thank Professor Seiichi Ogata for his support and guidance in the last part of my studies.

I would also like to extend my gratitude to my thesis reviewer, Professor Hiroshi Shimoda. He provided me with insightful comments, guidance, and suggestions that helped me improve this work significantly.

Thank you also to all my colleagues in the laboratory throughout the years, which have always been supportive and amazing friends. Special thanks to the secretaries of the lab: Nozomi Kamura, Shiho Nakamura, and especially Tomoko Tomomatsu, who has helped me with constant patience and kindness to successfully navigate the bureaucracy at the busiest time of my PhD.

I am extraordinarily grateful for the warm welcome, the amazing moments and unforgettable encounters that Japan offered me during my stay. I feel incredibly

lucky to have met the wonderful people that are my friends in Kyoto. Thank you so much for making these past years an amazing time.

Finally, I am grateful for my family, especially my parents. They are the reason why I could study and arrive at this point. There are no words to convey my gratitude for having a family that always believed in me, always supported me unconditionally, and always allowed me to find my own path and succeed in it. Grazie.

Table of contents

List of Figures

List of Tables

Abbreviations and acronyms

Abbreviations and acronyms used throughout the work are reported here. Further specific nomenclature is reported for each chapter.

BAU	Business as usual
BEP	Break-even price
DG	Distributed generation
EMD	Earth Mover's Distance
EV	Electric vehicle
GHG	Greenhouse Gas
HEV	Hybrid electric vehicle
JPY	Japanese Yen
JEPX	Japan Electric Power Exchange
MA	Moving average
MILP	Mixed integer linear programming
MINLP	Mixed integer nonlinear programming
MIQCP	Mixed integer quadratically constrained programming
MLIT	Ministry of Land, Infrastructure, Transport and Tourism (Japan)
MPC	Model predictive control
NOAA	National Oceanic and Atmospheric Administration
O&M	Operation and maintenance
PV	Solar photovoltaic
RE	Renewable energy

SAV	Shared autonomous vehicle (non-electric)
SAEV	Shared autonomous electric vehicle
SOC	State of charge
TEPCO	Tokyo Electric Power Company
TOD	Time of day pricing
TPD	Trips per day
TPH	Trips per hour
USD	U.S. Dollars
V2G	Vehicle to grid
VPP	Virtual power plant

Chapter 1

Introduction

1.1 Background

The ubiquitous presence of the internet and smartphones is allowing a shift from car ownership to intelligent car sharing models of transportation. One-way free-floating car sharing services (in which cars can be taken wherever they are currently parked and left at any other place within a specified area) are already commonplace in large cities in Europe [2]. The diffusion of shared transportation can significantly change the vehicle ownership rate: each car sharing vehicle is estimated to remove 9 to 13 vehicles from the roads [3], as most private cars are used less than 10% of the time [4]. It can also improve the efficiency of the transport sector, as high annual vehicle-km traveled per vehicle create a strong economic incentive towards highly efficient vehicles [3]. Shared transport is also expected to be cheaper than private transportation. Savings for the average American household are estimated to be about $6,000 a year by joining a shared transport program instead of owning a private vehicle [5].

The advent of autonomous driving technology will further speed up the adoption of this transport mode, making it more convenient: vehicles can move to pick up customers autonomously without the need to move to a parked vehicle, a service comparable to that of a taxi without the cost of the driver. The popularity of similarly convenient but relatively expensive services such as Uber show the potential

(a) **(b)**

Figure 1.1: *Two of Google's Waymo prototype autonomous cars. [Images: Wikimedia Commons]*

for this kind of transport mode. Autonomous driving technology has been extensively tested and is planned to be commercially available by the next decade [6]. Figure 1.1 shows two of Google's Waymo prototype autonomous cars, an example of a company at the forefront of autonomous driving technology. The combined Waymo fleet has driven over 10 million km autonomously [7], demonstrating the viability of the technology. Waymo is planning to introduce a commercial ride-hailing service using autonomous cars in Phoenix, Arizona in late 2018 [8]. Advantages of a car sharing system (or ride-hailing service) using autonomous vehicles include the efficiency gains from automated driving, with fuel economy improvements of 4 to 10%, elimination of the time spent for parking, and decreased need for parking spaces in cities [5]. Autonomous vehicles also have the potential to significantly decrease greenhouse-gas emissions in the transport sector, with estimated 87%-94% decreases in per-mile GHG emissions compared to current private vehicles in the United States by 2030, mainly due to the possibility of using vehicles sized to the specific trip [9].

Shared autonomous vehicles can also facilitate the electrification of the transport sector, as the cars involved can optimize their state of charge (SOC) and their charging schedule while reliably ensuring service to the user [10, 11]. This can overcome several problems currently hindering the wider adoption of electric vehicles, such

as the scarcity of charging stations [12], high cost, and range limitations [13]. It is therefore important to study the impact of this system on the electricity grid [11]. This type of car sharing—using autonomous driving technology and battery electric vehicles—will be referred to as Shared Autonomous Electric Vehicles (SAEV) in this work.

It is predicted that the widespread adoption of electric vehicles could significantly change the management and balancing of the electricity system and facilitate the integration of intermittent renewable energy in the grid [14]. For example, Dallinger and Wietschel [15] found that EVs can absorb over 50% of the yearly excess renewable generation in the high renewable scenario of Germany in 2030 that would have been curtailed otherwise. Electric vehicles with vehicle-to-grid (V2G) power capability can also offer several additional services to the electric grid, such as peak power generation, operating reserve, and regulation [16]. Implementation of V2G can also allow a higher renewable energy penetration by further increasing grid flexibility [17]. However, private electric vehicles are expected to put a large burden on distribution systems, especially when considering large scale V2G implementation [18]. By contrast, SAEVs can be more easily controlled and optimized to implement fast, large-scale demand response [19]. This would allow a deeper grid integration, which is fundamental to achieving the potential environmental benefits of vehicle electrification [20].

SAEVs would also allow easier utilization of electric vehicles for providing ancillary services, which may be uneconomical for private vehicles [21]. Another potential advantage of SAEVs is their ability to move autonomously to specific charging stations. This allows for a direct connection to the high voltage electricity transmission system in designated points without overloading the low-voltage distribution network. The centralization of grid connection may also help to implement efficient V2G connections by providing more balanced and controlled electricity flow and improved safety equipment.

The integration of SAEVs with the grid is not only a remarkable opportunity to supply much needed grid storage in a grid with increasing penetration of renewable

energy, it is also a necessity to ensure grid stability and a sustainable electrification of the transport sector. A successful transition to a new energy and transport paradigm is only possible through a holistic approach that considers both as one system. The shift to a grid reliant on intermittent renewable energy means that a much more flexible, smart, and resilient grid is needed. On the other hand, a sustainable transportation system needs to decrease its reliance on private transport to limit resource waste and increase its efficiency.

This is even more important considering the fast pace of progress in the world today. Countries such as China and India are increasing their consumption at very fast rate. This is an extremely positive development that will finally bring most of the world to a level of prosperity that was only known to a fraction of humanity until very recently. However, this transition can be sustained only through an increase in efficiency and a decrease of wasteful consumption.

The advent of transport as a service could mean less material needs (less vehicles), more efficient use of resources, and higher marginal cost of car transport. Although SAEVs have prices per km traveled that are comparable to private vehicles, these costs would be all marginal costs to the user, instead of fixed sunk costs. This incentivises a more thoughtful use of this resource. Potential passengers would consider alternatives such as public transport, walking or riding a bicycle whenever convenient. This is in contrast to a private car, where each trip is marginally so inexpensive that there are often no incentives to try an alternative mode. On the other hand, the fact that no upfront payment is necessary means that a large part of the population that could not have access to the flexibility of a private car can now afford this luxury whenever they think it is worth it, only paying the relatively low marginal price.

1.2 Aim of the work

The aim of this work is to quantitatively predict and evaluate the potential for SAEVs to offer grid services, such as operating reserves and storage for renewable

energy. For this purpose, simulation models were developed in this work to study SAEV systems in the context of a electricity grid with increasing penetration of renewable energy. A grid with dynamic electricity prices that reflect a competitive electricity market is considered throughout the work. The aim of the first model presented (Chapter 2) is to evaluate the optimal fleet size considering electricity price-aware charging and the potential for operating reserve provision. The aim of the second model (Chapter 3) is to study the possibility of integrating SAEVs with renewable energy in the context of a grid-connected Virtual Power Plant (VPP) and an isolated microgrid. The aim of the third model (Chapter 4) is to develop a more systematic simulation framework to study the simultaneous optimization of charging and relocation of SAEVs.

The models presented in this work are based on present transport patterns taken from surveys, and do not consider the effect of SAEV on transport fluxes. This aspect is still a topic of debate in the literature and it is highly uncertain, thus as a first approximation this work assumes that transport patterns remain unchanged in the case studies presented. This thesis does not include experimental work, and the results are intrinsically uncertain to some extent due to the lack of real-world data of SAEV systems for validation. However, the models were subjected to extensive sensibility analyses to ensure their internal consistency, and can be a valuable tool to quantitatively predict the effects of these systems on the electricity system.

1.3 Related work

This section provides a summary of the relevant literature related to this work. The section is divided into four sub sections. The first section deals with the literature on generic (non-electric) shared autonomous vehicle systems. The second section summarizes the specific literature on systems that deal with charging. A summary table detailing the methodology of the selected literature is also included. A third section briefly presents a selection of the literature on electric car sharing systems. The fourth and last section discusses concisely the existing vast literature on the

integration of electric vehicles with the grid.

1.3.1 Shared autonomous vehicles

Most of literature dealing with shared autonomous vehicles does not explicitly consider the vehicle energy source, and is mostly focused on the transportation aspects of the problem. In particular, most of the studies focus on the minimization of waiting times for passengers through the optimization of vehicle redistribution.

Burns et al. [22] simulate a fleet of shared autonomous vehicles (SAV) fulfilling the transport demand of a city in which numerical and analytical models were developed with simplified assumptions, such as homogeneous trip rates and simplified distance calculations without a road network. The model was applied to several case studies in different contexts, and the authors concluded that in all cases SAVs offered higher efficiencies, lower costs and higher convenience to users, when compared to other public and private transport modes. In the specific case study of Manhattan, it was found that 9,000 SAV could replace over 13,000 taxicabs by satisfying the same transport demand with a total cost of 0.31 $/km, compared to 2.5 $/km for current taxis, while decreasing waiting times from an average of 5 minutes to 1 minute.

Fagnant and Kockelman [4] also developed an agent-based model of SAV using simplified transport assumptions. Macro areas with homogeneous trip generation rates and gridded road network were used. They concluded that SAV could provide adequate service with a fleet size of about a tenth of the equivalent fleet of private vehicles, and that the quality of service was dependent on the density of users.

In [23], the transport modeling framework MATSim was employed to predict the impact of SAV on the modal share of the transport sector. On a simplified road network, the results showed that SAV could be the dominant transport mode, potentially also disrupting public transport.

Liu et al. [24] used MATSim to simulate a fleet of SAV in Austin, Texas, to investigate the rate of penetration of SAV at different price levels. They found that mode split reaches over 50% with a 0.31 $/km fare. The authors did not consider

changes in transport patterns due to SAVs, but only change in mode split for the same trips. Other authors have explored the impact of SAV on urban form, including urban parking demand, suggesting that SAV could eliminate the need for 90% of current parking space for users of the system [25].

Spieser et al. [26] used a more detailed and realistic transport model to study the fleet sizing problem and estimate the economic benefits of a fleet of SAV replacing all other private transport modes in Singapore, based on actual transport data. The authors determined both the minimum fleet size to meet the transport demand of the city and the fleet size necessary to obtain a certain peak waiting time. The results show that, for the specific case of Singapore, the personal mobility needs of the entire population can be met with a fleet size of a third of the total number of passenger vehicles currently in operation. This work also assumes unchanged transport patterns.

Levin et al. [27] focused on studying the effect of SAVs on traffic congestion by introducing SAVs in existing traffic simulation models. The results show that the level of service of SAV may be lower than predicted by previous studies when accounting for traffic congestion, since SAV may shift demand from other modes and increase the number of passenger-km traveled by car. However, they found that ride-sharing (more passengers sharing the same vehicle) was effective at solving this problem. Moreover, differential pricing (peak price) may also be beneficial in limiting peak congestion.

Several other studies have dealt with the problem of shared autonomous vehicle rebalancing strategies [28, 29, 30]. In all these studies the energy aspects were not considered, and the vehicle energy source was generally not specified.

1.3.2 SAEV

Some studies considered the constraints associated with the charging of electric vehicles, thus dealing with SAEVs. A summary of selected works on SAEV that consider vehicle charging is given in this section. In these studies, the charging is generally secondary to the transport optimization, and vehicles are assumed to

charge as fast as possible independently of the grid conditions. As these systems are deployed at scale, however, the problem of optimal charging becomes apparent, as the increased load and charging peaks on the grid would be problematic if not managed. Moreover, electric vehicles offer the opportunity for large scale demand response that can help increase the penetration of intermittent renewable energy in the grid, as mentioned previously [15].

Most studies agree that SAEVs can significantly reduce green-house gas (GHG) emissions and increase electrification in the transport sector [11]. Greenblatt and Saxena [9] estimate that SAEVs could reduce GHG emissions by 87%-94% compared to current private vehicles in the United States. Even when accounting for a substantial increase in distance traveled due to higher convenience, SAEVs are still found to reduce emissions compared to the baseline scenario.

Chen et al. [10] studied the operation of a SAEV system with methods based on a previous model developed by Fagnant and Kockelman [4]. The agent-based transport model methodology is similar, but the investigation is expanded by including charging of the electric vehicles serving 10% of trip demand in a medium-sized metropolitan area. The analysis includes a charging station generation phase to find the number and position of charging stations needed to serve passengers within a certain waiting time. The model was run in different scenarios to investigate the sensitivity to several parameters. The study considers short- and long-range type of vehicles, with slow and fast charging. It was found that although double the number of vehicles are needed for the case with short-range and slow charging vehicles, this is the most profitable scenario. For the case study in Austin, Texas, the results indicate that each SAEV can replace between 5 and 9 private vehicles, depending on range and speed of charge. The model does not consider 'smart' charging and found that simultaneous charging of the fleet at peak times may be problematic for the electric grid.

Rigas et al. developed a mixed integer programming optimization for shared electric vehicles with battery swapping [31]. Biondi et al. [32] propose an optimization formulation for the positioning of charging station for electric car sharing

systems and analyze the impact of these fleets on the electricity grid.

Pourazarm et al. [33] developed a theoretical optimization of vehicle routing with charging constraints. The problem is solved as a mixed integer nonlinear program (MINLP). The work also presents a faster problem with a sub-optimal solution that is however more computationally manageable and obtains almost the same results. The model allows for a variable electricity pricing at charging stations, however time-vaying pricing is not considered.

Chen et al. [34] developed a framework for the optimal routing and charging of electric vehicles in a fleet context. The problem is formulated as an extended pick-up and delivery problem in a graph and is solved as a mixed-integer quadratically constrained program. The work also includes a discussion of the possible impacts of the system on the electricity distribution network, although with simplified assumptions. The peak load of stations is found and it is suggested that future work may address the problem of sitting and sizing of charging stations. As in [33], charging optimization also considers different electricity pricing at stations but no time-varying electricity pricing is considered.

Bauer et al. [35] developed an agent-based model for the simulation of SAEV. The model proceeds through the day assigning trips to the nearest vehicle. If vehicles are not available within a threshold waiting time, a "new" vehicle is added to the necessary vehicles to satisfy demand. An iterative process was used to optimize the positioning of charging stations by starting with chargers everywhere and eliminating at each iteration the least used chargers. The model was tested in Manhattan with transport data from taxi trips. They find the optimal battery size and number of charging stations to minimize costs through sensitivity analysis. They conclude that vehicles with 50-90 miles range and 66 chargers per square mile (25 per square km) with a 11 kW connection can provide service with a cost of \$0.29-\$0.61 per mile (\$0.18-\$0.38 per km), about 10 times lower than normal taxis and lower than if the service was provided by any non-electric vehicle. They also calculate that SAEVs would reduce GHG emissions by 73% compared to current taxis with the current power grid thanks to higher vehicle efficiency.

Zhang et al. [36] present a model predictive control approach for the optimization of an autonomous car-sharing system with optimal rebalancing and consideration of vehicle charging constraints. The problem is solved as a mixed integer linear program (MILP). The algorithm is shown to outperform all the previous control strategies considered. The model formulation as a global optimization is however unsuitable for large-scale simulations, with the computational time increasing fast for larger systems. The proposed optimization assumes uncontrolled charging of vehicles.

One paper deals with time-varying electricity price [37], however dealing with a personal usage (not shared) scenario of autonomous electric vehicles.

1.3.3 Electric car sharing systems

Shared non-autonomous electric vehicles (car sharing systems) have also received much interest in recent years, and there are a number of studies focused on the integration of these vehicles with the electricity system.

Freund et al. [38] developed a control and optimization system to manage the charging of shared electric vehicles in a smart microgrid in order to maximize the use of renewable energy sources.

In another study [2], a model of an electric vehicle car sharing system with reservation was developed. The model is based on charging stations serving requests in the vicinity. The fact that demand is known in advance through reservation allows for the use of an optimization algorithm, which is also used to determine the optimal fleet size by maximizing the car sharing operator's net revenues and the user's benefit, also taking into account the necessary car relocation among charging stations.

Several authors explore the feasibility of taxi services using electric vehicles. Bischoff and Maciejewski [39] studied a fleet of electric (non-autonomous) taxis through MATSim. The authors conclude that electric vehicles can be used as taxis and only a limited number of charging pods is sufficient. However, the work does not focus specifically on the grid-side aspects. In another study [40], the operation of a

Table 1.1: *Summary of the selected literature on SAEV modeling with focus on methodology. Information on the case study used is also given where applicable and available. Only works dealing explicitly with charging during simulation time were considered. Opt. rel. = optimal relocation; Det. = deterministic model; C.S. = charge scheduling*

	Methodology							Case study			
	Opt. rel.	Det.	Comments	Realistic road net.	C.S.	Charging stations	Formulation	Place	Size	Trips	Vehicles
[32]	no	no	Stochastic optimization of charging station deployment considering parking availability, quantification of electric demand (non-autonomous free floating car sharing system)	no, based on cells	no	yes, optimized positioning and size	set cover problem	Netherlands		51,000 total trips	400
[35]	yes	yes	Analysis of impact of dynamic electricity prices without change in charging behavior. Detailed cost analysis, emissions impact	yes, with traffic conditions	no	optimized position, sensitivity to number of c.s.	agent-based	Manhattan, NY		350,000 TPD	minimum 6470

[34]	-	yes	Studied the effect of different pricing at charging stations. Also considers load on electric distribution networks	simplified, based on graph	no	yes	MIQCP	Sioux Falls, South Dakota	24 nodes		6
[10]	yes	no	Trips generated stochastically	no	no	yes, optimized with heuristics	agent-based	Austin, Texas	10,000 sq. mi (100x100 miles)	680,000 TPD	30,000-57,000
[41]	no	no	Framework integrating 4 sub-problems: fleet size and assignment schedule; number and locations of charging stations; vehicle powertrain requirements; and service fees	no	no	yes, optimized positioning	nearest neighbor assignment	Ann Arbor, Michigan	121 sq. mi (11x11 miles)		

[33]	yes	yes	Theoretical optimization of vehicle routing with charging constraints. Developed suboptimal solution that is however more manageable and obtains almost same results. Case of different pricing at charging stations.	possible, with congestion	no	yes, at specific nodes	MINLP global optimization	-	-	-	-
[37]	-	no	Personal usage scenario (not shared vehicles). Stochastic energy consumption model	not explicitly	yes, price based	yes, at specific locations	dynamic programming	-	-	-	-
[36]	yes	both cases	Global optimization of vehicle redistribution and charging allows for flexibility of constraints	no, based on nodes	no	at each node	MILP global optimization	Manhattan, New York	15 nodes	2,300-3,500 TPD	40

electric taxi fleet with trip reservation in Singapore was investigated. An interesting aspect of the results is that changing the number of charging stations had limited effect on the performance of the system.

1.3.4 Electric vehicles grid integration

Electric vehicles can offer several services to the grid, such as grid storage and ancillary services. Ancillary services are those services that are necessary to support the electricity grid, and in particular its real-time stability and the real-time balancing of demand and generation. Batteries are especially valuable providers of ancillary services, since they can ramp-up instantly and at no cost [42, 43]. This is in contrast with conventional generators which generally have a significant ramp-up delay and cost. The possibility for electric vehicles to offer ancillary services has been extensively studied [42, 17].

Almost all literature on electric vehicles' grid integration deals with private vehicles. However, there has been some work focusing on shared vehicles. Kahlen and Ketter [43] developed an algorithm for the control of vehicles in a carsharing system. Decisions concern the commitment of vehicles for operating reserve, the charging of vehicles, or the commitment for transport service. The decision is determined by comparing expected profits over future time steps for each action, and it is calculated with a multiple linear regression model. By testing the model with data from a free floating carsharing system they found that profits could increase by 7-12% with practically no decrease in vehicle availability.

The use of electric vehicles as grid service providers for integrating renewable energy has also been studied extensively [44], demonstrating the feasibility and effectiveness of using these vehicles for grid stabilization and to replace fossil fuel power plants in grids with high penetration of renewable energy [45]. Electric vehicles offer great opportunities for grid balancing and integration of renewable energy sources, because of the charging flexibility.

Hu et al. present a review of smart charging literature for electric vehicle fleet operators [46]. Nosratabadi et al. [47] present a useful review of distributed energy

scheduling in microgrid and virtual power plants, including work that considers electric vehicles.

In conclusion, although the literature on electric vehicle grid integration is extremely developed, there has been limited work on the development of intelligent charging strategies for car sharing systems that take into account grid integration, or on the assessment of the potential for these systems to provide grid services.

1.3.5 Summary

The literature presents several possible methodologies for the simulation of shared autonomous vehicles. Some works do not consider relocation optimization, and the simulation usually progresses in time steps with assignment of trips to the nearest vehicle. This approach generally produces longer waiting times, especially in the case of highly asymmetrical passenger fluxes. In the cases with optimized relocation, the main types of models are those based on some form of heuristics and those that use a global optimization approach. In the first case, the simulations are more easily scalable, while in the latter the feasibility of the problem is limited to relatively small domains in terms of number of vehicles, number of nodes (geographic size of the simulation or resolution) and passenger request rate.

The literature explicitly dealing with electric vehicles in the context of shared autonomous vehicle systems is more limited. Existing work approach the problem from the point of view of the transport service, thus focusing on the minimization of waiting time without considering the impact on the grid. As mentioned, this approach is not realistic if these vehicles were to account for a large part of the transport modal share in certain areas. Their uncontrolled charge would risk increasing the congestion on the electric distribution network, increasing the cost of grid balancing, and missing out on the opportunity of providing a useful service for the integration of renewable energy in future grids. Some models [34, 33] assume price differences among charging stations. This however neglects the most important aspect of electricity price variability, which is the temporal variability. Although service (connection) price may change across different private charging stations [34],

electricity prices do not generally vary across small regions, as this would imply strong grid congestion effects. Another paper [35] considers the impact of variable electricity price (time of use tariffs) on the cost performance of the SAEV system, however without considering any responsive strategy (passive sensitivity analysis).

In summary, there has been very limited work dealing with the interaction of SAEVs with the electricity grid. As this is considered a fundamental problem for the large scale implementation of these systems, as well as an important opportunity for the future smart grid, this work aims at filling this gap in the literature.

1.4 Contributions of this study

The academic contribution of this study is the extension of the current research on electric vehicles grid integration in the context of shared transportation with autonomous vehicles. The problem of grid integration has been largely overlooked in the literature on SAEVs, as detailed in Chapter 1.3. This work aims at putting the foundations of this important topic of research by looking at several aspects of the problem. In particular, the work focuses on the transport and economic implications of SAEVs with electricity-price-aware charging, their potential to provide ancillary services, their possible integration with renewable energy, and the formulation of a more systematic methodology for the simulation of shared transport systems with optimized charging.

The practical contribution of this study is the development of models to quantitatively assess and simulate the impact of SAEVs on the grid. As mentioned previously in the Introduction, this is of primary importance in order to develop appropriate policy and facilitate the electrification of the transport sector and its integration with the grid. This would be a key element to allow a wider adoption of intermittent renewable energy sources. A wide deployment of smart-charging SAEVs would allow the implementation of large scale demand response and grid storage to support renewable energy deployment.

1.5 Overview of the work

Chapter 1 is an introduction to the work. This includes a general background on Shared Autonomous Electric Vehicles, their differences with conventional and private electric vehicles, and their potential for grid integration; a review of the literature on shared autonomous vehicles, SAEVs, and more generally on electric vehicles' grid integration and ancillary services provision; a statement of academic contribution, in which the relevance of this work is summarized and put in the context of the literature.

Chapter 2 presents a novel methodology to simulate SAEVs, taking into account electric charge scheduling based on price signals from the grid with a heuristics-based approach and the possibility of providing operating reserves. A detailed description of the model is presented, including the transport model, the trip assignment, and the charge scheduling algorithm. The model is applied to a case study in Tokyo, and the cost of the system, waiting times for users, and operating reserve provision potential are investigated. The results and conclusions from the case study are then discussed, and their potential implications for policy are discussed.

Chapter 3 deals with the potential synergies of SAEVs when combined with intermittent renewable energy. In order to quantify this effect, a model is presented where SAEVs provide transport and storage for renewable energy in a virtual power plant (VPP) or a microgrid. In the first section the problem is introduced and discussed. The second section the methodology is presented. The model is then applied to the Tokyo case study using stochastic renewable energy generation data. The results are divided in two parts. In the first part, the results for the VPP are reported and discussed. This part includes a comprehensive sensitivity analysis. In the second part, the model is applied to the case of an isolated microgrid including dispatchable distributed generators. The conclusions and recommendation for future work are reported in the last section.

In Chapter 4 the problem of SAEVs' charge scheduling is analyzed more in depth, with the use of an analytic optimization model for the price-based charge scheduling while also considering the rebalancing of vehicles. The methods are

reported in section 2, including a summary of the model from the literature and a detailed description of the extension proposed. The model is then applied to the case study in the central district of Tokyo and the findings are discussed. Finally, the conclusions and the possible future developments of the model are reported.

Chapter 5 reports the conclusions of the work and the future possible research directions.

An Appendix chapter presents the methodology for the transport survey data analysis and stochastic trip generation. This data is used throughout the work to test the simulation models developed.

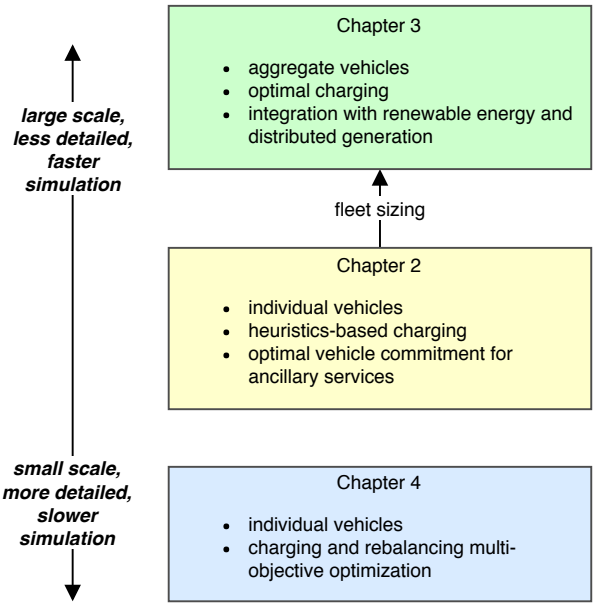

Figure 1.2: *Summary of the characteristics of the models presented in each chapter*

Figure 1.2 presents an overview of the models presented in each chapter. Below, a summarized outline of the work is presented:

Chapter 2

- developed first model of SAEV operation to incorporate demand response with dynamic electricity price

- fast heuristics algorithm allows for fast computation on large systems: extensive sensitivity analysis performed for parameter selection and fleet sizing

Chapter 3

- developed first model of SAEV in a grid with renewable energy incorporating power flow balance
- aggregate model of the system based on results from previous chapter: fast simulation allows for sensitivity analysis to identify best deployment scenarios for SAEV and renewable energy

Chapter 4

- developed first model of SAEV operation with multi-objective optimization of relocation and charging with demand response
- slower simulations but optimal analytical solution of the problem: allows to test other models by comparing them to results of this model (benchmark) with a scaled-down scenario

Chapter 2

A novel SAEV transport model with charge scheduling and operating reserve provision

2.1 Introduction

In this chapter, a novel model for simulating a Shared Autonomous Electric Vehicle system and its interaction with the power grid is presented. The work includes a static transport model based on the transport survey data detailed in Section A.1 to simulate the transport patterns. The vehicles satisfy trip requests while charging their batteries according to a heuristics-based demand-response strategy based on electricity price signals from the grid. Subsequently, the model is used to evaluate the potential for the system to participate in the operating reserve market and the influence of several parameters on the results.

It is assumed that vehicles are managed by a company or entity that oversees the shared transport service. Control is of two types: the vehicle routing control is centralized, with a central authority (control center) assigning available vehicles to new passenger trips; the decision to move to charging station, and how much to charge, is decentralized, and depends on each vehicle's SOC, waiting times, and the current and expected price of electricity and aggregated transport demand. The

vehicles are assumed to communicate with the control center reporting their status and SOC in order for the control center to optimize the assignment of trips.

SAEVs can potentially offer more significant operating reserve than private vehicles thanks to their ability to move autonomously to specific charging stations. These charging stations can be positioned strategically to access the high-voltage transmission system without overloading the distribution network, and making the prospect of large scale grid injections more realistic. Figure 2.1 is a map of high-voltage substations in the Tokyo grid, showing possible positions of large charging stations for autonomous vehicles. The limited number of charging stations needed also make the required high power V2G connections more affordable.

A new system for responding to grid capacity requests is proposed and tested to evaluate the SAEV system performance as an operating reserve provider. Operating reserve is surplus electricity generation capacity that can respond to sudden drops of generation (such as a power plant failure or a sudden drop in renewable energy generation) or sudden increases in load. This provides a margin that ensures the stability and reliability of the electricity system [48]. Operating reserves can be distinguished in two types, depending on response time: spinning reserve and non-spinning reserve. The first is the reserve that can respond instantly, while the second is the reserve generation that can respond with a delay of several minutes, up to 15 minutes [48]. In the system, the fleet of SAEVs provide spinning and non-spinning operating reserve in response to grid operator requests (both to generate energy and to absorb surplus generation). In case of grid requests, the charging decisions are centralized and controlled by the control center to reach the aggregated power generation needed. The results show that a SAEV system can be used reliably as an emergency supply of energy when coordinated with the electric grid.

The aim of this chapter is to evaluate the feasibility of an autonomous car sharing systems with charge scheduling in terms of transportation service quality and economic performance, and its potential to effectively respond to price signals from the grid and provide ancillary services.

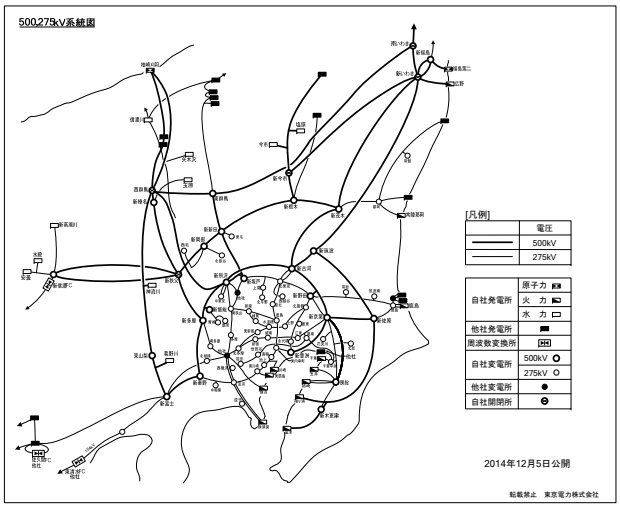

Figure 2.1: *Map of high voltage substations in the Tokyo grid. Stations used in the model (Section 2.2.3) could be positioned at these points to take advantage of the high voltage transmission without overloading the distribution network.*

2.2 Simulation model

This section describes the methods used in this chapter. The first part of the section deals with the general methodology for the transport model and the operating reserve request model. In the second part, the specific case study methods are reported. These include the calculation of the parameters used.

Nomenclature

A. Indices

h	Hour
k	Trip
t	Time step
v	Vehicle

B. Simulation variables

A_i	Area of node i
$a_v(t)$	Waiting time variable
BEP	Break-even price

$d_{i,j}$	Distance between node i and j
$e_v(t)$	Energy exchanged
$f(h)$	Frequency of trips at hour h
ℓ	Length of time step (minutes)
$m(t)$	Price of electricity
$p_v(t)$	Charging power
$q_v(t)$	State of charge (SOC) of battery
rd_k	Destination node of trip k
ro_k	Origin node of trip k
rt_k	Time (hour) of trip k
rw_k	Weight of trip k
${}^i s_v$	Binary state variable i
T	Total number of time steps
TPH	Average trips per hour
V	Total number of vehicles
$w_v(t)$	Distance to current destination
$W_{pass,v}$	Total distance traveled with passengers
$W_{tot,v}$	Total distance traveled
$\lambda(t)$	Expected number of requests at time step t
Δ_{max}	Price of electricity at which car charge at maximum rate
$\pi_v(t)$	Agent price
C. Operating reserve simulation variables	
$r_{max}(t)$	Total power available for request at time t
α_v	Initial delay of v before connection
Γ	Duration of the request
δ	Allowed delay of request
$\epsilon_v(\tau)$	Energy delivered by v at minute τ
τ	Time step
D. Parameters and constants	
a_{con}	Time needed to connect to charging station

a_{idle}	Maximum idle time
a_{charge}	Minimum charging time
$C_{battery}$	Cost of battery
C_{car}	Cost of car (with no battery)
CAP	Battery capacity (kWh)
EC	Electricity consumption of cars (kWh/km)
hz	Prediction horizon
$L_{battery}$	Life of battery in equivalent full cycles
L_{car}	Life of car not including battery (years)
$p_{i,j}(t)$	Probability of a trip starting in i with destination j
p_{max}	Maximum charge rate (kW)
p_{peak}	Peak charge rate for short periods (kW)
q_{charge}	SOC at which car move to charging stations
q_{max}	Maximum SOC in normal operation
q_{min}	Minimum SOC in normal operation
$u(t)$	Average speed of vehicles (km/time step)
PSP	Passenger service priority factor (JPY/km or USD/km)
β	Ratio of trip distance to Euclidean distance
η	Battery round-trip efficiency

2.2.1 Transport model

The first, and fundamental component of this study, was the transport route and trip selection model. This is used to determine where SAEVs travel, which is primarily in order to satisfy customer requests. The model applied in this study was developed in MATLAB™ and is based on a simplified road network, represented by nodes at specific coordinates and their associated areas.

The simulation evolves through T time steps. At each time step, trip requests can arrive at each node of the model, with an associated destination node. A fleet of V autonomous electric vehicles move from one node to another satisfying trip requests.

In order to have an acceptable computational time for the simulation, the actual street layout is not considered. The distance is calculated as the Euclidean distance times a tortuosity factor β that represents the lengthening due to the city's street layout. The distance between nodes is stored in a distance matrix where each element $d_{i,j}$ represents the distance between node i and node j.

Distances inside the same node (for trips starting and ending in the same node) are calculated using the approximation of the average distance between two uniformly distributed random points in a square:

$$d_{i,i} = 0.52 \cdot \sqrt{A_i} \cdot \beta \tag{2.1}$$

Where A_i is the area associated with node i.

These assumptions do not alter the probabilistic location of requests' origins or destinations, as these are the initial given conditions of the model. They do, however, fail to consider the congestion effect and the fact that a real road network is not homogeneous. This is considered acceptable for this work, as the aim is not to simulate the change in the city traffic patterns, but to understand the energy aspects of SAEV as a 'marginal' player (that does not significantly alter the transport patterns) in the transport system. This also makes the model readily adjustable to alternative cities if the other required data is available. It is, however, important to consider the average effect of traffic congestion, because it can significantly change the pattern of availability of vehicles during peak times. Traffic congestion is therefore introduced in the model as a variable average speed of vehicles. This is represented with a periodic time-varying vector $u(t)$ which represents the distance traveled by each vehicle in a time step of the simulation. This is related to the average speed of vehicles in km/h by a factor $\ell/60$.

The current state of each vehicle v is registered as a binary variable ${}^{i}s_v(t) \in \{0, 1\}$, representing different situations. If the vehicle is currently in state i, the corresponding state variable ${}^{i}s_v(t)$ is set to 1, otherwise it is set to 0. A summary of the different states is presented in Table 2.2 and Figure 2.2. Vehicles can be in only one state at any given time.

Table 2.2: *States of vehicles*

state	description
0	charging, not available
1	charging, available
2	idle, available
3	moving, available after drop-off
4	moving to charging station, not available
5	connecting to charging station, not available

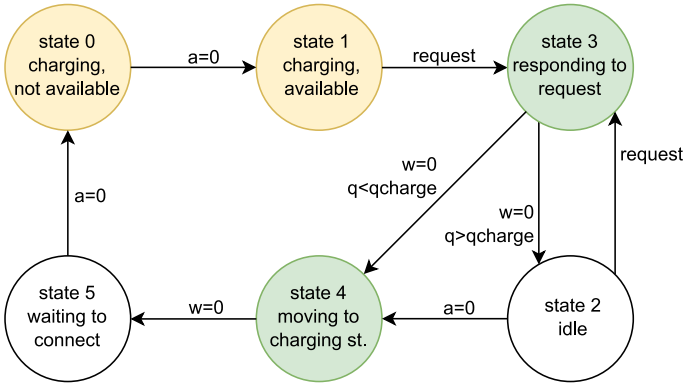

Figure 2.2: *Simplified outline of the model. Yellow backgrounds indicate connection to the grid, green backgrounds indicate movement.*

2.2.2 Trip requests

Trip requests are generated stochastically during the simulation. The number of requests at each time step t is decided through a Poisson process with a periodically time-varying rate $\lambda(t)$. The number of requests in each time step t is therefore sampled from the Poisson distribution with a cumulative mass function (CMF) defined as:

$$CMF(x) = \sum_{i=1}^{x} \frac{\lambda(t)^i \cdot e^{-\lambda(t)}}{i!}; \tag{2.2}$$

Each request is then associated with a starting node and a destination node $[i, j]$. The origin/destination pair is extracted from a periodically time-varying distribution where $p_{i,j}(t)$ is the probability associated with the pair $[i, j]$ at time t and

$\sum_i \sum_j p_{i,j}(t) = 1$. It is assumed that no reservation is possible: all passenger requests are expected to be fulfilled immediately. This can be considered to be the worst case (conservative) scenario, because if reservations were possible, this would always allow cars to be repositioned more efficiently. This is a significant difference from much of the previous work that includes reservations, making the system predictable in advance, and potentially more efficient.

Trip requests generated are assigned at each time step to available vehicles through the Kuhn-Munkres algorithm (Hungarian algorithm, [49]), which matches vehicles and requests to minimize total travel distance. A vehicle is considered to be available in any of the following cases:

- it is charging and has been charging for more than a minimum charging time (state 1);
- it is parked idle (state 2);
- it is currently transporting a passenger (state 3)

In the last case, the vehicle will travel to pick up the next passenger after the current one has reached their destination. In terms of system states the constraint is:

$$ {}^1s_v + {}^2 s_v + {}^3 s_v = 1 \tag{2.3}$$

A further necessary condition is that the vehicle has enough charge for the specific trip request:

$$(w_v(t) + d_{k,i} + d_{i,j}) \cdot EC < (q_v(t) - q_{min}) \cdot CAP \tag{2.4}$$

Node k is the last destination of the vehicle (or the current position for idle or charging vehicles), w_v is the distance to the last destination, EC is the energy consumption, q is the SOC and CAP is the battery capacity. Note that the charge available is calculated considering that vehicles should never be below a minimum SOC when the destination is reached, in order to have enough charge to move to a

charging station. When a request is assigned, the vehicle's distance to destination w_v is increased, the destination node k is updated and the vehicle's state is changed:

$$\begin{aligned} w_v(t+1) &= w_v(t) + d_{k,i} + d_{i,j} \\ {}^1s_v(t+1) &= 0 \\ {}^2s_v(t+1) &= 0 \\ {}^3s_v(t+1) &= 1 \end{aligned} \tag{2.5}$$

At each time step, the distance to destination will decrease: $w_v(t+1) = w_v(t) - u(t)$, until $w_v(t) = 0$ and the destination is reached.

The request is rejected if it is not assigned to a vehicle in the same time step, thus not allowing request queuing. The number of these rejected requests is later used as one indicator of system performance.

2.2.3 Charging stations

Vehicles can only charge their batteries at designated charging stations. The charging stations are placed at specific nodes in the grid, and vehicles need to travel to these nodes in order to charge. Autonomous vehicles are assumed to be able to connect to a charging pod automatically and with minimum delay. Several implementations of this technology have been proposed [50]. Charging station congestion has not been assessed in this work, so it is assumed that charging spaces are always available. This is considered reasonable since charging stations would be sized according to usage patterns.

A vehicle with no requests pending moves to a charging station either when its battery's SOC is below a certain level q_{charge}, or when it has not been assigned requests for a certain period of time (maximum idle time a_{idle}). In this last case, this also helps the re-positioning of vehicles that find themselves in peripheral nodes with limited request rates. Vehicle reaching a charging station start charging after a certain delay a_{con}, to account for the time to physically connect to the pod. Once it starts charging, the vehicle keeps charging for at least a minimum charging time

a_{charge} to avoid continuous disconnection (see Table 2.3). After the time threshold is reached, the vehicle becomes available for passengers, while still connected to the grid. It therefore participates in the assignment algorithm, although with lower priority compared to an idle vehicle: if the two vehicles have the same distance to the request, the idle vehicle is chosen. The vehicle stays connected otherwise and it therefore counts as an additional storage for the grid.

The number of time steps of delay in each case is assigned to the variable $a_v(t)$, which evolves as follows:

$$\begin{aligned} a_v(t+1) = \max(a_v(t) - 1 \\ + ({}^0s_v(t+1) \cdot^5 s_v(t)) \cdot a_{charge} \\ + ({}^2s_v(t+1) -^2 s_v(t)) \cdot a_{idle} \\ + ({}^5s_v(t+1) \cdot^4 s_v(t)) \cdot a_{con}, 0) \end{aligned} \tag{2.6}$$

The first two terms inside the max expression in (2.6) accounts for the decreasing delay at each time step. The third term accounts for the minimum charging time, the fourth term for the maximum idle time, and the fifth term for the time to connect to a charging station. Note that a_v is always non-negative. Moreover, when terms 3 and 5 are nonzero, they are always positive and $a_v(t)$ in (2.6) is necessarily zero per (2.12) and (2.17).

2.2.4 Charging

All vehicles in the simulation are battery electric and therefore need to charge to be able to serve the passenger requests. A heuristics-based charge scheduling algorithm is used in the simulations, and the interaction between the power grid and the vehicles is mediated by the electricity price from the grid. A price-based demand response is helpful in balancing the grid in the case of high penetration of renewable energy [51].

The charge scheduling algorithm is based on an 'agent price' π_v. In this work, the agent price is a measure of the value of electricity stored in each vehicle. In other

words, the agent price is the 'perceived' value of electricity for each agent (vehicle) at a certain time.

The vehicle will buy electricity when the agent price is higher than the electricity price. In particular, the vehicle will charge at a rate proportional to the difference between π and the electricity price, up to a maximum Δ_{max}, which corresponds to the maximum charging rate p_{max}. The unconstrained rate of charge, or the proportion of the maximum power that would be used in absence of other constraints, can therefore be defined as:

$$b_v(t) = \max(\min(\frac{\pi_v(t) - m(t)}{\Delta_{max}} \quad , \quad 1) \quad , \quad -1) \tag{2.7}$$

Where $m(t)$ is the price of electricity from the grid. Δ_{max} was set at 30 JPY/kWh. This behavior was introduced to increase the system stability when the agent price is close to the price of electricity. The energy exchanged (in kWh) at time step t is therefore:

$$\begin{aligned} e_v(t) = ({}^0s_v(t) + {}^1 s_v(t)) \cdot \max \Bigg(\min \Bigg(b_v(t) \cdot \frac{p_{max} \cdot \ell}{60}, \\ CAP \cdot (q_{max} - q_v(t))^+ \Bigg), CAP \cdot (q_{min} - q_v(t))^- \Bigg) \end{aligned} \tag{2.8}$$

The shorthand notation used in (2.8) is defined as: $x^+ := max(x, 0)$, $x^- := min(x, 0)$. Equation (2.8) refers to the energy reaching the vehicle and thus does not account for the efficiency of the battery, which is counted only for the charging cycle when calculating the cost of the energy. $e_v(t)$ is positive when the vehicle is charging, and negative when discharging.

It is assumed that in order to calculate the agent price, predictions of short-term future price and transport demand are available to the system up to a certain horizon. Moreover, it is assumed that the electricity price is not influenced by the behavior of SAEVs (the model simulates a small enough fleet of SAEVs). This is justified by the scale used in the simulations. Even assuming 2000 vehicles (the maximum number used in simulations) charging at the same time at 10 kW, the

total load would be 20 MW, which is less than a thousandth of the average power generation by Tokyo Electric Power Company (TEPCO) of ∼23 GW in 2015 [52].

The algorithm is based on the average of expected future prices and transport demand as follows:

$$\pi_v(t) = \frac{\sum_{j=1}^{hz} \left(m(t+j) + \lambda'(t+j) \cdot PSP/EC\right)}{2 \cdot q_v(t) \cdot hz} \tag{2.9}$$

$$\lambda'(t) = \frac{\lambda(t) \cdot 60}{\ell \cdot \sum_{t-1440/\ell}^{t-1} \lambda(t)} \tag{2.10}$$

Where π_t is the agent price at time t, hz is the prediction horizon for future prices, PSP is the passenger service priority factor, and λ' represents the relative rate of requests in the time step compared to the total in the previous 24 hours, normalized as a rate of trips per hour. The PSP (expressed in JPY/km or USD/km) is a weighting parameter used to allocate a certain amount of energy to transport requests as opposed to energy storage. A higher PSP would put more priority on passengers, reducing probability of dropped requests and possibly waiting times, but also rendering storage less effective. The simple equation allows for a fast calculation of the agent price at each time step for each vehicle.

The state of charge of each vehicle will then evolve according to:

$$q_v(t+1) = q_v(t) + \frac{e_v(t)}{CAP} - \frac{u(t) \cdot EC}{CAP} \cdot ({}^3s_v(t) + {}^4 s_v(t)) \tag{2.11}$$

In accordance with the model described, the state variables evolve according to the following equations:

$${}^0s_v(t+1) = {}^0 s_v(t) + ({}^5s_v(t) - {}^0 s_v(t)) \cdot (1 - \operatorname{sgn}(a_v(t))) \tag{2.12}$$

$${}^1s_v(t+1) = {}^1 s_v(t) + {}^0 s_v(t) \cdot (1 - \operatorname{sgn}(a_v(t))) \tag{2.13}$$

$${}^2s_v(t+1) = {}^2 s_v(t) + {}^3 s_v(t) \cdot (1 - \operatorname{sgn}(w_v(t))) \tag{2.14}$$

$$^3s_v(t+1) =^3 s_v(t) \cdot \text{sgn}\left(w_v(t)\right) \tag{2.15}$$

$$^4s_v(t+1) =^4 s_v(t) -^4 s_v(t)) \cdot (1 - \text{sgn}\left(w_v(t)\right)) \tag{2.16}$$

$$^5s_v(t+1) =^5 s_v(t) -^5 s_v(t) \cdot (1 - \text{sgn}\left(a_v(t)\right)) +^4 s_v(t) \cdot (1 - \text{sgn}\left(w_v(t)\right)) \tag{2.17}$$

with $\text{sgn}(x)$ the sign function which is 0 when $x = 0$, 1 when x is positive and -1 when x is negative.

2.2.5 Transport system evaluation

In order to evaluate the economic feasibility of the SAEV system, a conservative estimate of the costs was made (see Table 2.4). The values were estimated based on currently available electric vehicles and on estimates of the price of autonomous vehicle control hardware (see section 2.3.2). The life expectancy of the vehicle is defined in years, while the life of the battery is defined by its total number of full cycles (100-0-100% SOC). The cost of the vehicle will therefore be considered a fixed cost based on the lifetime of the vehicle, while the cost of the battery will depend on its use (charge/discharge cycles).

To assess the cost of the system, the break-even price (BEP) is used. This is defined as the minimum price per km the passengers have to pay to cover the total costs of the SAEV system. Any price higher than the BEP will be a net profit for the system. The BEP is calculated based on the results of the simulation:

$$BEP = \frac{\sum_v (VC_v + FC_v)}{\sum_v W_{pass,v}} \tag{2.18}$$

where VC_v and FC_v are the variable and fixed cost, respectively, for vehicle v, and $W_{pass,v}$ is the distance traveled with passengers for vehicle v. The BEP is expressed in JPY/km (or USD/km).The system would incur further overhead costs, such as the cost for managing the assignment system. However, for simplicity, these

are assumed to be included in the overall price of the vehicle (fixed costs). The variable and fixed costs are:

$$VC_v = \frac{\sum_t e_v(t)}{L_{battery} \cdot CAP} \cdot C_{battery} + \sum_T e_v(t) \cdot m(t) \tag{2.19}$$

$$FC_v = \frac{C_{car} \cdot T \cdot \ell}{L_{car} \cdot 525600} \tag{2.20}$$

Where $C_{battery}$ and C_{car} are the cost of the battery and the vehicle, respectively; $L_{battery}$ and L_{car} are, respectively, the life of the battery (in number of cycles) and the vehicle (in years); 525600 is the total number of minutes in a year.

The variable cost depends on the specific vehicle (function of the total distance traveled), while the fixed cost is the same for each vehicle. The total costs are then the sum of all the individual vehicles' costs. Moreover, the system efficiency is also calculated as:

$$Efficiency = \frac{\sum_v W_{pass,v}}{\sum_v W_{tot,v}} \tag{2.21}$$

where $W_{tot,v}$ is the total distance traveled.

2.2.6 Operating reserve model

The potential for the cars to act as operating reserve is subject to the speed at which they can deploy capacity, and for how long. To evaluate these factors, a request mechanism was implemented as an extension of the model developed in Chapter 2.

An operating reserve request in this model is characterized by a duration Γ and an allowed delay δ. At time step t of the simulation the system is tested to calculate the maximum theoretical operating reserve power available $r_{max}(t)$. This is the maximum constant power deliverable for the request duration.

It is assumed that during an operating reserve request the vehicles will put priority in satisfying the grid operator request over new passengers' requests if necessary. Vehicles can therefore be called back to charging stations to contribute. The rate

at which these vehicles can be called back determines the delay in fulfilling the request and the overall energy and power available. Vehicles with pending passenger requests (already accepted) can move to charging stations only after transporting their passengers, thus affecting their connection time or grid waiting time. Moreover, in these special cases, vehicles are allowed to reach the full range of battery capacity from 0% to 100% SOC if needed.

The calculation of the power available progresses with a time step τ through the duration of the grid operator request. For each vehicle v, the time needed to deploy capacity α is calculated, subtracting the allowed delay δ of the request:

$$\alpha_v = \max\left(0 \quad , \quad ({}^2s_v(t) +^3 s_v(t) +^4 s_v(t)) \cdot \left(\frac{w_v(t) + d_{i,j}}{u(t)} + a_{con}\right) +^5 s_v(t) \cdot a_v(t) - \delta\right) \tag{2.22}$$

with i the vehicle's node (or current passenger's drop-off node) and j the node with the closest charging station. Vehicles which are already connected to a charging station will always have a time delay of 0 minutes. The state of charge at the time of connection to the charging station is also calculated for each vehicle:

$$q_{v,conn} = q_v(t) - (w_v(t) + d_{i,j}) \cdot \frac{EC}{CAP} \cdot ({}^2s_v +^3 s_v +^4 s_v) \tag{2.23}$$

The energy delivered at each time step of the request by each vehicle is referred to with $\epsilon_v(\tau)$. In order to have the maximum energy delivered the following objective function should be maximized:

$$f_p(\epsilon_v) = \sum_{\tau} \sum_{v} \epsilon_v(\tau) \tag{2.24}$$

Also, it is desirable that the minimum number of vehicles are used for the grid request, in order to limit the disruption to the transport service. The cost function can therefore be introduced:

$$f_s(c_v) = \cdot \sum_{v} c_v \tag{2.25}$$

$$c_v \in \{0, 1\} \tag{2.26}$$

where c_v is a binary variable that represents the commitment of vehicle v for the request. Equation (2.25) can be considered the cost of commitment of each vehicle, which is paid only when the vehicle is used (called back to the charging station). The overall objective function to maximize is then:

$$f(x) = f_p(\epsilon_v) - b \cdot f_s(c_v) \tag{2.27}$$

b is the secondary objective's relative weight. Only vehicles that are connected at time τ can contribute to energy delivery:

$$\epsilon_v(\tau) = 0 \quad \tau < \alpha_v \tag{2.28}$$

moreover, the energy deliverable at each time step is constrained by the maximum power:

$$0 \leqslant \epsilon_v(\tau) \leqslant \frac{p_{peak}}{60} \tag{2.29}$$

The state of charge of each vehicle has to remain within the interval $[0, 1]$ at each time step:

$$0 \leqslant q_{v,conn} - \frac{\sum_{k=1}^{\tau} \epsilon_v(k)}{CAP} \leqslant 1 \quad \tau \in \Gamma \tag{2.30}$$

The commitment costs are introduced as:

$$\sum_{\tau} \epsilon_v(\tau) \leqslant \frac{p_{peak}}{60} \cdot \Gamma \cdot c_v \tag{2.31}$$

meaning that if the commitment variable c_v is 0, vehicle v can not supply energy. A limit to how many vehicles can be used was also introduced, to ensure that there are always enough vehicles left for the transport service:

$$\sum_{\tau} c_v \leqslant z \cdot V \tag{2.32}$$

where z is the maximum ratio of vehicles that can be used for the grid request. This value is only relevant during periods of relatively low passenger request rates, for example at night, since most of the times the number of vehicles used is limited by other factors. In the simulations, z was chosen as 0.7. Choosing a lower value would put more priority on the passenger requests. The last constraint dictates that the power delivered should stay constant during the request time:

$$\sum_v \epsilon_v(\tau+1) = \sum_v \epsilon_v(\tau) \quad \tau \in \Gamma \tag{2.33}$$

The problem can therefore be stated as:

$$\begin{aligned} &\underset{x}{\text{maximize}} \quad f(x) \\ &\text{subject to} \quad (2.26), (2.28), (2.29), (2.30), (2.31), (2.33) \end{aligned} \tag{2.34}$$

The problem (2.34) is a mixed integer linear program and was solved with the built-in MATLAB$^{\text{TM}}$ function *intlinprog*.

The disruption to the transport service during and after the request is also investigated. During a request, the vehicles participating will stay in state 0, thus not available, and their power exchange will be determined by the optimization results. Vehicles not participating in the operating reserve request are not permitted to exchange power with the grid during the request time, so that the system acts as a single agent. Moreover, as mentioned previously, during the request vehicles can discharge until they reach 0 state of charge. The final impact on the transport service is assessed by the number of extra rejected requests and extra minutes of waiting times when compared to the base scenario.

2.2.7 Model assumptions, validation and limits

Validation of the model is important in ensuring the credibility of the results. While it is not possible to validate the model with real world demonstration or experiment, it is possible to validate the internal consistency and performance against theoretical expectations. The influence of model parameters was verified with sensitivity analysis. Model parameters such as idle time and battery capacity were chosen

through sensitivity analysis to maximize BEP and minimize waiting times. The model's limitations come primarily from the assumptions made to make the simulations possible with limited data. The main simplifying assumption is related to the transport simulation, as the city's road network is not considered. This is to allow for a faster simulation time and also due to the difficulty of properly considering traffic congestion in the simulations.

Other simplifying assumptions are related to the energy aspects of the model. Detailed charge and discharge behavior of batteries is not considered: charge power and charging/discharging efficiency are assumed to be the same at any SOC level. This is considered acceptable for this level of analysis. This is further justified by the fact that the simulations assume relatively conservative charging power levels. Moreover, the detailed electric grid is not considered: the model assumes that there are no transmission capacity constraints, and does not consider transmission losses. This is justified by the assumption that the centralized nature of charging stations allow vehicles to be connected directly to the medium or high voltage transmission grid, as opposed to the distribution network. Moreover, the positioning of these charging stations could be optimized to minimize power losses. These aspects were not considered in this paper, and are planned as the focus of future work.

Another limitation of the model is the consideration of static transport patterns. It is possible that the service will also attract people currently using public transportation or other means, thus affecting the position and time of trips from the survey. All these simplifying assumptions have been previously used in most of the models reviewed in Chapter 1.3. Numerical assumptions in the case study were backed by references whenever possible. The results are intrinsically uncertain due to the lack of real-world examples of commercial shared autonomous vehicle fleets and due to the experimental nature of this technology, which makes it impossible to compare the model with real data. However, despite this limitation, the internal and theoretical consistency should provide sufficient validation of the model‘s demonstrative analytical capacity for the case study presented.

2.3 Numerical data for simulations

2.3.1 Transport data

The case study examined here is based on the Tokyo Person Trip Survey 2008 [1]. In order to have a representative collection of trip characteristics for a city, the area of service in the simulations was limited to a central 40x40 km area of Tokyo, so only trips starting and ending in zones in this area were considered. This is approximately equivalent to the 23 special wards of Tokyo, which are the core and the most populous part of the city. The selected area includes 514 zones, which are selected as the nodes in the model. 34.5% of all the trips in the survey start and end in the central zones selected. Figure 2.4 shows the distribution of trip distances and starting time for the selected trips. The centers of the nodes selected are shown in Figure 2.3. Figure 2.5 shows the origin (blue spikes) and destinations (red spikes) of trips in the morning and evening. The asymmetry between origin and destination at the morning peak and evening peak is evident in the figures, with a large concentration of red spikes in the central area in the morning and blue spikes in the evening showing commuters' trips. The details of the stochastic trip generation methodology and the determination of the tortuosity factor of roads are reported in Section A.1.

30 charging stations were positioned in total, chosen with a sensitivity analysis. The results of the sensitivity analysis are reported in Figure 2.6. Although increasing the number of charging stations continue to decrease waiting times and BEP, the effects were deemed not large enough to justify the added expense of a larger number of charging stations. The position of charging stations in the case study was determined in order to minimize (to a large extent) the distance of travel from each node to the closest station. The first station was positioned in the node for which the sum of the distances to all other nodes is minimal. Subsequent stations were positioned in the same way, taking into account the presence of previous stations (i.e. considering only distances to the closest station). This algorithm is not optimal, but provides a good approximation of a distribution minimizing travel distances from

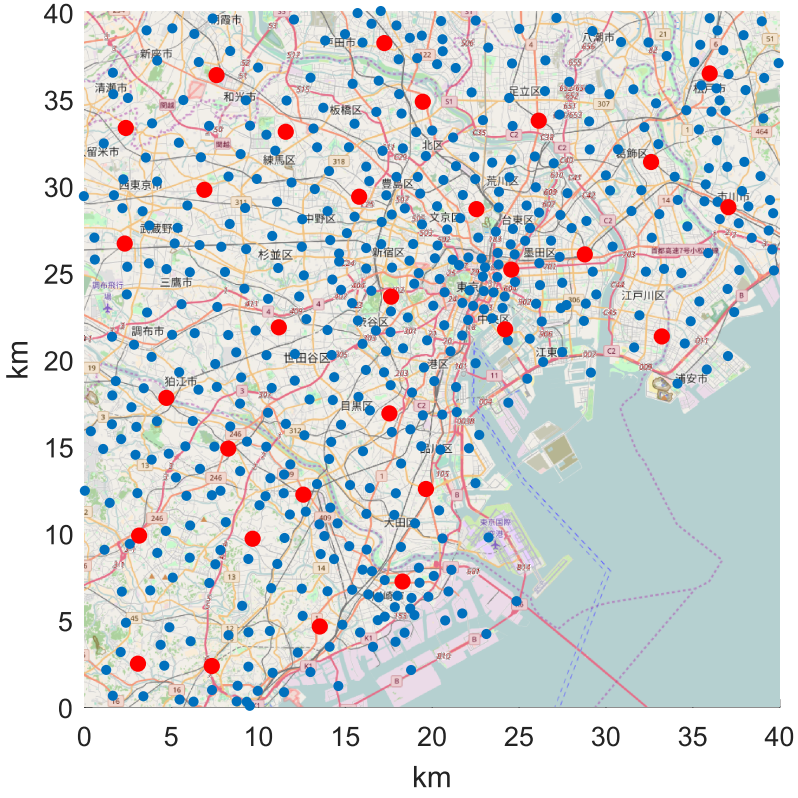

Figure 2.3: *Map of nodes in central Tokyo. Dots represent the approximate location of the center of the node. From [1]. Red dots represent nodes with charging stations in the simulation.*

each point.

Three levels of traffic congestion were considered: peak, average, and off-peak, at 20, 30 and 40 km/h, respectively. Figure 2.7 show the chosen speeds at each time of the day. The lowest speed of 20 km/h was chosen as the reported average speed in central Tokyo at peak time [53]. The average and off-peak speeds were chosen as 1.5 and 2 times the peak speed, as precise data on average speed in Tokyo could not be found. In setting this at these levels it also makes evaluation of the performance of the model corresponding to these changes more facile. Moreover, the actual speeds depend on type of road and origin/destination pair. Considering the average speed allows for the consideration of the effects of traffic congestion without simulating the actual road routing and congestion, which would render simulations

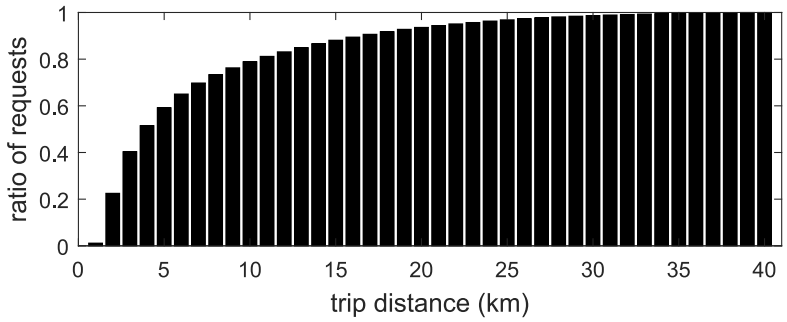

(a)

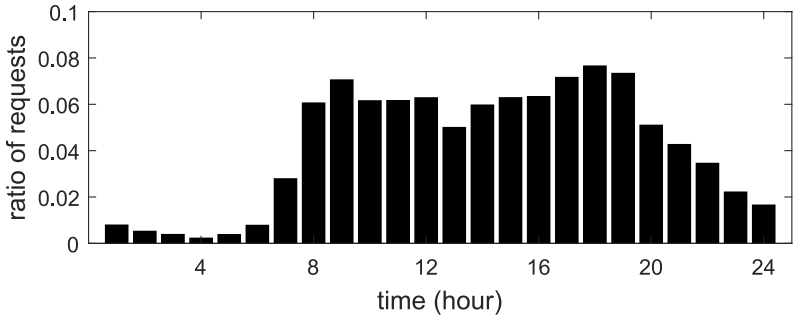

(b)

Figure 2.4: *(a) cumulative distribution of trip distance and (b) distribution of trip starting time from transportation survey [1]*

of this scale impractical. It should be noted that the off-peak speed does not affect results significantly, since the limiting factor for fleet sizing and operating reserve service is the minimum speed at the moment of maximum transport request rate. The results of a sensitivity analysis for the average speed is reported in Figure 2.8. The figure confirms that the choice of off-peak speeds is less critical also for waiting times, since while the sensitivity of results on peak speed at peak transport demand is very high, the sensitivity to off-peak speeds is very low, as shown in the figure. The peak/off-peak times were chosen to coincide with the pattern of trip requests (more trips translates into slower average speeds). The speed in km/h is related to the distance traveled in one time step $u(t)$ in the simulation as: $u(t) = \text{speed} \cdot \ell/60$.

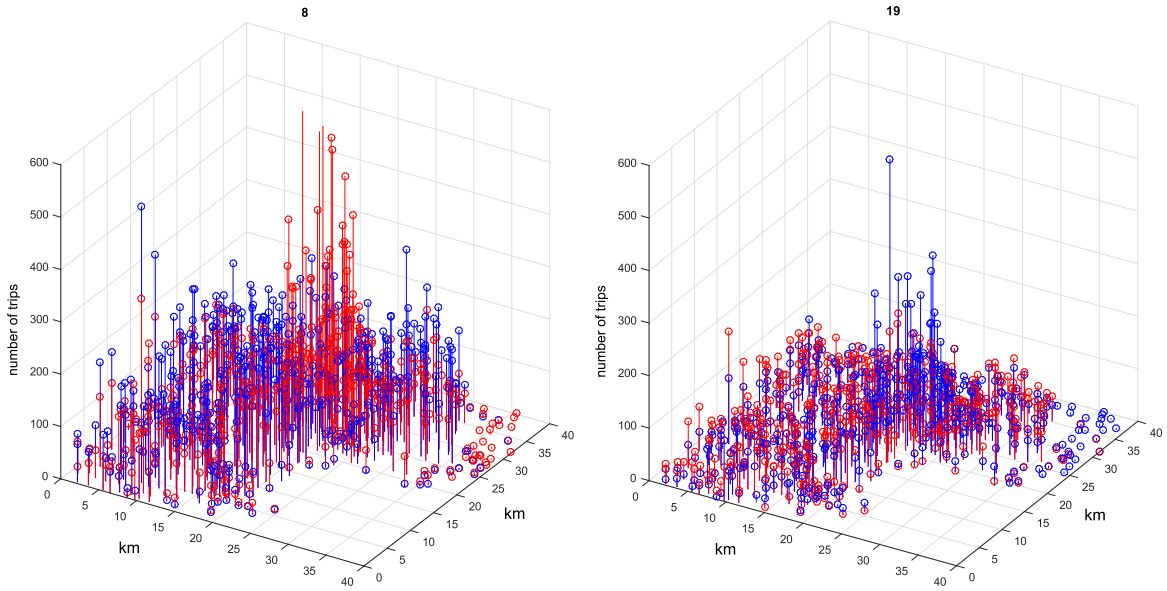

Figure 2.5: *A visual representation of trips origin and destination for the central 40x40 km area at different times in the day: (a) 8 am (b) 7 pm. Blue spikes represent origins, while red spikes represent destinations. Higher spikes correspond to higher trip frequency.*

2.3.2 Vehicle characteristics and costs

The parameters chosen for the vehicles are summarized in Table 2.4. Electricity consumption of vehicles EC was chosen at 0.15 kWh/km, taken from [54] and similar to the Nissan Leaf energy consumption at city speeds [55]. Battery cycle life was estimated at 1500 full cycles. Studies show that lithium-ion batteries for electric vehicles have low capacity fade even after 1000 cycles [56]. Real-life examples for lithium-ion batteries confirm these findings. Tesla Model S batteries have shown less than 10% capacity degradation over 700 cycles in surveys of private users [57] and the Powerwall (stationary Li-ion battery) from the same company offers a warranty of 60% capacity retention after 10 years with unlimited cycles [58]. A more controlled charging schedule can also contribute to increase battery life. Uddin et al. demonstrate an increase in battery life for electric vehicles when using smart charging with V2G compared to private charging at home [59]. Capacity fade of the battery is not considered in the model, thus the stated capacity should be considered

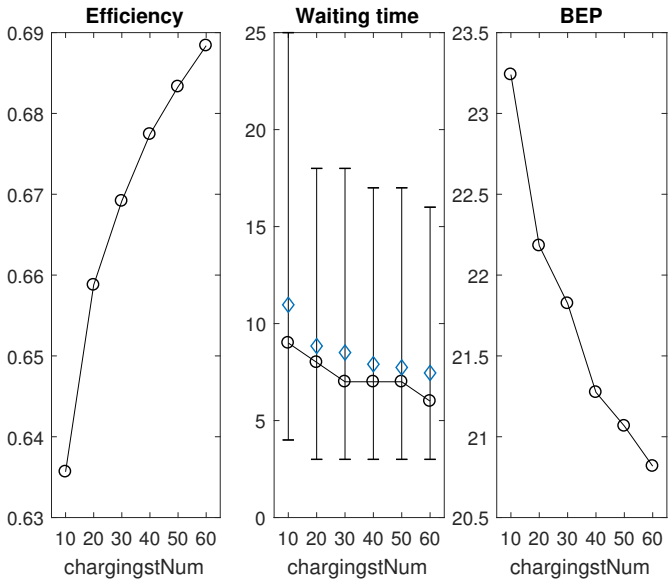

Figure 2.6: *Sensitivity of results on number of charging stations. Simulations with 1000 TPH. The blue diamond is the average waiting time.*

as an average during the battery life.

Prices are given in Japanese Yen (JPY) and US Dollars (USD), with a conversion rate of 1 JPY=0.009 USD (rate as of January 2018). Autonomous driving technology is expected to add $7,000 to $10,000 to the price of a vehicle by 2025 [60]. Fagnant and Kockelman estimate $10,000 added cost for early adoption [61]. A conservative estimate of 5 million JPY ($45,000) was used for the cost of the vehicle and other expenses (such as control center, maintenance etc.), excluding battery. The cost of the battery was calculated assuming 200 USD/kWh (22,200 JPY/kWh) [62].

Maximum charging/discharging power was set at 10 kW for normal operation and at 20 kW for short times (peak power when responding to grid requests). These power levels can be provided by several existing technological standards [44], which are not discussed in this work. Simulations were also run with a hypothetical 50 kW connection to investigate the influence of charging speed on performance.

Minimum SOC was set at 25% in order to enhance durability of the battery (see Table 2.3) [63]. The maximum SOC was set at 80% in normal operation, to increase the ability to absorb excess generation from the grid when needed. This has also been shown to further extend battery life as lithium-ion batteries suffer higher stress

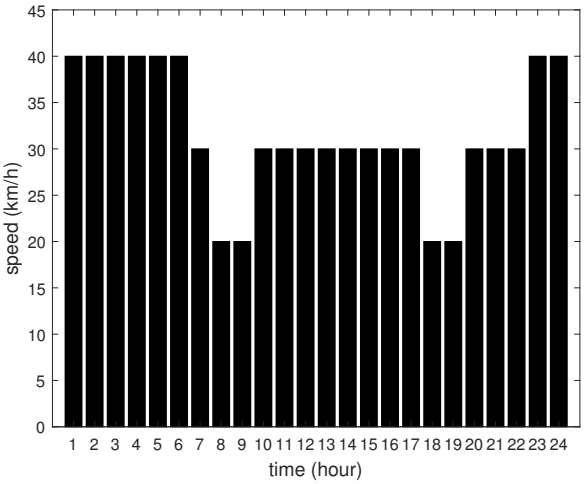

Figure 2.7: *Average speed during the day.*

at high SOC [64].

Table 2.3: *Summary of simulation parameters*

Name/symbol	Value	Unit
q_{charge}	0.35	-
q_{min}	0.25	-
q_{max}	0.8	-
ℓ	1	minutes
a_{con}	3	minutes
a_{charge}	30	minutes
a_{idle}	5	minutes

The time needed for the vehicle to connect to a charging station has been assumed to be 3 minutes. This includes the time to park the vehicle and connect it to a charging pod. Internal parameters of the model, such as minimum charging time and maximum idle time, were chosen through sensitivity analysis to minimize waiting times and BEP.

Due to the uncertainties related to future implementations of autonomous driving technology, conservative parameters were chosen in the simulations. However, it is possible that prices and vehicle performance would be better than in the current

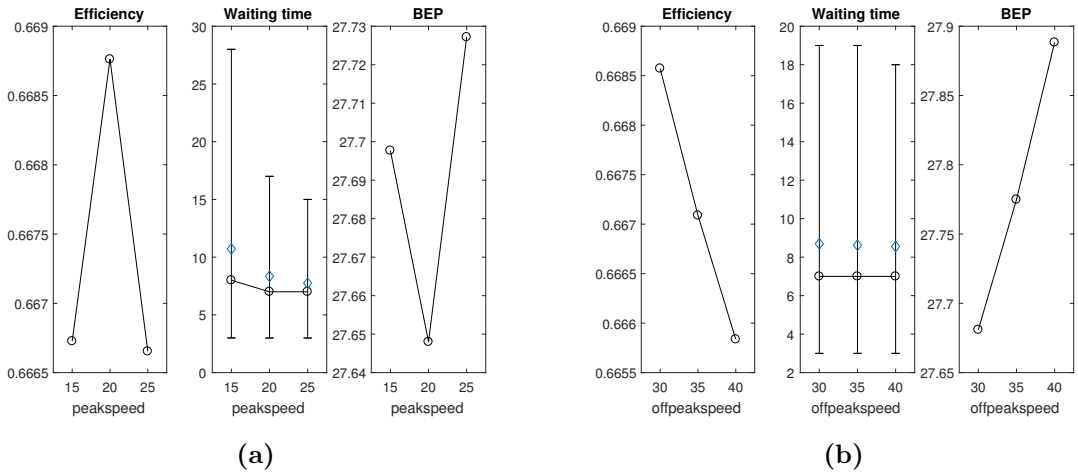

Figure 2.8: *Sensitivity of several output parameters to (a) peak speed (b) off-peak speed. The blue diamond is the average waiting time.*

study. For example, cheaper and more durable batteries could increase the energy available and the storage capability, while keeping costs low.

2.3.3 Electricity prices

The influence of electricity pricing was also studied. Three example price profiles were considered to test the model (see Figure 2.9):

1. *TOD* - Time-of-day pricing with 2 price periods (peak/off-peak).
2. *TOD+solar* - TOD with high solar penetration, with peaks at early morning and evening.
3. *HighRe* - Wholesale electricity market with high renewable energy penetration: random price profile extracted from a gamma distribution with shape parameter $k = 2$ and scale parameter $\theta = 20$.

The electricity market in Japan is undergoing a process of liberalization, and some electricity providers already offer several time-of-day pricing options [65].

All price profiles were normalized to the same average value of 40 JPY/kWh (0.36 USD/kWh), in order to investigate the ability of the proposed charge scheduling

Table 2.4: *Summary of technical and economic assumptions*

Name/symbol	Value	Unit
EC	0.15	kWh/km
CAP	50	kWh
η	0.9	-
p_{max}	10	kW
p_{peak}	20	kW
L_{car}	5	years
$L_{battery}$	1500	full cycles
C_{car}	5,000,000	JPY
	45,000	USD
$C_{battery}$	1,110,000	JPY
	10,000	USD

algorithm to minimize energy expenditures. The average price is conservatively higher than current average prices (about 20 to 30 JPY/kWh for TEPCO, depending on type of connection [65]) to account for a possible future rise of energy prices. This may happen due to the rising cost of renewable energy subsidies and dispatch and cost of energy imports. In the third case, the system buys and sell electricity in the wholesale electricity market as a price taker. Gamma distributions were shown to fit the current prices on the Japanese wholesale markets. Figure 2.10 shows histograms of spot prices for the main regions in Japan on the Japanese electricity exchange (JEPX) between April 2013 and end of 2017 with associated gamma distributions fitted. A random distribution for prices that could simulate the variability and range of prices in a market was needed to test the stochastic model. Although the generated price profiles in this case may not reflect the specific time distribution of prices in current markets, the temporal variability is justified by the high intermittent renewable energy penetration that is assumed in this scenario.

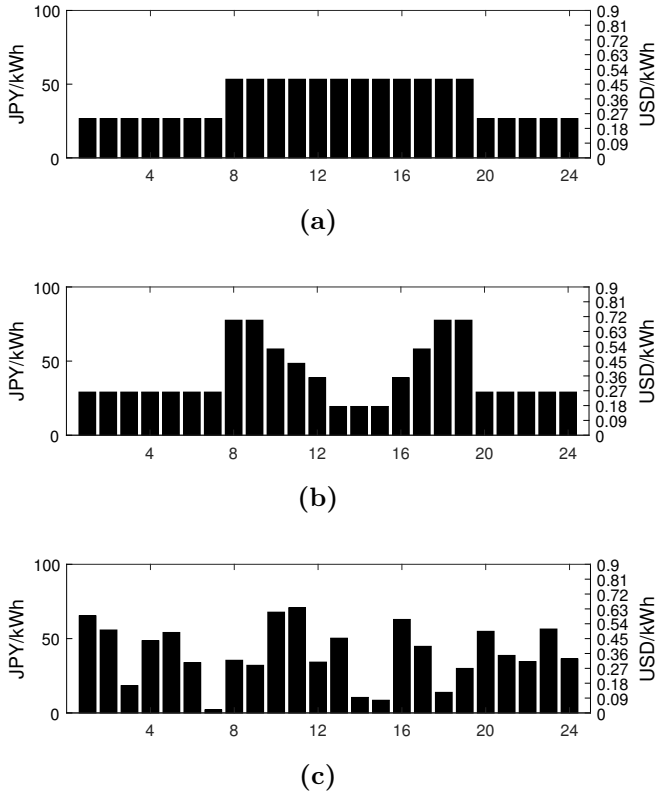

Figure 2.9: *Comparison of 24-hours samples of price profiles used in the simulations. The average for all profiles is 40 JPY/kWh (0.36 USD/kWh). (a) Time-of-day pricing with two periods; (b) time-of-day pricing with high solar penetration; (c) free market with high renewable energy penetration, modeled with a gamma distribution.*

2.4 Results and discussion

In this section, the results from the case study are presented. In the first section, the model is tested with different trip rates and number of vehicles to investigate the optimal fleet size as a trade-off between costs and transport service performance. In the second section, the effect of different price profiles on costs and transport performance is investigated using the optimal fleet size from the previous section. In the third section, the results of operating reserve simulations are presented for several request characteristics.

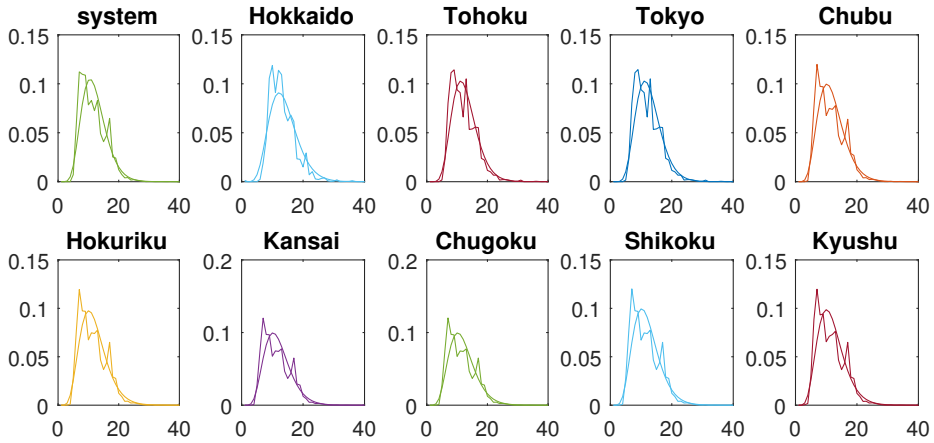

Figure 2.10: *Histograms of spot prices for the main regions in Japan on the Japanese electricity exchange (JEPX) between April 2013 and end of 2017 at half-hour intervals, with associated gamma distributions fitted.*

2.4.1 Fleet sizing

The aim of the first part of the simulations is to estimate the number of vehicles needed to satisfy the transportation requests. Simulations were run with different numbers of vehicles to estimate the optimal fleet size based on a number of output parameters. The parameters chosen were the waiting time for passengers, the break-even price of the system and the number of rejected requests.

The simulations have a time step of 1 minute over a period of 20 days. One extra day was added at the beginning to avoid start-up transients. The forecast horizon was set at 12 hours (720 time steps). Considering that both electricity price and passenger request rates change hourly, there are effectively only 12 distinct forecast values for each. Several trip rates were tested to show the influence of the rate on the system performance. This is useful to understand the sustainability of the system at different levels of request density, for example during the initial implementation phase when adoption rates are low. The passenger priority factor (PSP) was set at 100 JPY/km (0.9 USD/km). This value implies a bigger priority for transport service compared to grid services, as it corresponds to an equivalent electricity price of 667 JPY/kWh (6 USD/kWh), considering the electricity consumption of vehicles.

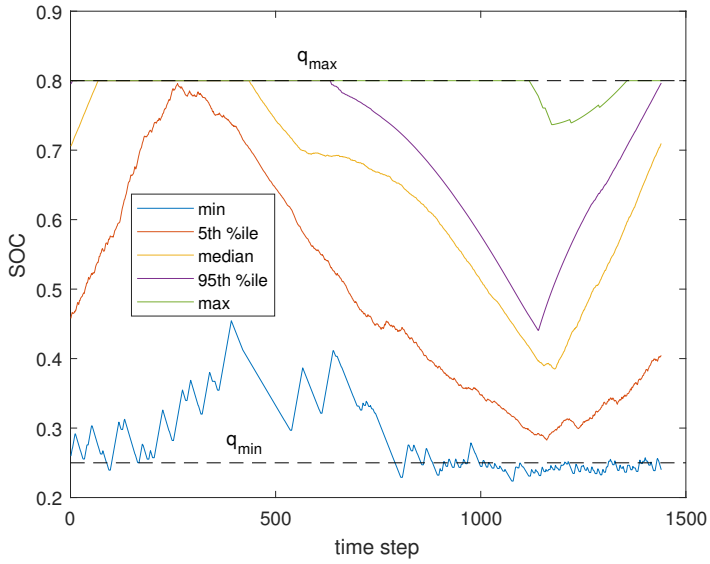

Figure 2.11: *Example of SOC evolution in a day (1440 time steps). At each time step, the minimum, maximum, median and 5th and 95th percentile of vehicles' SOC are reported (simulation with 1000 trips per hour and 1400 vehicles).*

The simulations are based on numbers of vehicles that are constant proportions of the average rate of trips in order to compare the results. For example, if the average rate of trips per hour is 500, then a proportion of 1.4 vehicles per average rate of trip per hour would be a fleet of $500 \cdot 1.4 = 700$ vehicles. The charging of the vehicles is managed by the charging algorithm introduced in section 2.2.4. A simple time-of-day hourly price profile with two periods was chosen for the electricity price (Figure 2.9a), with an average electricity price of 40 JPY/kWh (0.36 USD/kWh).

Figure 2.12 shows an example of the movements of a vehicle during simulation time. Results are shown in Figure 2.15 and 2.16. Waiting times tend to stabilize when the number of SAEVs available is more than 1.2—1.4 times the average rate of trips per hour.

The median waiting time drops to 7 minutes and 95% of requests are fulfilled within 18 minutes for a simulation with 1000 TPH and 1400 vehicles (Figure 2.15). Waiting times tend to reach a plateau with a certain amount of vehicles over TPH, depending on the TPH. After this plateau is reached, the waiting times are essentially not dependent on the number of vehicles. Figure 2.17 show the cumulative

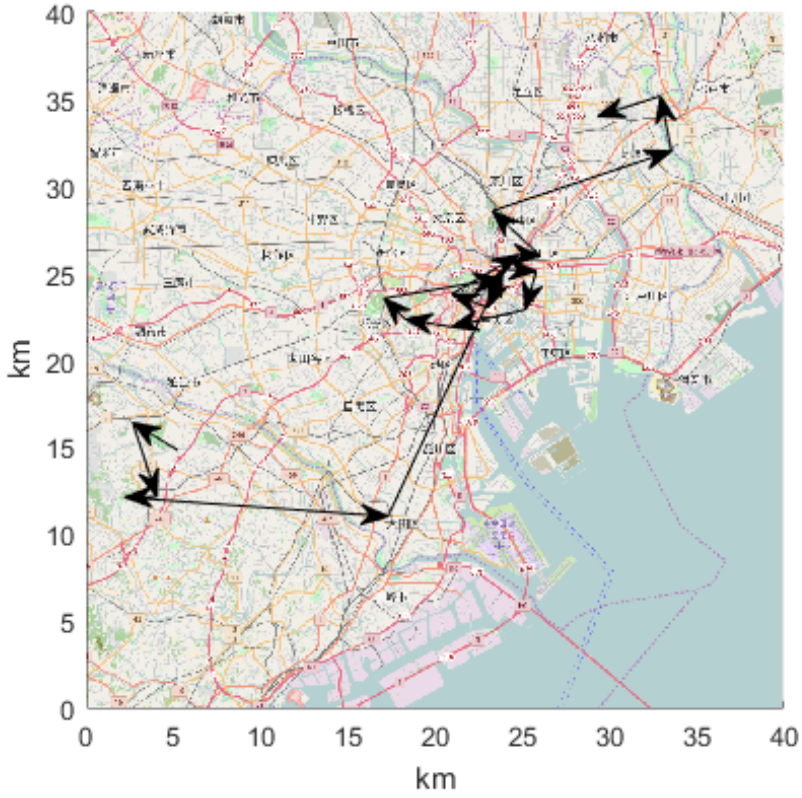

Figure 2.12: *Example of the first 20 movements of a vehicle during simulation time.*

waiting time distribution for simulations with 1000 TPH, for varying fleet sizes. Waiting times are strongly dependent on position and time of day, with increased waiting for requests in peripheral areas and during peak demand. An important characteristic of the system is that the expected waiting time is always known when a trip request is accepted (otherwise the request is rejected), so in a real case scenario the user can always plan in advance for the time needed (or use another means of transportation). Moreover, waiting times are quite predictable, depending on a certain time and position of the trip request. All these factors may be investigated further in future work.

Break-even prices tend to increase as the fleet size increases (Figure 2.16a). This is due to the increased investment needed for a larger fleet while efficiency levels and number of passengers served are stable (no rejected requests). Overall, BEP decreases as the TPH increase, together with the increase in efficiency of the system

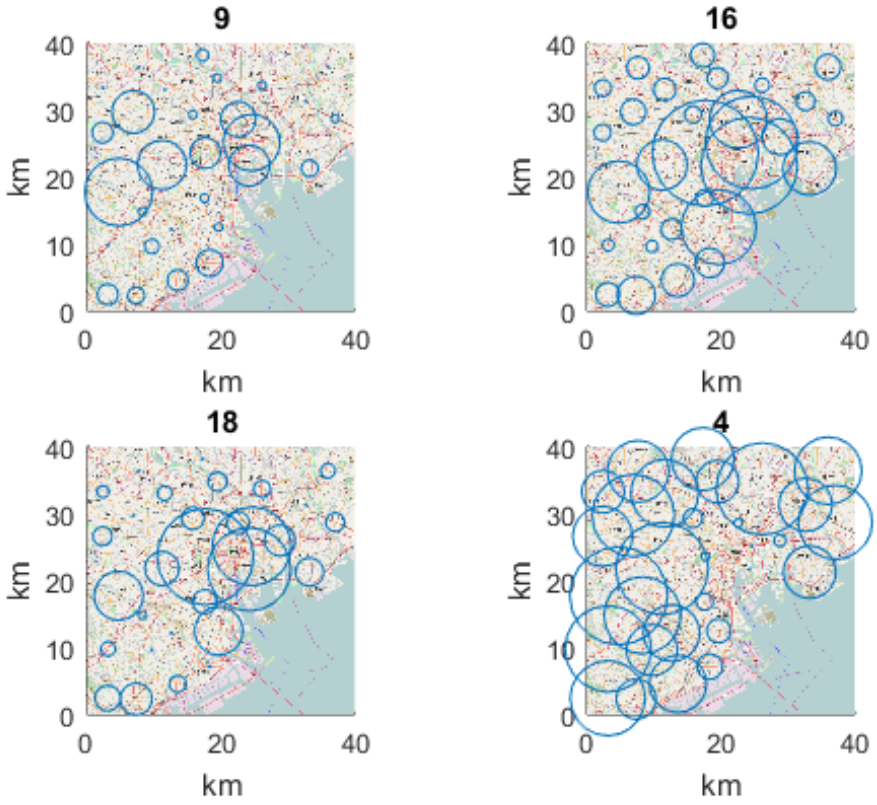

Figure 2.13: *Occupancy for each station at different time of day (hour of the day displayed on top of each figure). Size of circle is proportional to the number of vehicles connected to that charging station.*

(Figure 2.16b). For 1000 TPH and a fleet size of 1200 vehicles the BEP is about 30 JPY/km (0.27 USD/km), about 10 times lower than the average Japanese standard taxi fare of about 300 JPY/km (2.70 USD/km) [66]. This is a price comparable with public transport fares.

The efficiency of the system tends to increase with larger fleets, thanks to a more ubiquitous presence of vehicles to satisfy transport demand without extra empty trips (Figure 2.16c). However, as with waiting times, efficiency also tends to reach a plateau, the value of which is a function of the total TPH. Higher TPH values are associated with higher overall efficiency of the system. Rejected requests drop to zero for fleet sizes larger than a threshold size, which is dependent on the total TPH (Table 2.5).

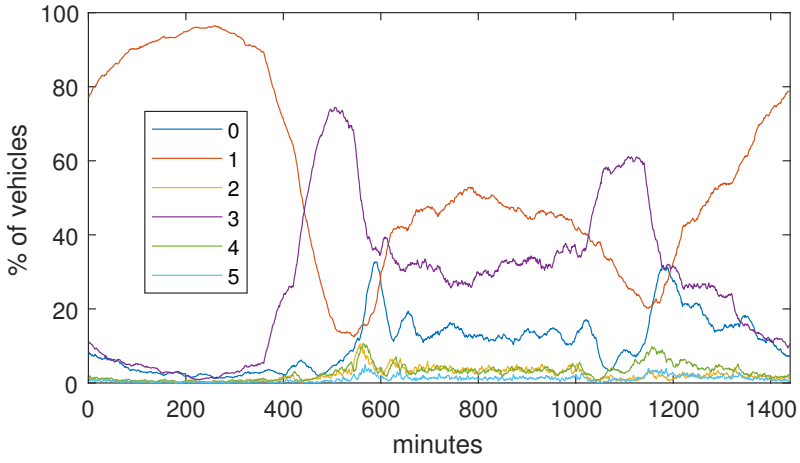

(a)

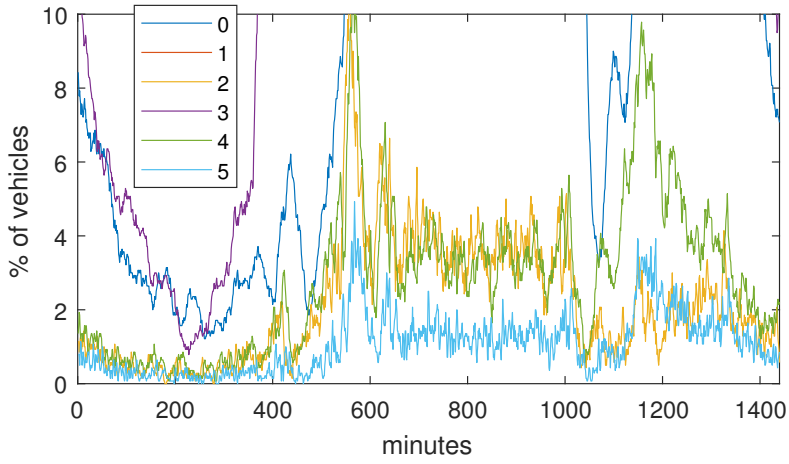

(b)

Figure 2.14: *Example of vehicles' status (see Table 2.2) during a day. The curves show the percentage of vehicles at each state at any given time. (a) Overall (b) Zoom-in to the lowest 10% to show transitional states with few vehicles at any given time*

Results show that the system is able to operate efficiently with between 1.2 and 1.6 vehicles per trip per hour, or about 5 to 7 vehicles per 100 trips per day. Assuming an average of 2 trips per private vehicle per day, this suggests that autonomous vehicles can replace private vehicles with a proportion of about 1:7 to 1:10, depending on the expected quality of service (waiting times and prices), in accordance with previous studies as discussed in section 2. The results also demonstrate the feasibility of the system even without planned active re-balancing of the vehicles. However,

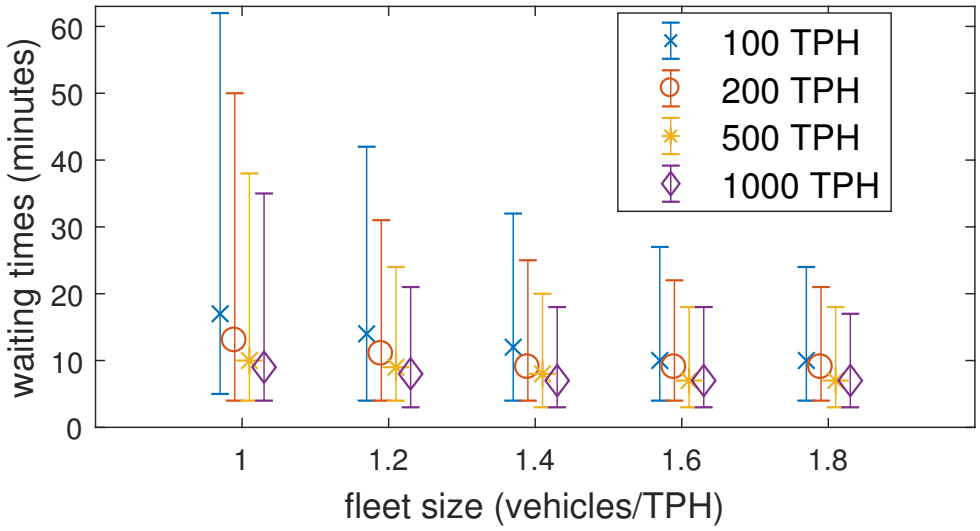

Figure 2.15: *Waiting times as a function of the number of SAEVs and trips per hour (tph). The marker indicates the median value and the error bars the 5th and 95th percentiles.*

with an effective re-balancing strategy waiting time can be reduced further. For the rest of this work, a fleet size of 1.4 vehicles/TPH was chosen. This represent a compromise between waiting times and costs.

2.4.2 Charge scheduling algorithm

The influence of electricity pricing was investigated by testing the model with the price profiles introduced in section 2.3.3. Figure 2.18 shows the results of different charging strategies with the different price profiles. In all the simulations there are no rejected requests and the waiting times are the same as those found in section 2.4.1, thus demonstrating that the charge scheduling algorithm has no negative effect on the transport service quality.

The charge scheduling algorithm lowers the BEP, with the benefits substantially higher when employing V2G. The non-V2G strategy differs only in that the vehicle can not sell back to the grid, thus only the positive values of (2.8) are considered. The savings are particularly significant with highly volatile price profiles such as profile 3. V2G can therefore play a role in making the system more economically

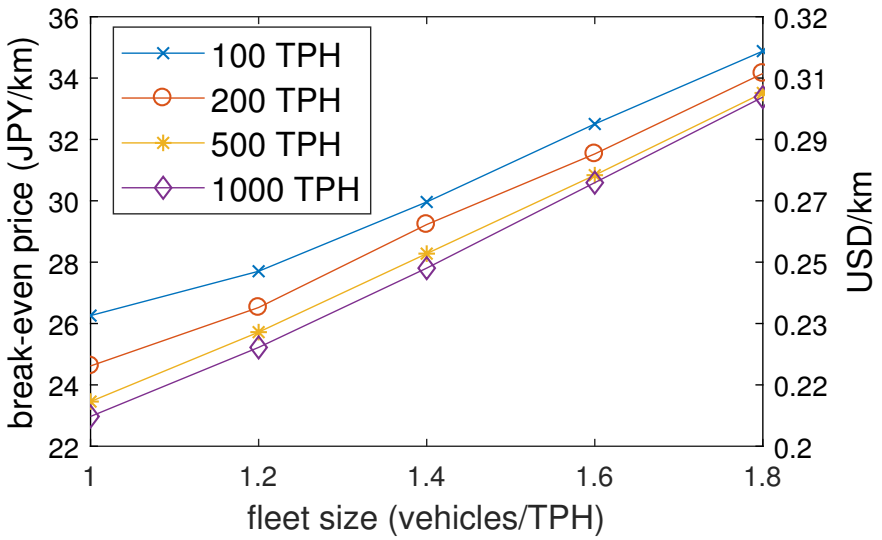

(a)

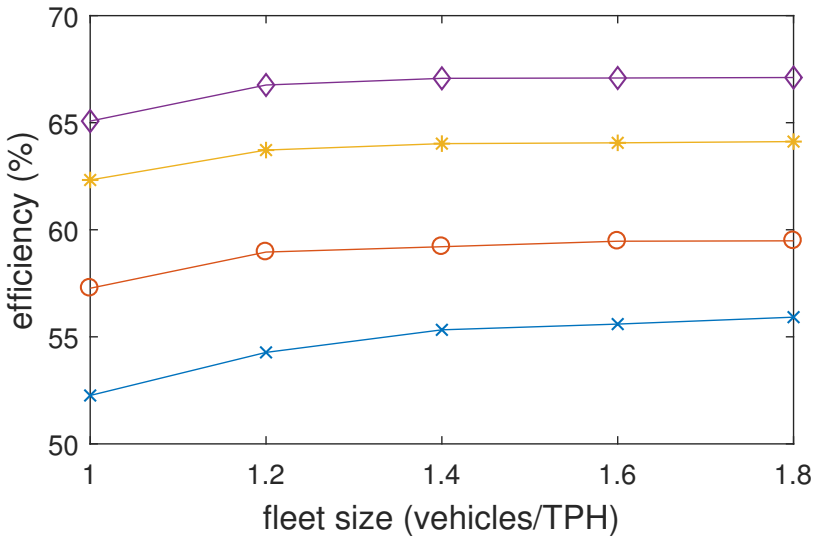

(b)

Figure 2.16: *System performance parameters as a function of the number of SAEVs and trips per hour (tph). (a) Break-even prices; (b) efficiency*

Table 2.5: *Requests served*

	vehicles/TPH				
TPH	1	1.2	1.4	1.6	1.8
100	95.65%	99.64%	99.98%	99.99%	100%
200	98.16%	99.95%	99.99%	99.99%	100%
500	99.70%	99.99%	100%	100%	100%
1000	99.79%	99.99%	100%	100%	100%

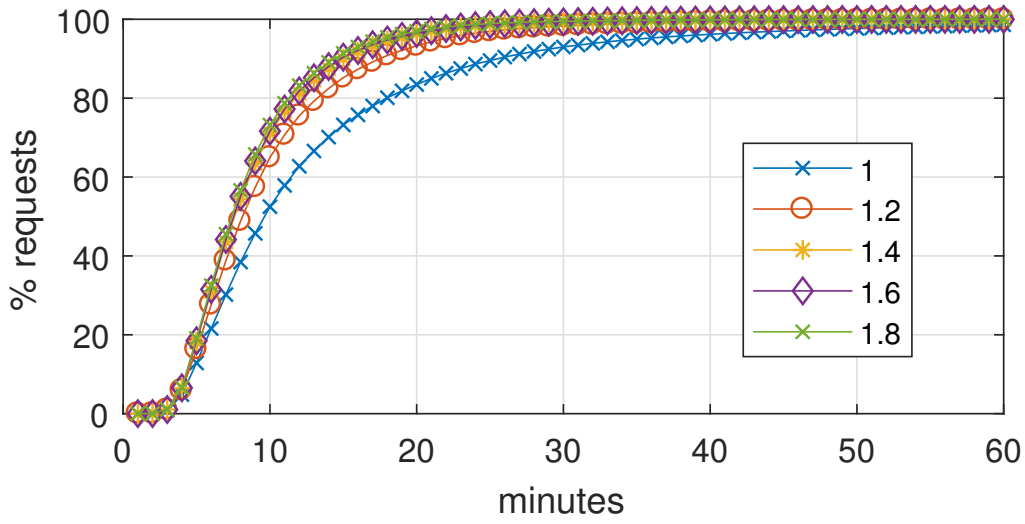

Figure 2.17: *Cumulative waiting time distribution for simulations with 1000 TPH and 1 to 1.8 vehicles per TPH.*

viable. In a scenario with rapidly changing electricity prices, that is, with a high penetration of non-dispatchable generation, under the assumptions of this work V2G has the potential to significantly decrease the energy costs for the system and help to balance the grid.

2.5 Operating reserve model

Two types of operating reserve were tested: spinning reserve, modeled with requests with no allowed delay; and non-spinning reserve, modeled with an allowed delay of 15 minutes. In both cases, the capacity of the system was tested for different request

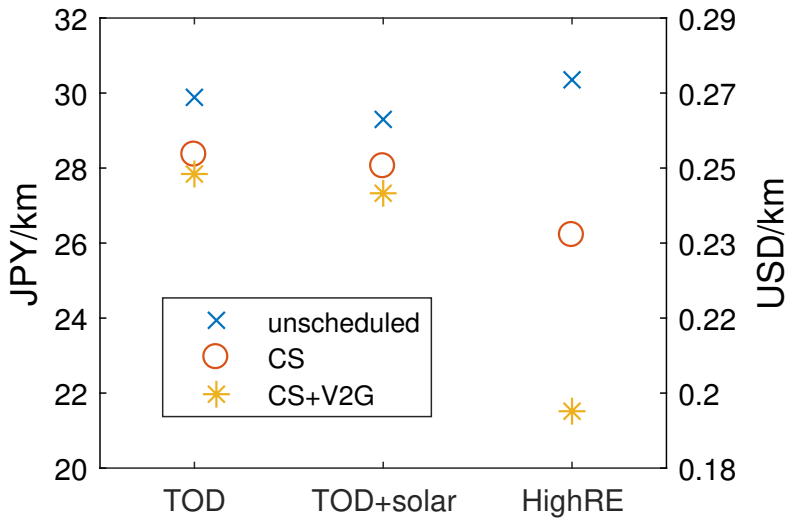

Figure 2.18: *BEP for different charging strategies and price profiles. Simulation with 1000 trips per hour and 1.4 vehicles/TPH over 20 days.*

duration of 30 and 60 minutes. Two types of grid connection for peak power were also tested: 20 kW and 50 kW. Moreover, the possibility for the system to be used to supply reserve storage was also tested in the same way. The secondary objective weight in (2.27) was chosen as 0.001. This is an arbitrarily small value in order not to affect the main optimization, while still allowing for the optimization of the use of vehicles for the same amount of power delivered. The results would not change as long as the secondary objective weight is small enough.

The available power varies significantly depending on the time of day, due to variable number of vehicles connected to charging stations and the available SOC. Figure 2.13 shows the occupancy for each station at different time of day. Central stations are busier during afternoon (hours 16:00 and 18:00, upper right and lower left panel), while peripheral stations are more occupied at night (4:00 am, lower right panel). Lowest level of occupancy is during the morning rush hour at 9:00 am (upper left panel). Figure 2.11 shows an example of SOC evolution during a day. The SOC evolution depends on transport demand and electricity prices. Figure 2.14 shows the status of vehicles during a day. States 0 and 1 represent vehicles connected to charging stations. The limiting period was identified as the peak transport demand

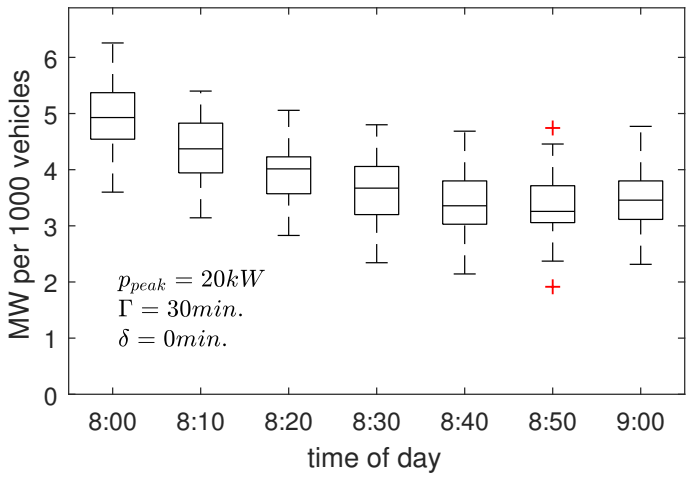

Figure 2.19: *Results of 50 tests for operating reserve capacity with no delay for 30 minutes. Results for 60 minutes duration were found to be the same. Whiskers in the boxplot include the upper and lower values up to 1.5 IQR distance from the third and first quartiles, respectively. Red plus signs indicate outliers.*

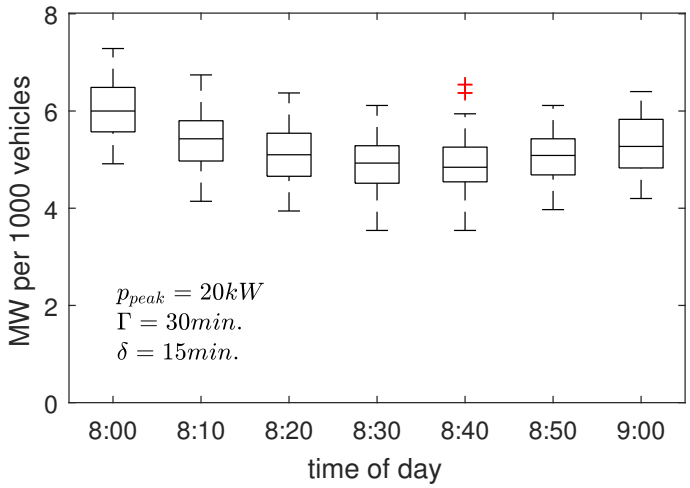

Figure 2.20: *Results of 50 tests for operating reserve capacity with 15 minutes delay for 30 minutes. Results for 60 minutes duration were found to be the same.*

between 8 and 9 in the morning, when the lowest number of vehicles are connected. The system was therefore tested for this period, to calculate the minimum power available. The tests were run at 10 minutes intervals for 50 times.

Figure 2.19 and 2.20 show the results with a maximum power connection of 20 kW and duration of 30 minutes. The results of the tests with a duration of 60

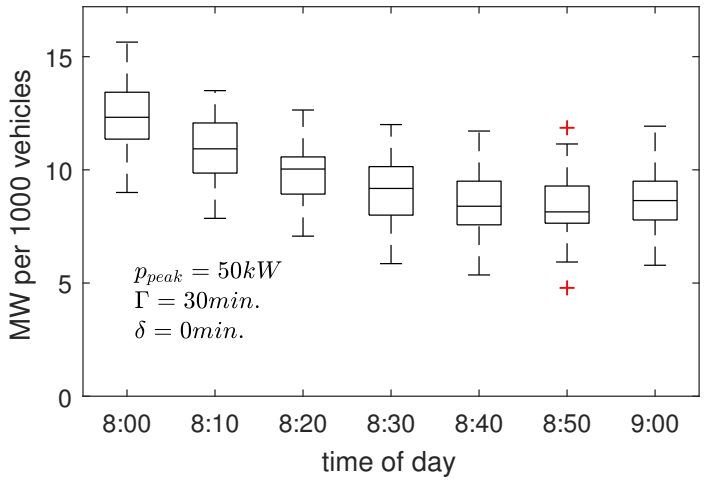

Figure 2.21: *Results of 50 tests for operating reserve capacity with no delay for 30 minutes, with a 50 kW connection*

minutes were the same as for the 30 minutes, thus are not shown. The allowed delay is the most significant factor in determining the amount of available power for a 20 kW connection: when 15 minutes delays are allowed, the power available grows by about 1-1.5 MW per 1000 vehicles. This results from the fact that the limiting factor in this case is the power deliverable (that is, the number of vehicles connected to charging stations), and not the energy stored in the batteries. A longer allowed delay allows more vehicles to move to charging stations to contribute during an operating reserve request. This conclusion is supported by the results of the 50 kW connection in Figure 2.21, which are almost exactly increased by a factor 50/20.

Figures 2.22-2.23 show the results for negative operating reserve capacity, or to absorb excess generation (storage). This service may become relevant as penetration of intermittent renewable energy increase.

The impact on the transport service was also investigated. In Figure 2.24 the average waiting times are shown for a 30 minutes non-spinning request in the morning peak and at the afternoon peak. Note that the 15 minutes allowed delay is the worst case scenario since with no allowed delay the vehicles participating in the request will necessarily be fewer.

Providing operating reserve with 20 kW connection does not influence the request

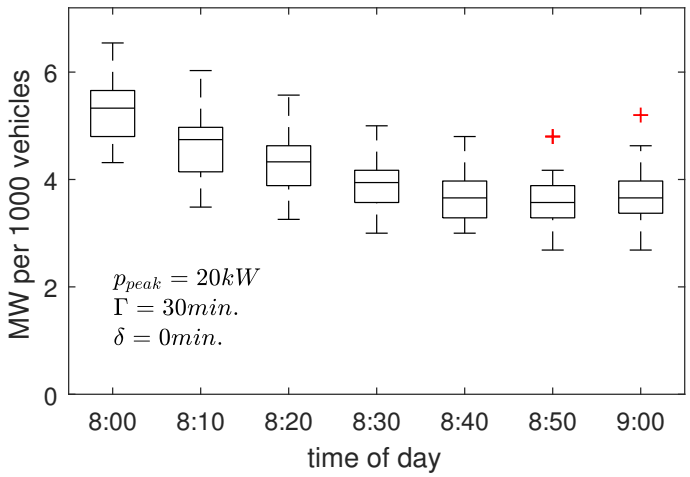

Figure 2.22: *Results of 50 tests for negative operating reserve capacity (storage of excess generation) with no delay for 30 minutes, with a 20 kW connection*

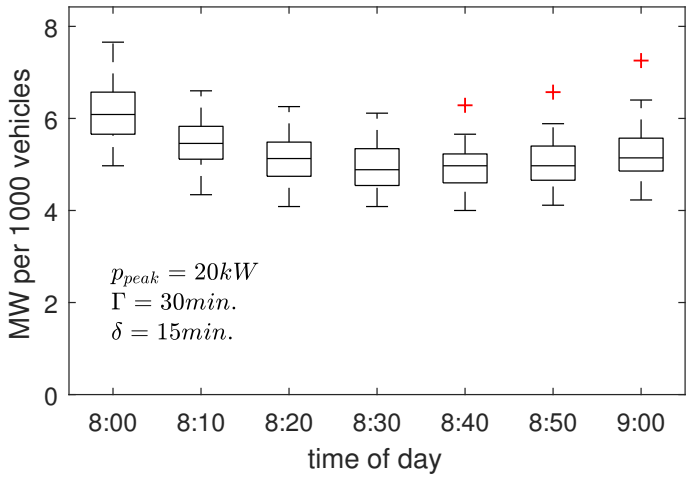

Figure 2.23: *Results of 50 tests for negative operating reserve capacity (storage of excess generation) with 15 minutes delay for 30 minutes, with a 20 kW connection*

rejection rate, and momentarily increase the average waiting time for passengers during peak times.

2.6 Conclusions

A simulation model was developed in MATLAB^{TM} to study the feasibility of a shared autonomous electric vehicle transport system and its integration with the

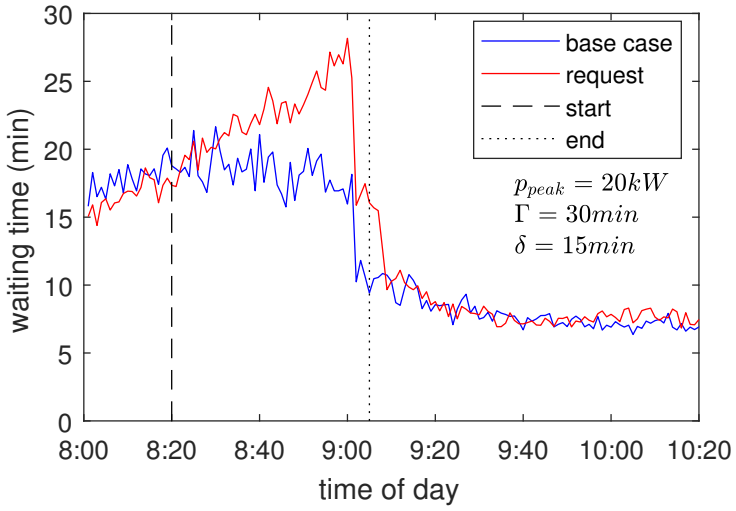

(a)

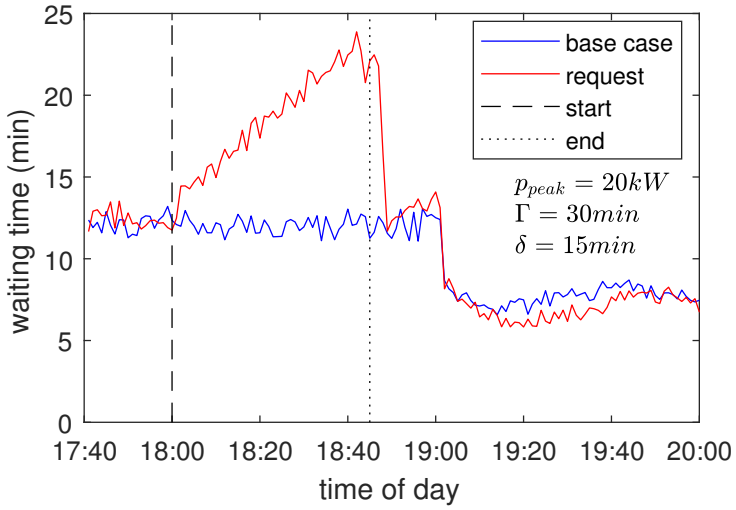

(b)

Figure 2.24: *Average waiting times for base case (no reserve request) and for a case with a 30 minutes non-spinning operating reserve request. (a) morning peak; (b) afternoon peak. Average over 10 simulations for each case. For all the simulations, there were no rejected requests.*

electricity grid. The model simulates a SAEV fleet serving passengers and charging at designated charging stations. A charge scheduling algorithm based on electricity prices was used and tested with several price profiles. A new model for estimating the availability of vehicles for operating reserve was developed and used to estimate

the potential for the SAEV system to provide spinning and non-spinning operating reserve to the grid.

The city of Tokyo was taken as a case study, with passenger data based on a transport survey. The system is studied in a transitional phase, with the assumption of unchanged transport demand patterns and a limited number of vehicles, and assuming that the power flow of vehicles does not influence electricity prices or transmission congestion levels.

The results of the simulations show that every shared vehicle in a fleet of SAEVs in Tokyo could replace 7 to 10 private cars, depending on the trade-off between waiting time and cost of the system. The system's break-even price per km is significantly lower than the fare of traditional taxis, and comparable to the average cost of car ownership and public transport. The results also suggests that the integration of a charge scheduling algorithm can further lower the cost of transport by providing load shifting and storage for the grid. In the case of highly volatile price profiles, the break-even prices of the system drop by up to 30% thanks to charge scheduling with vehicle-to-grid.

For the operating reserve model, the results show that the amount of operating reserve power available depends strongly on the time of day and the allowed delay. In particular, the system is able to supply spinning reserve of up to about 3.5 MW per 1000 vehicles even at the worst time for 1 hour with a 20 kW connection. This increase to 8-9 MW per 1000 vehicles when using a 50 kW connection.

In a scenario of a wide implementation of this system, the model suggest that SAEVs could provide significant grid-scale storage and spinning reserves. However, to assess the real impact of this technology implemented at large scale, a dynamic transport model needs to be developed to account for the change in transport patterns and congestion levels. Moreover, a model of the electricity transmission network could be included in future work to account for transmission constraints for a full-scale system.

Chapter 3

SAEVs as storage for renewable energy

3.1 Introduction

As detailed in Chapter 1.3, most studies on the charging of electric vehicles and their interaction with renewable energy have focused on private vehicles, mostly assuming that vehicles are used once or twice a day and charged at night [67, 68, 14]. This chapter presents a new methodology for the optimization of SAEVs charging with distributed dispatchable generators (DG), renewable energy generators, grid electricity with variable pricing, vehicle-to-grid, and considering vehicles' rebalancing requirements. The costs and carbon emissions of a SAEV system is investigated in the context of a grid-connected VPP and of an isolated microgrid compared to alternative energy storage and transport options.

The economic performance of SAEVs is expected to improve in the case of larger fluctuating renewable energy penetration. This is considered to be a synergy effect of SAEVs and renewable energy. Therefore, the aim of this study is to evaluate this synergy effect quantitatively by using the proposed method for optimizing the charging of SAEVs.

3.2 Methods

A mixed-integer linear optimization model is used to schedule the optimal charging and discharging of the aggregate fleet of SAEVs in order to minimize total costs for the VPP or microgrid. Transport demand, non-transport load and renewable energy generation are considered external inputs. Transport demand and renewable energy generation profiles are generated stochastically based on transport survey and historical weather data, respectively.

3.2.1 Transport demand generation

Nomenclature

A. Indices and simulation variables

$c(t), q(t)$	Charge energy and V2G discharge energy
$d_{i,j}$	distance between node i and j
$e(t)$	Energy stored in vehicles
$e_{max}(t)$	Maximum energy exchangeable
$f_{pass}(t)$	Distance for passenger trips
$f_{rel}(t)$	Distance for rebalancing
$f_{tot}(t)$	Total distance
$G_{re}(t)$	Generation from renewable sources
$g_j(t)$	Generation from DG
$o_j(t)$	DG operation binary variable
$i(t), k(t)$	Energy imports and exports
$L(t)$	Non-transport electricity load
$m_{av}(t)$	Vehicles available
t	Time step
$v_j(t), w_j(t)$	DG start-up and shut-down binary variables
$\lambda(t)$	Rate of Poisson process

B. Parameters and constants

$C_{battery}$	Cost of battery (yen/kWh)
C_{car}	Cost of car (with no battery)
$C_{startup}$	Start-up cost
CAP	Battery capacity (kWh)
EC	Electricity consumption of cars (kWh/km)
$e_{v,max}$	Maximum energy exchangeable per vehicle (kWh/km)
i_{max}	Maximum power exchangeable with grid (kW)
$L_{battery}$	Life of battery in equivalent full cycles
L_{car}	Life of car not including battery (years)
m	Total number of vehicles
$u(t)$	Average speed of vehicles (km/time step)
$y(t)$	Electricity price (yen/kWh)
$z_{i,j}$	Markov transition probability between state i and j
β	Ratio of trip distance to Euclidean distance
η	Battery round-trip efficiency

The transport demand is based on transport survey data. The total number of passengers at each time interval t is determined stochastically with a Poisson process with rate $\lambda(t)$ dependent on the relative frequency of trips at that time of day and the average trips per hour of the simulation. The scaling of the simulation is determined by the average trips per day (TPD) or average trip rate.

Each passenger request is generated at a specific node of the simulation, which is extracted from the trip origin and destination node distributions for the specific time of day. The generated trips are stored in matrix $A(t)$, where a_{ij} is the number of passengers originating from node i with destination node j. The distance between each node and each other node is stored in the symmetric square matrix D, where each element d_{ij} is the distance between node i and node j. The values are calculated from the Euclidean distance between nodes multiplied by an average tortuosity factor to account for the street layout. The total distance traveled to transport passengers can therefore be expressed as:

$$f_{pass}(t) = \sum_j \sum_i a_{ij}(t) \cdot d_{ij} \tag{3.1}$$

Passenger origin and destination distributions are typically not symmetric during any period of time shorter than a day. Vehicles would therefore tend to accumulate at certain nodes with higher destination rates and would be unavailable at nodes with high origin rates. In order to ensure service to all passengers, redistribution of vehicles is needed. It has been shown that the minimum amount of additional distance to travel for redistribution is equivalent to the Earth Mover's Distance (EMD) between the origin and destination distributions during a certain period of time [26]. This is also known as Wasserstein or Kantorovich distance. The EMD is a theoretical minimum rebalancing distance, which can however be reached in practice with an efficient routing strategy [26]. For the purpose of this work, the EMD is calculated for each time interval from the trip distributions using the algorithm in [69]. This extra relocation travel distance $f_{rel}(t)$ is added to the total distance traveled for trips with passengers to account for the energy needed for rebalancing.

The model assumes that the distribution of trips within a time period is uniform. Also, the position of electricity load and injections in the grid is not considered, since the actual position of specific vehicles is not simulated.

3.2.2 Charge scheduling model

The total energy stored in the vehicles e evolves as:

$$e(t+1) = e(t) - d(t) + c(t) - q(t)/\eta \tag{3.2}$$

where d, c, and q are respectively transport energy demand, charge, and V2G discharge during time t, all non-negative. η is the efficiency of V2G, set at 0.9. $q = 0$ for simulations without V2G. The electricity flow balance is stated as:

$$G_{re}(t) - L(t) + i(t) - k(t) - c(t) + q(t) + \sum_j g_j(t) \geq 0 \tag{3.3}$$

Where G_{re} is the renewable energy generation, L is non-transport electric load in the system, i is the grid import, k is the grid export, and g_j is the generation from unit j.

The dispatchable distributed generators (DG) units are controlled with three binary decision variables: $v_j(t)$, $w_j(t)$, $o_j(t)$, all $\in \{0, 1\}$, to account respectively for startup, shutdown and operation of generator j at time t. The constraints for the generators are:

$$o_j(t) - o_j(t-1) = v_j(t) - w_j(t) \tag{3.4}$$

$$g_{j,min} \cdot o_j(t) \leq g_j(t) \leq g_{j,max} \cdot o_j(t) \tag{3.5}$$

with $g_{j,min}$ and $g_{j,max}$ respectively the minimum and maximum generation for generator j when operational. The grid import/export capacity should also be less than the maximum capacity i_{max}:

$$0 \leq i(t) \leq i_{max} \tag{3.6}$$

$$0 \leq k(t) \leq i_{max} \tag{3.7}$$

The energy stored is constrained by the battery capacity of vehicles and the initial energy stored at the beginning and at the end of the time period:

$$e(0) = CAP \cdot m \cdot SOC_0 \tag{3.8}$$

$$CAP \cdot m \cdot SOC_{min} \leq e(t) \leq CAP \cdot m \tag{3.9}$$

$$e(t_{end}) \geq CAP \cdot m \cdot SOC_{end} \tag{3.10}$$

With CAP the battery capacity of each vehicle, m the number of vehicles, SOC_{min} the minimum state of charge of the combined fleet, and SOC_0 and SOC_{end} respectively the initial SOC and the minimum final SOC at the end of the period.

The amount of energy that can be charged or discharged from vehicles during a time interval is constrained by the number of vehicles connected to a charging station during the interval. Assuming a uniform distribution of passenger trip requests during the period, the average number of vehicles connected is:

$$m_{av}(t) = m - \frac{f_{pass}(t) + f_{rel}(t)}{u(t) \cdot t_{len}} \tag{3.11}$$

where u is the average speed of vehicles and t_{len} is the length of the time step interval. The maximum energy exchangeable is therefore:

$$e_{max}(t) = m_{av}(t) \cdot e_{v,max} \tag{3.12}$$

$$0 \leq c(t) \leq e_{max}(t) \tag{3.13}$$

$$0 \leq q(t) \leq e_{max}(t) \tag{3.14}$$

where $e_{v,max}$ is the maximum energy that can be exchanged by each vehicle during a time interval. This is a function of the choice of power connection and the length of the interval. The actual instantaneous power exchangeable during the period may vary depending on the specific position of vehicles. In this work it is assume that the power connections allow for higher power levels if required.

The model objective is the minimization of total cost. This includes costs from the grid, from the generators, and the cost of battery cycling. The cost function for the grid interaction is:

$$C_{grid}(t) = i(t) \cdot y(t) - k(t) \cdot y(t) \cdot \eta_{grid} \tag{3.15}$$

η_{grid} is an efficiency parameter representing the cost of selling to the grid and to avoid simultaneous import and export. This was chosen at 0.99. The cost function for DG considers the start-up costs and cost of generation:

$$C_{DG}(t) = \sum_{j} (i_j(t) \cdot C_{op,j} + v_j(t) \cdot C_{start,j}) \tag{3.16}$$

The objective function is therefore:

$$min \sum_{t} \left(C_{grid}(t) + C_{DG}(t) + \frac{\gamma_{cycles} \cdot c(t) \cdot C_{bat}}{L_{bat}} \right) \tag{3.17}$$

with $y(t)$ the price of electricity from the grid at time t. γ_{cycles} is the fraction of the battery costs amortized by cycling as opposed to aging, which was chosen as 0.5 (see also section 3.3.4). The model presented can be solved with mixed integer linear programming methods.

A model predictive control (MPC) approach (also known as receding horizon control) was used in the simulations to account for the limited prediction horizons for weather patterns and transport demand. This allows us to obtain results from optimization based on realistic prediction horizons, while still allowing us to study the behavior of the system over long simulation periods. An optimization period (horizon) of 2 days was used. At each step of the MPC, the first day of the optimization is implemented, and the optimization is rerun with an updated prediction horizon for the next day. For more accurate results but slower simulation times, the optimization can be run at each hour with only the first hour implemented.

3.2.3 Renewable energy generation

Two intermittent renewable energy sources are considered: wind and solar power. Renewable energy generation profiles g for both sources were generated stochastically based on historical data. Load, solar, and wind profiles were assumed to be independent.

Wind speed profiles were generated with a Markov model based on historical wind speed observation. Markov models are often used to generate wind speed profiles based on historical data [70]. Each element of the Markov transition probability matrix Z was determined as:

$$z_{i,j} = \frac{w_{i,j}}{\sum_i nw_{i,j}} \tag{3.18}$$

Where $nw_{i,j}$ is the number of transitions from state i to state j in the historical

data, where each state corresponds to a range of wind speeds, discretized into 20 states. The wind power generation P_w is then calculated considering the wind turbine characteristic curve, which was linearized for simplicity:

$$P_w = \begin{cases} P_{rated} \cdot \min(1, \max(0, \frac{W - W_{cutin}}{W_{rated} - W_{cutin}})) & if \quad W \leq W_{\text{cutoff}} \\ 0 & if \quad W > W_{\text{cutoff}} \end{cases} \tag{3.19}$$

where W is the wind speed.

Solar irradiance profiles were generated from hourly extraterrestrial solar irradiation profiles for the simulation days and location and a stochastically generated average daily clearness index K. The probability distribution of K was calculated by comparing computed values for the maximum daily extraterrestrial solar irradiation over actual measured historical irradiation values for each day. Extraterrestrial irradiation was calculated based on methodology reported in the HOMER software documentation [71].

3.3 Numerical simulations

The model was developed in MATLAB$^{\text{TM}}$ and tested with a case study in Tokyo.

3.3.1 Transport data

The transport request probability is based on the Tokyo Person Trip Survey 2008. More information about the survey extraction methodology can be found in Section A.1. Trips by car in a central 20x20 km area of Tokyo were considered for this work. This area includes about 300 nodes (origin and destination points). Figure 3.4 shows the location of the selected nodes. Figure 3.3a shows the amount of vehicles-minute traveled during a day with the selected trips from the survey, and the corresponding calculated EMD.

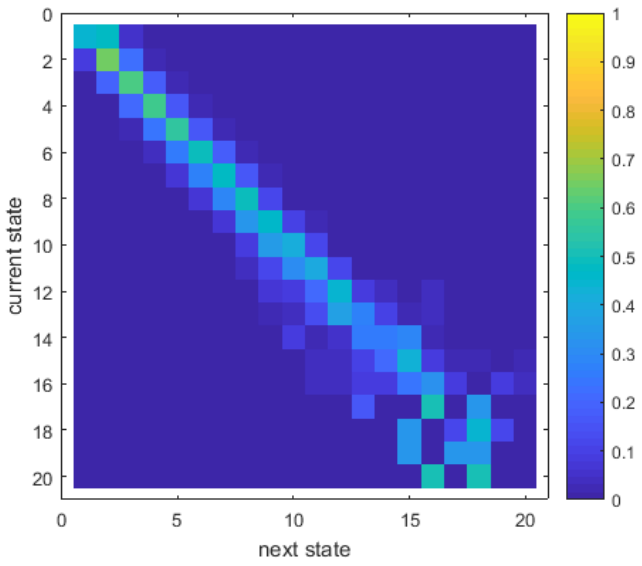

Figure 3.1: *Markov transition probability matrix for the wind speed historical observations.*

3.3.2 Electricity load and price

The electricity load profile was taken from the Tokyo Electric Power Company (TEPCO) [72]. Data for the year 2017 was used in the simulations. The electricity load profile was normalized to a daily electricity consumption of 6.3 kWh per person, the average for Japanese residential consumers [73]. It is assumed that the VPP has access to the wholesale electricity market as a price-taker. This is justified by the scale of the VPP relative to the total electricity market.

The electricity price was taken from the Japan Electric Power Exchange (JEPX) historical day-ahead trading data for the corresponding electricity load in 2017.

3.3.3 Renewable generation data

Hourly solar irradiation data was taken from the Japan Meteorological Agency for Tsukuba weather station (near Tokyo) in the years 2011-2015 [74]. Figure 3.2a shows the theoretical extraterrestrial daily solar irradiation and the historical measured irradiation levels for the period considered. Seasonal variations are clearly visible. Seasonality effect is much less prominent in the clearness index, shown in Figure

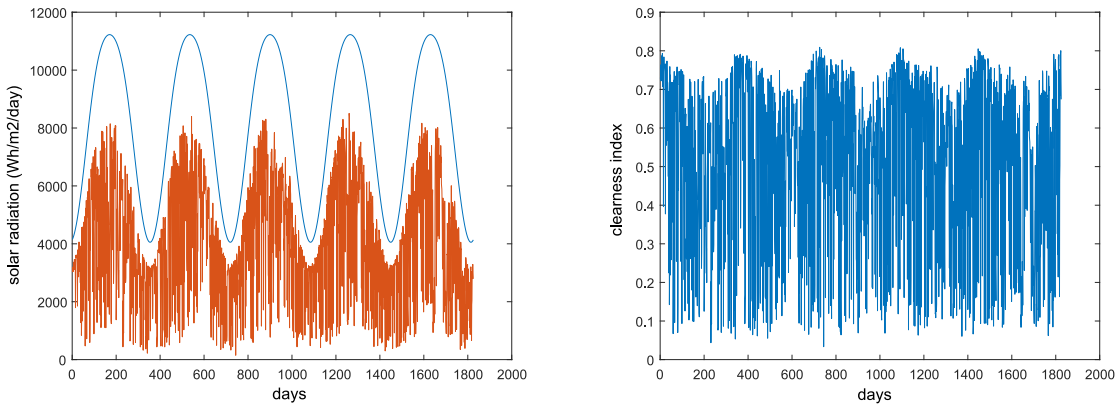

(a) **(b)**

Figure 3.2: *Calculation of solar power distribution for stochastic solar power profile generation. (a) Theoretical extraterrestrial daily solar irradiation (blue) and actual measured daily irradiation during five years (red). (b) clearness index K during the five years.*

3.2b for the same period. Solar panels are assumed with tilt equal to the latitude (36°) and peak generation at $1kW/m^2$, resulting in an average yearly capacity factor of 13%.

Wind model data was based on 6 years of historical observations from 2010 to 2015 at Tokyo Haneda Airport, taken from NOAA [75]. The Markov transition probability matrix obtained from historical observations is reported in Figure 3.1. Each element represents the probability of a transition to the next state from each current state. To obtain wind power generation profiles from wind speeds, an hypothetical typical wind turbine was used with cut-in speed of 4 m/s, rated speed of 12 m/s and cut-off speed of 25 m/s, resulting in an average yearly capacity factor of 21% with the considered wind speed profile.

The generation capacity was sized to generate the total non-transport electricity consumption over a year. For simulation with solar power only, this is equivalent to about 2 kW of solar PV per person, which is consistent with a rooftop solar PV system size considering the number of people in the household. In Japan, residential rooftop solar installation average size ranges between 4 and 6 kW [76]. Figure 3.3b shows an example of solar and wind power generation during a week.

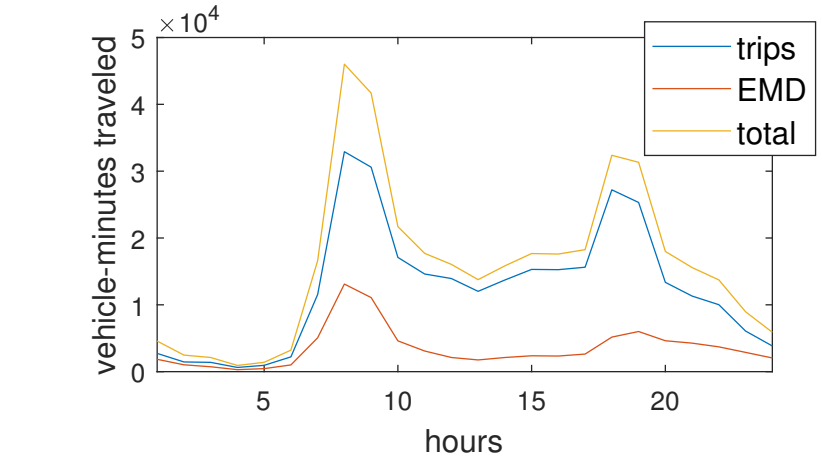

(a)

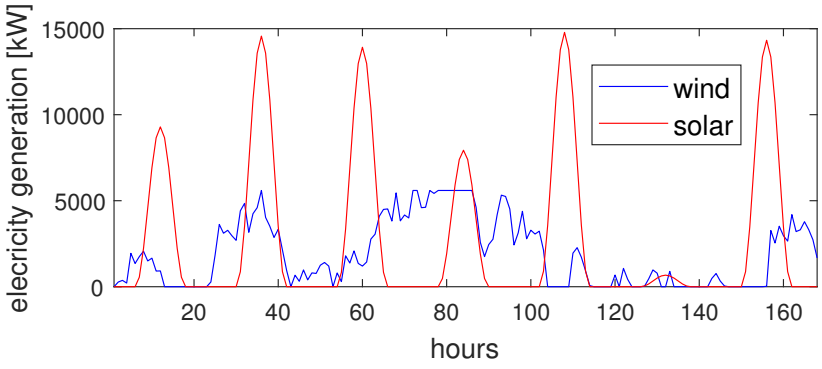

(b)

Figure 3.3: *(a) EMD for trips from the transport survey during a day; (b) Example of profiles for solar and wind power generation during a week.*

3.3.4 Cost and emissions assumptions

The exchange rate used in this work was 1 USD=100 JPY (similar to the current exchange rate as of April 2018). Battery costs were estimated at $200/kWh [62], with a cycle life of 1500 cycles. Costs of the battery were divided in equal parts between amortization costs (calculated over 5 years) and cycling costs, thus reflecting the practical life of batteries and avoiding underestimating costs of underused storage. Life-cycle emissions of batteries were also included at 50 kg CO_2/kWh capacity, similar to lithium-ion batteries manufactured in the United States [79].

The private vehicle for comparison was assumed to be a hybrid electric vehicle (HEV) with a high fuel efficiency of 23 km/l, similar to those of the 2016 Toyota

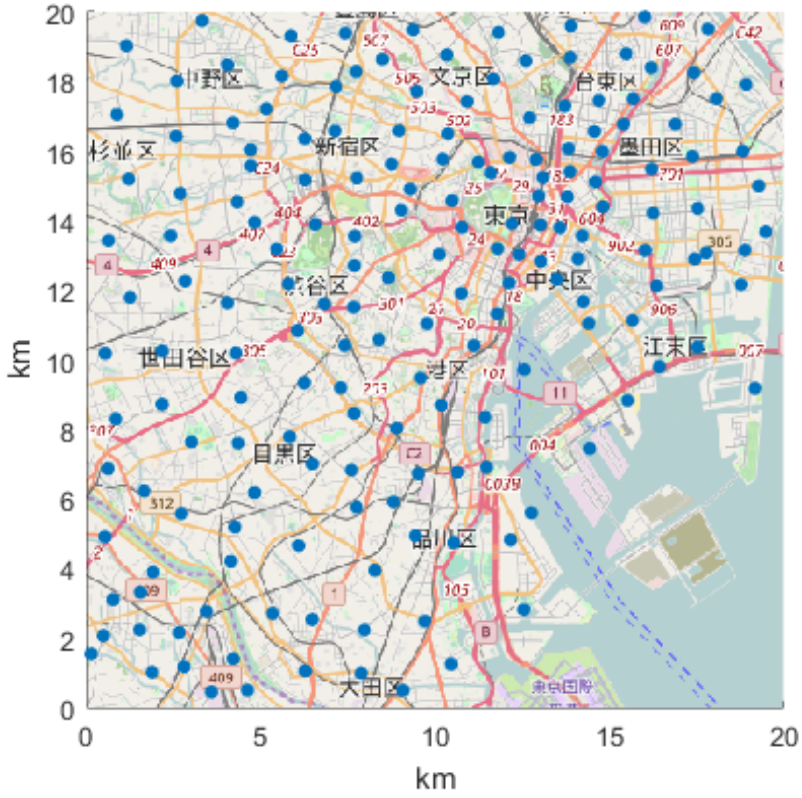

Figure 3.4: *Map of origin/destination nodes in the central 20x20 km area of Tokyo, taken from transport survey [1].*

Prius in city driving [80]. This value is conservative, as it is considerably higher than current average new vehicle efficiency in Japan and higher than the 2020 target for new vehicles of 20.3 km/l [81]. Gasoline prices were assumed at 150 yen/liter. The cost of the vehicle was taken as 2 million yen or $20,000 with a life expectancy of 12 years, the current average for new vehicles in Japan [81]. Emissions from gasoline consumption is 2.3 kg CO_2/liter.

Autonomous vehicles costs (excluding battery) were conservatively estimated at 5 million yen or $50,000 with a life expectancy of 5 years. This is supported by literature putting the extra price of fully autonomous technology at about $10,000 [61, 60]. The extra cost was assumed to be necessary due to the heavier usage of the vehicle compared to a private car, and by the extra cost of maintenance and other expenses which is assumed included in the capital cost. The vehicles'

Table 3.2: *Transport mode characteristics*

	HEV	SAEV
capital cost	2 million yen	5 million yen
consumption	4.3 l/100km	0.15 kWh/km
expected life	12 years	5 years

Table 3.3: *Summary of renewable energy characteristics*

	solar	wind	ref
capital cost [million yen/kW]	0.25	0.20	[77]
O&M cost [yen/kW/year]	0	7600	[77]
payback [years]	10	10	-
capacity factor [%]	13	21	-
emissions [kg CO_2/kWh]	0.041	0.011	[78]

battery capacity was set at 50 kWh and the maximum power exchange (charging or discharging) at 10 kW. A summary of the transport cost assumptions can be found in Table 3.2. Grid emission intensity was set at 0.452 kg CO_2/kWh, the average between the value for the Japanese electricity supply in 2015 (0.534) and the 2030 target (0.37) [82]. Renewable energy costs, operation and maintenance costs, payback periods, capacity factors and emissions are summarized in Table 3.3.

As of 2018, Japan had a residential solar feed-in tariff of 26 yen/kWh [83]. High feed-in tariffs in recent years have caused a sharp increase in photovoltaic installations in the country with about 50 GW of cumulative installation at the end of 2017, a 10-fold increase from 2011. It is expected that the feed-in tariff will be progressively decreased and phased out in the coming years to favour self-consumption [84]. In this work, it is assumed that excess PV power is bought at the price of electricity in the wholesale electricity market (marginal cost of generation). The price of electricity for households was set at 20 yen/kWh, which is close to the average price for TEPCO.

For the microgrid case, hypothetical DG units representing a gas turbine, a diesel

Table 3.4: *Summary of distributed generation characteristics*

DG unit	min. kW	max. kW	cost yen/kWh	CO_2 kg/kWh
gas turbine	2000	5000	20	0.6
diesel engine	100	1000	25	0.65
biomass	1000	2000	15	0.4

generator, and biomass steam plant were used. Table 3.4 presents a summary of the characteristics of these units. Approximate values were taken from [85]. Start-up costs for each unit were chosen as the cost of running the unit at full power for one hour.

3.3.5 Simulation parameters and scale

The time interval length for the simulations presented was set to 1 hour and the tortuosity factor of roads was set to 1.5 (see also Section A.1.2). The fleet size was selected at 1.4 vehicles per average trip per hour (TPH). This ratio was found in previous work to be a good compromise between minimizing waiting times and operating costs of the system (see Chapter 2). Assuming an average of 2 trips per private vehicle per day, this suggests that autonomous vehicles would replace traditional vehicles with a proportion of about 1:8.6, in accordance with previous studies [4], [61]. The total population assumed in these simulation was chosen as 12,000 people, resulting in a total of 24,000 trips per day (1,000 trips per hour average).

3.4 Results and discussion

In this study, two cases were considered for analysis: grid-connected VPP without DG, and isolated microgrid with DG. Each data point represents 100 week-long simulations, taken from Mondays to Sundays of the load profile.

Table 3.5: *Summary of scenarios. VPP does not apply to the microgrid case.*

scenario	trans-port	storage	charge sched.	V2G	VPP	RE
BAU	HEV	×	×	×	×	◯
Battery	HEV	◯	◯	×	◯	◯
SAEV1	SAEV	◯	×	×	◯	◯
SAEV2	SAEV	◯	◯	×	◯	◯
SAEV3	SAEV	◯	◯	◯	◯	◯

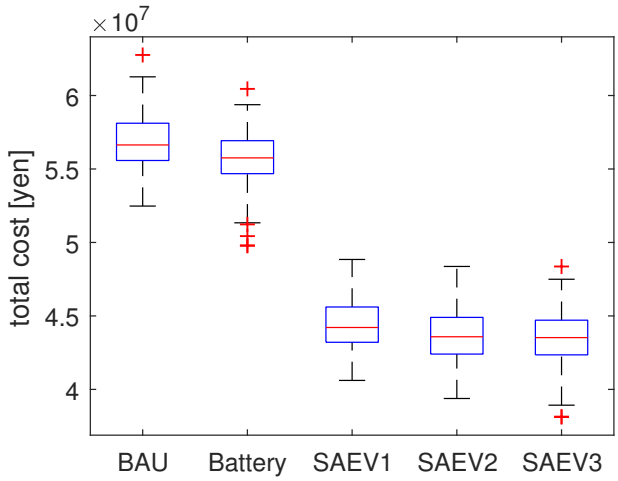

Figure 3.5: *Weekly total costs for 100 iterations for each case considered.*

3.4.1 VPP case

5 scenarios were considered to compare the cost and emissions performance of SAEV to other options and the effectiveness of the optimization algorithm in the context of a VPP. These are summarized in Table 3.5. The Business as usual (BAU) case assumed private vehicles and electricity from utility at a fixed price of 20 yen/kWh and excess generation sold at the marginal price (see section 3.3.4). The battery case assumes that households install a battery and join a VPP with an energy management system that minimizes total costs. The 3 SAEV scenarios assume that households join a VPP that also provides transport services via SAEV (thus they avoid buying a private vehicle) without installing a battery. The 3 scenarios

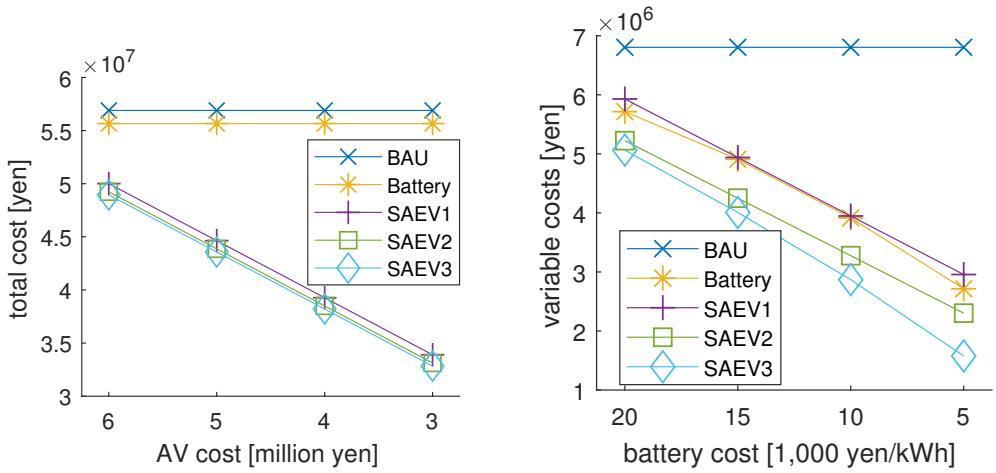

Figure 3.6: *Sensitivity of (a) total costs to autonomous vehicle cost and (b) variable costs (electricity, fuel, and battery costs) to battery costs.*

differ with regard to the charging strategy applied, and correspond respectively to unscheduled charging, optimized charging without V2G, and optimized charging with V2G.

Total costs for each scenario are reported in Figure 3.5. The breakdown of costs and the CO_2 emissions for each scenario are reported in Table 3.6. The cases with transport provided by SAEV (scenarios 4 to 6) are the lowest cost options. The cost savings are dominated by capital costs, as vehicles are shared among all participants in the VPP while avoiding the cost of each individual buying a private vehicle. However, the cost of electricity becomes significantly higher in the case of SAEV, although it is still lower than the fuel costs it replaces. The proposed algorithm decreases electricity costs by 32% and 75%, respectively for the scenario with no V2G and with V2G over the unscheduled charging. The difference would increase with more variable electricity prices in markets with higher penetration of intermittent sources.

Carbon emissions increase significantly in the SAEV cases, due to the combined effect of high carbon intensity of the Japanese grid and the high efficiency of hybrid cars. Another important factor is the higher total distance traveled by SAEV com-

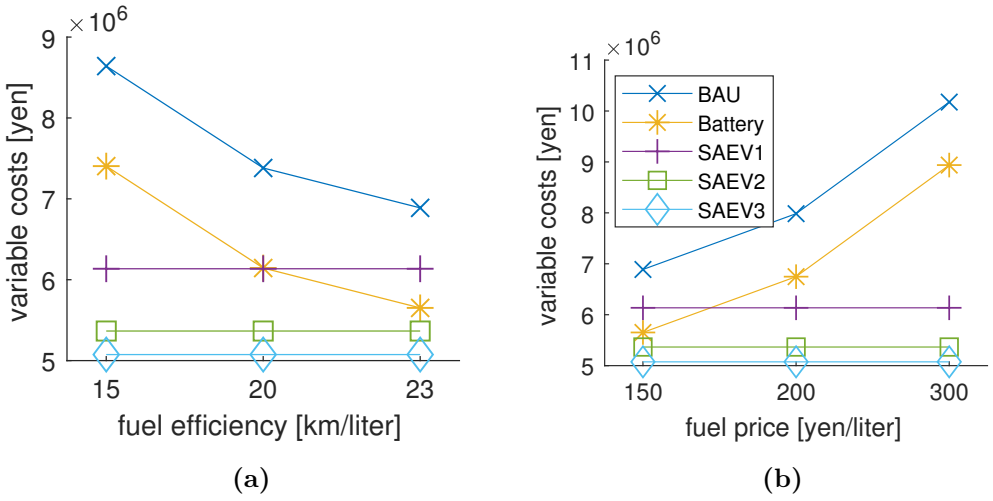

Figure 3.7: *Sensitivity of variable costs to (a) HEV fuel efficiency and (b) fuel cost.*

Table 3.6: *Costs and emissions for VPP scenarios. Capital includes the cost of vehicles and solar panels.*

	Costs (million yen)					CO_2
	ele.	fuel	batt.	capital	total	(t)
BAU	3.60	3.29	0.00	49.94	56.83	86.7
Battery	-0.99	3.29	3.35	49.94	55.59	94.6
SAEV1	2.17	0.00	3.96	38.44	44.57	129.2
SAEV2	1.47	0.00	3.90	38.44	43.80	124.2
SAEV3	0.77	0.00	4.30	38.44	43.51	128.9

pared to private vehicles due to the need to rebalance empty vehicles, as discussed previously. However the life-cycle emissions were not considered, which would likely be significantly lower due to the need for less vehicles. The optimization objective function could also be expanded with carbon pricing and hourly carbon intensity to minimize the emissions. This was not considered in this work due to lack of data.

Sensitivity to autonomous driving technology costs

Autonomous driving technology costs are the most important factor determining the total cost of the system. This is because capital costs dominate the total costs,

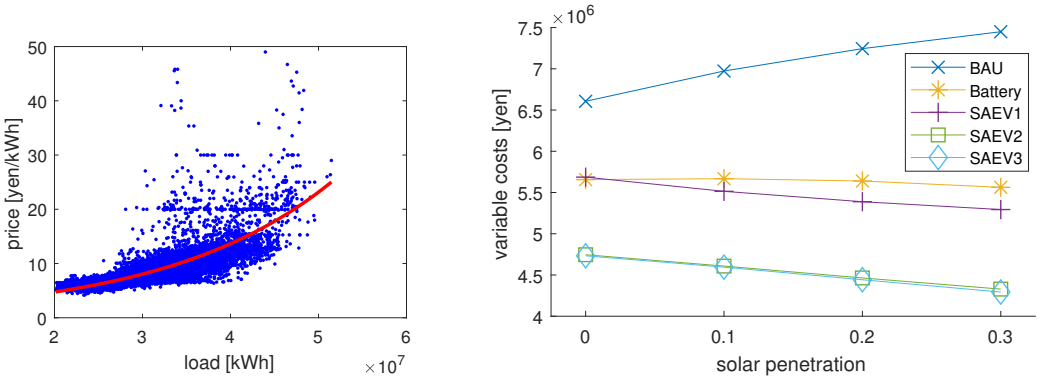

(a) **(b)**

Figure 3.8: *(a) Exponential fit of the relation between prices and dispatchable generation on the Japan Electric Power Exchange (JEPX) in 2017. (b) Effect of increasing solar penetration in the grid.*

being about 10 times the variable costs (Table 3.6). However, even for the case in which vehicles cost 6 million yen ($60,000), the SAEV+VPP systems are cheaper than the alternative (Figure 3.6a).

Sensitivity to battery costs

The sensitivity to battery costs is presented in Figure 3.6b. Battery costs are a major factor in determining the operating or variable costs. Costs for SAEV with V2G decrease faster than other cases, as the lower cost of battery cycling allows vehicles to be used for grid storage. It should be noted that battery prices are expected to fall significantly in coming years. Bloomberg New Energy Finance 2017 Lithium-Ion Battery Price Survey gives average pack prices of $209/kWh (20,900 yen/kWh) in 2017, and they expect they will fall below $100/kWh (10,000 yen/kWh) by 2025 [86].

Sensitivity to fuel prices and fuel efficiency

Operating or variable costs (fuel, electricity and battery) are very sensitive to fuel prices and HEV fuel efficiency. While variable costs for the BAU and battery cases are similar with SAEV cases in the baseline scenario, these costs diverge significantly

with less optimistic assumptions for HEV. This is shown in Figure 3.7. A fuel efficiency of 20 km/liter is the target for new vehicles sold in Japan in 2020 [87]. 15, 20 and 23 km/liter are equivalent to 35, 47 and 54 mpg, respectively. This is still very optimistic for HEV, and the average fuel efficiency of vehicles may be towards the lower end of the range, thus favoring SAEVs. Fuel prices may also increase as oil prices increase.

Effect of increasing solar grid penetration

The value of grid storage is higher with higher grid penetration of intermittent renewable energy. To test the effect of different levels of intermittent renewable energy penetration on the grid, the approximate aggregate cost curve of dispatchable generation in the TEPCO area was estimated by fitting an exponential curve to the demand/price data from JEPX (Figure 3.8a). This allows the generation of artificial electricity price profiles depending on load and renewable energy generation profiles. The case of increasing penetration of solar power in the grid was tested, with the results reported in Figure 3.8b. Higher solar penetration depresses prices paid for excess solar generation and encourages self-consumption and storage. This especially favours SAEV cases that can charge when prices are lower. The V2G case shows almost no difference with the scheduled case without V2G. This is because this simple analysis neglects some side-effects of higher solar penetration, such as the fast and expensive ramping needed at evenings. This would further increase the value of V2G providing peak generation.

3.4.2 Microgrid case

The same transport, load and weather data used for the VPP was used to test the microgrid case, assuming an isolated microgrid with no grid connection ($i_{max} = 0$). The same scenarios presented in Table 3.5 were used with renewable capacity sized to cover all electrical loads over a year with a 50/50% share of wind and solar power. Total costs for each scenario in the microgrid case are reported in Figure 3.9. The breakdown of costs, the installed renewable energy generation capacity, and the

Table 3.7: *Costs, installed renewable generation capacity, and emissions for microgrid scenarios. Fuel includes cost of fuel for cars and cost of dispatchable generators. The renewable generation capacity is sized to cover all load in the system during a year with 50% wind and 50% solar. SAEV scenarios have higher RE capacity (and associated higher costs) because of the higher load from the electrified transport.*

	Costs (million yen)				RE (MW)		CO_2
	fuel	batt.	capital	total	solar	wind	(t)
BAU	8.14	0.00	48.10	56.24	12.15	7.52	181.3
Battery	5.09	3.56	48.10	56.75	12.15	7.52	117.9
SAEV1	6.64	3.96	40.11	50.71	16.55	10.24	184.5
SAEV2	4.61	3.87	40.11	48.59	16.55	10.24	131.0
SAEV3	2.62	4.46	40.11	47.19	16.55	10.24	92.7

carbon emissions for the microgrid case are listed in Table 3.7. An example of the results for one week with and without V2G is presented in Figure 3.10.

SAEV scenarios are the lowest cost options, even considering the increased renewable energy capacity installed. The difference between non-scheduled, scheduled without V2G, and with V2G is much more evident than for the VPP case. The scheduled SAEV model with V2G is able to avoid the use of more expensive generators and maximize the use of renewable energy. This also significantly decreases carbon emissions, which are about half for the SAEV+V2G case compared to the BAU case.

In Figure 3.11 the average utilization and load factors are reported. These are defined respectively as the share of time a generator is active over the whole period, and the load level of the generator when active. As generators are less efficient at lower load factors, higher load factors are preferable. The effect of lower load factor on varying the per unit carbon emissions or costs were not considered for simplicity. The cases with batteries and with SAEV+V2G show the highest load factors and the lowest utilization factors. In particular, this implies the possibility to re-size the system with less generators, thus reducing the capital costs. This effect was not

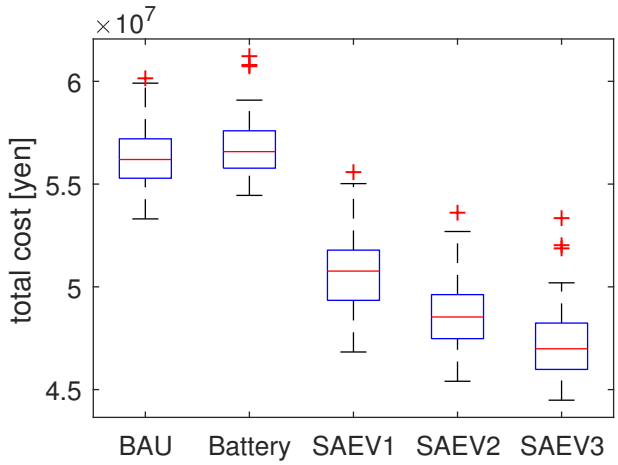

Figure 3.9: *Weekly average total costs for the cases considered in the microgrid case.*

considered in this work (the generators are assumed to be already present).

Sensitivity to renewable energy capacity

The sensitivity to renewable energy capacity is shown in Figure 3.12. The values of capacity represent the share of yearly load generated by renewable energy. These correspond to RE capacities listed in Table 3.7. SAEVs are effective at integrating renewable energy in the system. The total cost for the BAU case with no renewable energy is approximately the same as for the case with SAEV+V2G with 150% renewable energy. As shown in Figure 3.12b, this allows a drastic decrease in carbon emissions at the same cost level.

3.4.3 Implications for policy and practice

The results suggest that there would be significant advantages for households shifting from a private vehicle to a SAEV system in the context of a VPP or in a microgrid. This could help accelerate transport electrification, provide large amount of grid storage to integrate intermittent renewable sources, and avoid the problems connected with the introduction of a large amount of non-controlled EVs on the grid. Rapidly decreasing costs of batteries and autonomous driving technology would make the system even more favorable. However, in the current situation the system

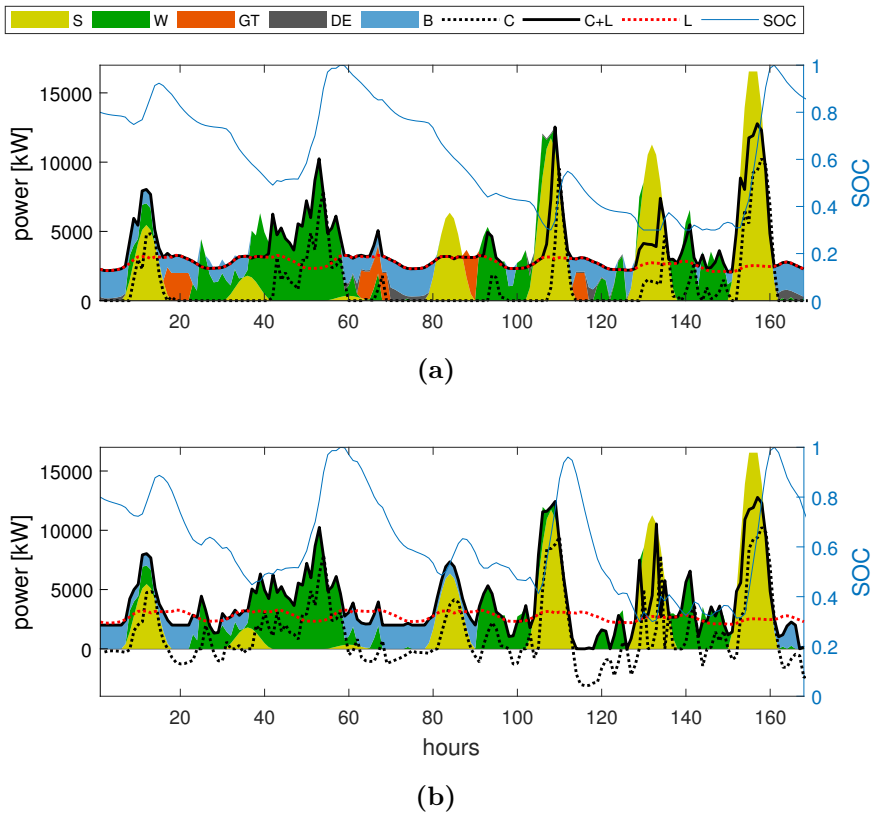

Figure 3.10: *Example of SOC, charge [C], load [L] and generation from gas [GT], diesel [DE], biomass [B], solar [S] and wind [W] (a) without V2G (b) with V2G. V2G discharge (negative charge) allows to avoid gas turbine and diesel generator start-up.*

may increase carbon emissions in the Japanese context. The introduction of carbon pricing with a real-time carbon intensity signal from the grid may not only solve this problem, but actively decrease the total carbon emissions. It should also be noted that, even though in this work the carbon intensity was considered constant and equal to the average, vehicles tend to charge at periods of excess electricity generation and low prices, which often correspond to high renewable energy generation and thus lower carbon intensity.

The results may also apply to non-autonomous car sharing systems, although the cost of manual rebalancing would likely make the system more expensive and the absence of autonomous capability less attractive to users.

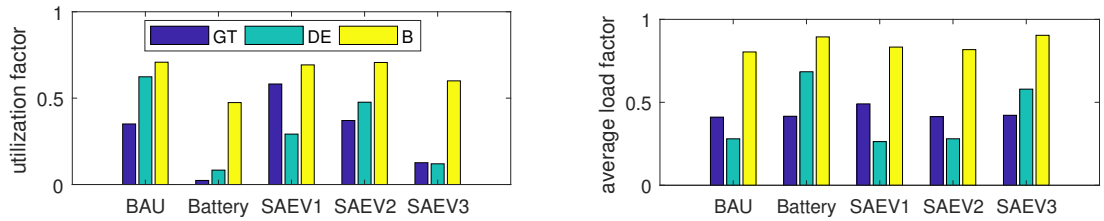

(a) **(b)**

Figure 3.11: *Utilization factor and load factor for gas turbine [GT], diesel engine [DE], and biomass [B] in the microgrid case.*

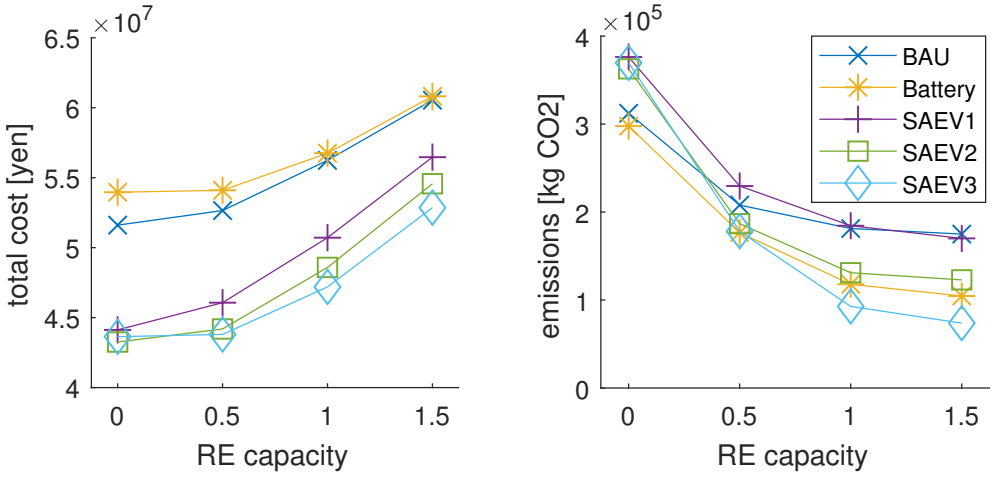

(a) **(b)**

Figure 3.12: *Microgrid case: sensitivity to total renewable energy (RE) capacity of (a) total costs (b) carbon emissions*

3.5 Conclusions

The synergies between SAEVs and renewable energy sources were studied in the context of a grid-connected Virtual Power Plant (VPP) and an isolated microgrid. An optimization methodology was developed for the charge and discharge of the vehicles to minimize costs for the system. The model was tested with several scenarios using weather data and transport patterns for the Tokyo region. The results for the case study show that SAEVs with the optimized charging are effective at decreasing the overall costs in the VPP. The proposed algorithm also decreases electricity expenditures by 75% over the unscheduled charging in the case of SAEV+V2G. Total

cost savings are however dominated by capital cost savings due to lower number of vehicles needed. Overall, total costs are about 20% lower for households with rooftop solar power shifting from utility power and hybrid private vehicles to the VPP with SAEV. It was also shown that further electricity savings (and possibly profits) could be attained in a grid with higher penetration of intermittent renewable energy, demonstrating strong synergies existing between SAEVs and renewable energy. In the case of the isolated microgrid, SAEVs with V2G decrease cost by 16% and cut carbon emissions by half. This demonstrates the potential of SAEV to promote the integration of intermittent renewable energy while reducing total costs for the system.

This is an early work on the integration of SAEV with renewable energy, and several other aspects could be investigated in future work. Real-time grid carbon intensity could be used to extend the cost function to include carbon pricing to reduce vehicles' emissions. Also, an estimate of the life-cycle carbon emissions of the systems studied would allow to assess more realistically the impact of this technology. A more detailed model of dispatchable generation costs could be used to investigate more realistically the effect of increasing penetration of renewable energy in the grid and the potential for vehicles to provide grid storage. Moreover, the provision by vehicles of high revenue grid services such as frequency control or operating reserves could be included in the optimization.

Chapter 4

A novel approach to SAEV simulation: two-layer transport and charging optimization

4.1 Introduction

In Chapter 2 a model of SAEV charging was proposed. However, optimized vehicle relocation was not considered. This is a central problem in the operation of SAEV, and it is necessary to develop a charging optimization framework that can also incorporate intelligent vehicle relocation.

The difference in time scales for charging optimization and transport scheduling poses significant challenges for the simultaneous optimization of SAEV's transport and charging aspects. While the rebalancing of vehicles is generally optimized with a horizon of 15-30 minutes [36, 26], electric vehicle charging is typically optimized over several hours. The longer time frame for charging optimization is due to several reasons. Firstly, charging is relatively slow. Even with fast-charging it may take over one hour to fully charge a battery [88]. Charging for a relatively long time once a vehicle is connected is also more efficient, as it avoids the time wasted in continuous connection and disconnection. The most important consideration however is related to the challenges and opportunities that these vehicles offer to the grid as mentioned

before. In order to avoid grid congestion and provide useful service to the grid, the charge scheduling algorithm needs to optimize over the time frame of variability of electricity demand and intermittent renewable energy sources such as wind and solar, which can be several hours.

In this chapter, charge optimization based on electricity price is integrated into model predictive control (MPC) of a shared autonomous electric vehicle (SAEV) system based on the work by Zhang et al. [36]. The complexity and the computational time of the optimization increase more than linearly with longer time horizons, and optimizing the charge over several hours is impractical. The novel model therefore deals with the different time frames at which transport service and charging have to be optimized with a MPC routine which is run in parallel at two different time scales. Vehicle charging is optimized over longer time scales to minimize electricity costs. Vehicle routing and rebalancing for transport service is optimized at shorter time-scales to minimize waiting times for passengers, taking as constraints the results of the long-time-scale optimization. This approach allows the efficient optimization of both aspects of SAEV operation.

4.2 Methodology

The present chapter is based on the article by Zhang et al. [36] where an MPC was developed to find optimal management strategies for rebalancing of autonomous mobility-on-demand systems (shared autonomous vehicles). Although the work also proposed a version with charging constraints, the charging was not optimized and the vehicles would charge at maximum power as soon as they connect to charging stations.

4.2.1 Transport model from literature

The rebalancing problem is formulated as a MILP. The problem formulation ensures that the system always optimizes the rebalancing of the vehicles within the optimization horizon. However, the computational complexity of the MILP optimization

limits the feasibility to relatively small systems (in the order of a few tens of nodes). Nevertheless, the results of this model can be useful to estimate the performance in comparison to other systems.

Nomenclature

A. State variables	
$d_{i,j}(t)$	waiting passengers at node i with destination j
$u_i^k(t)$	vehicle k waiting at i
${}^T p_i^k(t)$	moving vehicles
$q^k(t)$	state of charge
B. Control variables	
$v_{i,j}^k(t)$	vehicle k transporting passengers between i and j
$w_{i,j}^k(t)$	vehicle k rebalancing empty between i and j
$e^k(t)$	energy charged
$g^k(t)$	energy discharged with V2G
C. Exogenous simulation variables	
$c_{i,j}(t)$	passenger arrivals at node i with destination j
$f(h)$	relative number of trips departing at hour h
$m(t)$	price of electricity
$p_{i,j}(t)$	probability of a trip from i to j at time step t
rw_x, rt_x, ro_x, rd_x	weight, hour of departure, origin node, and destination node of trip x from survey.
$\lambda(t)$	rate of trips arrival at time t
D. Parameters and constants	
J_x, J_u, J_m, J_s	cost of moving, rebalancing, charging, and final SOC
q_{min}, q_{max}	minimum and maximum SOC
t_{hor}	optimization horizon
$\alpha_c, \alpha_{v2g}, \alpha_d$	charge, V2G discharge, and consumption rate
β	temporal ratio between the 2 layers
ρ_1, ρ_2, ρ_3	weights of rebalancing, charging and final SOC secondary objectives

η	V2G efficiency

In this work, Zhang's model is extended to include electricity price-based charge scheduling and vehicle-to-grid discharge in the global optimization.

The general formulation of the model evolution is:

$$x(t+1) = Ax(t) + Bu(t) + c(t) \tag{4.1}$$

where $x(t)$ is the state of the system at time t, $u(t)$ is the set of control variables and $c(t)$ represents new passenger arrivals at nodes.

$$x(t) = \begin{bmatrix} d(t) \\ p(t) \\ u(t) \\ q(t) \end{bmatrix} \tag{4.2}$$

$$u(t) = \begin{bmatrix} v(t) \\ w(t) \\ e(t) \\ g(t) \end{bmatrix} \tag{4.3}$$

These variables are described as follows.

The controls for the optimization are encoded into binary variables. $v_{ij}^k(t) = 1$ when vehicle k is transporting passengers between i and j and $w_{ij}^k(t)$ is the equivalent for rebalancing trips (empty trips). $d_{ij}(t)$ and $c_{ij}(t)$ are, respectively, the number of passengers waiting and arriving at node i with destination j at time t. $d_{ij}(t)$ evolves as:

$$d_{ij}(t+1) = d_{ij}(t) + c_{ij}(t) - \sum_k v_{ij}^k(t) \tag{4.4}$$

Another variable is used to keep track of vehicles in movement: ${}^{T_i}p_i^k(t) = 1$ when vehicle k is at distance T_i from its destination i at time t. This evolves as:

$$
\begin{aligned}
&{}^{T_i}p_i^k(t+1) \\
&\quad = \begin{cases} {}^{T_i+1}p_i^k(t) + \sum_{j:t_{ji}-1=T_i}(v_{ij}^k(t) + w_{ij}^k(t)) & T_i < T_{max,i} \\ \sum_{j:t_{ji}-1=T_i}(v_{ij}^k(t) + w_{ij}^k(t)) & T_i = T_{max,i} \end{cases}
\end{aligned} \tag{4.5}
$$

The binary variable $u_i^k(t)$ represents waiting vehicles at nodes. $u_i^k(t) = 1$ when vehicle k is waiting at node i at time t. The variable evolves as:

$$u_i^k(t+1) = u_i^k(t) +^0 p_i^k(t) - \sum_k (v_{ij}^k(t) + w_{ij}^k(t)) \tag{4.6}$$

Vehicles can either be waiting or moving:

$$\sum_i u_i^k(t) + \sum_{i,T_i} {}^{T_i}p_i^k(t) = 1 \tag{4.7}$$

Also, vehicles can only do one action at each time step:

$$\sum_i \left(u_i^k(t) + \sum_j v_{ij}^k(t) + \sum_j w_{ij}^k(t) \right) \leq 1 \tag{4.8}$$

and vehicles cannot transport more passengers than are waiting at stations:

$$\sum_k v_{ij}^k(t) \leq d_{ij}(t) + c_{ij}(t) \tag{4.9}$$

Another constraint is associated with vehicles' charge state. The state of charge (SOC) of vehicles is encoded into a real variable $q^k(t) \in \{0, 1\}$ and $q_{min} \leq q^k(t) \leq q_{max}$. Vehicles need to have enough charge to be assigned a trip:

$$q^k(t) \geq v_{ij}^k(t)\alpha_d t_{ij} + q_{min} \tag{4.10}$$

$$q^k(t) \geq w_{ij}^k(t)\alpha_d t_{ij} + q_{min} \tag{4.11}$$

α_d is the energy consumption per time step, and t_{ij} is the number of time steps for the trip from i to j.

The cost functions to minimize are related to the waiting time for passengers and the rebalancing costs:

$$J_x(x(t)) = \sum_{i,j} d_{ij}(t) \tag{4.12}$$

$$J_u(u(t)) = \sum_{k} \sum_{i,j} t_{ij} w_{ij}^k(t) \tag{4.13}$$

For a more detailed description of the model, refer to [36].

As noted previously, in the original work the charging of vehicles was not a control variable, and vehicles would charge at a fixed rate when not moving until reaching a full state of charge or a movement was requested.

4.2.2 Charge scheduling

In this work the charging was added to the control vector, thus becoming part of the optimization. The state of charge (SOC) of vehicles $q^k(t)$ evolves as:

$$q^k(t+1) = q^k(t) + e^k(t) - g^k(t) \tag{4.14}$$

where $e^k(t)$ and $g^k(t)$ are, respectively, the energy charged and discharged to the grid in time step t, both non-negative.

The constraints for the charging rates are:

$$e^k(t) \leq \alpha_c \sum_i u_i^k \tag{4.15}$$

$$g^k(t) \leq \alpha_{v2g} \sum_i u_i^k \tag{4.16}$$

where α_c and α_{v2g} are the maximum charging and V2G discharging rates, respectively.

To take into account the charging rate in the optimization, a further cost function is added. This is stated as:

$$J_m(u(t)) = \sum_{k \in V} \Big((e^k(t) - \eta g^k(t)) m(t) + \omega g^k(t) \Big) \tag{4.17}$$

where $m(t)$ is the price of electricity, η is the V2G efficiency, and ω is the extra cost of cycling the battery incurred when supplying power to the grid. The system

is considered a price taker, therefore the electricity price is not affected by charging. It should be noted that since $\eta < 1$ and $\omega > 0$, the optimization would never charge and discharge at the same time. Cost function J_m is added as a further objective to the cost functions relative to the waiting time for passengers J_x and the redistribution trips for vehicles J_u.

Another cost function is added to put a premium on higher state of charge at the end of the optimization period:

$$J_s = -\sum_{k \in V} q^k(t + t_{hor} - 1) \tag{4.18}$$

This is to avoid vehicles reaching a minimum SOC at the end of the optimization horizon, and to account for future transport demand that is necessarily not represented in the optimization. The overall objective is therefore (the variables for each function have been omitted for compactness and clarity):

$$\underset{u(t),..,u(t+t_{hor}-1)}{\text{minimize}} \sum_t \Big(J_x + \rho_1 J_u + \rho_2 J_m \Big) + \rho_3 J_s \tag{4.19}$$

ρ_1, ρ_2, and ρ_3 in (4.19) are the relative weights assigned to each secondary objective.

4.2.3 Two-layer optimization

As mentioned in the introduction, vehicles rebalancing and charging optimization require very different optimization time frames. Rebalancing is generally optimized within an horizon of half an hour or less, while it would be preferable to have a longer horizon for charging optimization in order to take into account the availability of intermittent renewable energy sources and variability of electricity demand.

In order to optimize both transport and charging, a two-layers model predictive control optimization was implemented. In model predictive control (or receding horizon control), at each time step the optimization is performed over a time horizon and only the first control action is executed. This ensures that at each time step the

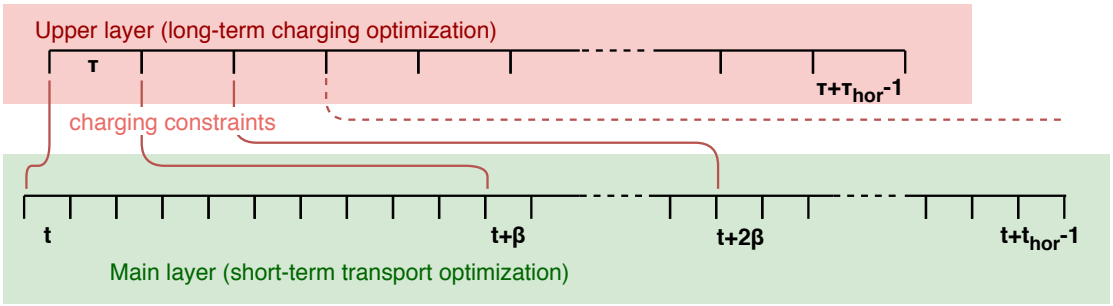

Figure 4.1: *Schematic diagram of the two-layers MPC optimization model*

control uses all the information available up to the future prediction horizon when taking the present action.

In this 2-layer MPC, a higher 'coarse' MPC layer optimizes for charging over longer time frames taking into account the requirements of transport service. The main layer optimizes transport service over short time frames, taking as constraints the optimal charging controls found by the higher layer. Both layers are based on the model presented in the previous sections.

The two layers are related by a step length ratio β that determines the relative length of a time step between the two layers. At the beginning of the simulation, the higher coarse layer determines the optimal charging schedule by optimizing over its own time frame. The results are passed down to the main layer as constraints on charging during each step. After β time steps in the main layer, the higher layer optimizes again over its own time frame, passing down the next charging constraints to the main layer for the next β time steps. A schematic diagram of the two-layers model is presented in Figure 4.1.

4.2.4 Upper layer and constraint assignment

In this section, the integration of the two layers is discussed. The upper layer simulation variables are denoted with Greek letters, so that d, p, u, q, t, e, c are respectively δ, π, μ, ϕ, τ, ϵ, κ. T_i^k is also defined as the distance from node i of vehicle k if moving, and $T_i^k = 0$ if the vehicle is waiting at node i. The upper layer's objective function has secondary weights that are related to the main one by division

by a factor β, to reflect the fact that a waiting passenger waits β times longer in the upper simulation for each time step, as the time step is longer. The arrivals at nodes is defined as:

$$\kappa_{ij}(\tau) = \sum_{t=(\tau-1)\beta+1}^{\tau\beta} c_{ij}(t) \tag{4.20}$$

At the start of an upper layer simulation at (main) time t', the situation at the main layer is assigned to the upper layer:

$$\delta_{ij}(\tau) = d_{ij}(t') \tag{4.21}$$

$$^{[T_i^k/\beta]}\pi_i^k(\tau) = 1 \quad if \quad T_i^k > 0 \tag{4.22}$$

$$\mu_i^k(\tau) = u_i^k(t') \tag{4.23}$$

$$\phi^k(\tau) = q^k(t') \tag{4.24}$$

The charging controls resulting from the upper layer optimization are assigned back to the main layer as constraints on charging and on movement. For vehicles moving, the constraints are assigned only after arrival.

$$e^k(t) = \begin{cases} \epsilon^k(\tau')/\beta & t > t' + T_i^k \\ 0 & t \leq t' + T_i^k \end{cases} \tag{4.25}$$

$$u_i^k(t) = \begin{cases} 1 & t > t' + T_i^k \\ 0 & t \leq t' + T_i^k \end{cases} \tag{4.26}$$

where τ' in (4.25) such that $(\tau - 1)\beta < t' - t \leq \tau\beta$.

4.3 Numerical data

The model was implemented in MATLAB^{TM} and solved as a mixed integer linear optimization with the built-in MATLAB^{TM} function *intlinprog*. To evaluate the performance of the model, several simulations were conducted using data from the transport survey in Tokyo.

4.3.1 Transport data

The Tokyo Person Trip Survey 2008 was used to test the model. More details about the survey analysis and trip generation methodology can be found in Section A.1. Only trips by car or taxi with origin and destination in a central 5x5 km area of Tokyo were considered. These were considered the trips with characteristics more likely to be similar to trips done with the SAEV system. This area was divided into 10 regions by grouping nodes with k-means clustering. The cluster's centroid for each area was considered as a discretized model of the origin/destination of trips in each area.

4.3.2 Secondary weights determination

Deciding the value of secondary weights is an important problem for multi-objective optimization models. The first weight in (4.19), ρ_1, is the easiest to set, as there is an optimal rebalancing that can always be achieved. If set low enough (0.01 in this work), the rebalancing will be optimized without influencing the main objective. Further decrease of rebalancing cost is impossible under this optimized rebalancing cost (this optimized distance is the same distance found with the Earth Mover's Distance calculation in Chapter 3). Determination of ρ_2 and ρ_3 is less straightforward. These two secondary objectives represent the cost of energy, not the 'waiting cost' like the main objective. Therefore, setting these objectives depend on the relative importance of minimizing monetary costs over minimizing the waiting times for passengers. This trade-off need to be decided by policy or by user preference. A sensitivity analysis was conducted to understand the influence of this parameter on

the cost and wait times. The results of the sensitivity analysis are shown in Figure 4.2. Each data point represents the median values over 10 simulations of the model. Total system costs increase and waiting time decrease with decreasing ρ_2. However, a plateau is reached for both values, as there is a charge schedule that ensures minimum waiting time while minimizing as much as possible the charging costs. This is reached for $\rho_2 \simeq 0.1$ in the simulations of Figure 4.2. In this work, ρ_2 was set to 0.001 to ensure the simulations are within the plateau region, as minimizing wait times is considered a priority over marginally lower charging costs. The objective for final SOC was set as $\rho_3 = \rho_2 m_{median}$ where m_{median} is the median price of electricity. This is equivalent to compensate for lower SOC by buying electricity at the median price up to 100% SOC.

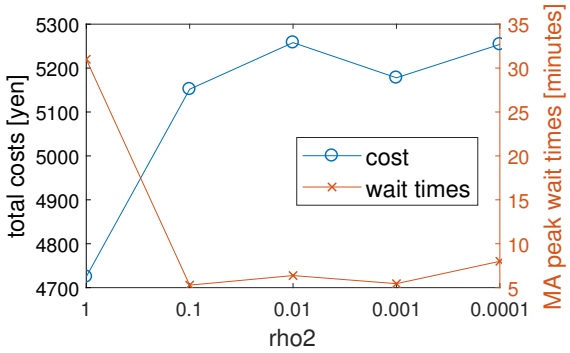

Figure 4.2: *Costs and moving average (MA) peak waiting times sensitivity to secondary weight* ρ_2

4.3.3 Electricity prices and scenario reduction

In order to investigate the influence of different electricity price profiles on the results, real electricity market price profiles were used in the simulations. Due to the computational time required for each simulation, studying an entire year of electricity prices would be extremely time consuming. A scenario reduction approach was therefore used to reduce the number of required simulations while assessing the behavior of the model in all the possible situations.

In this work, a scenario is defined as the electricity price profile during a single

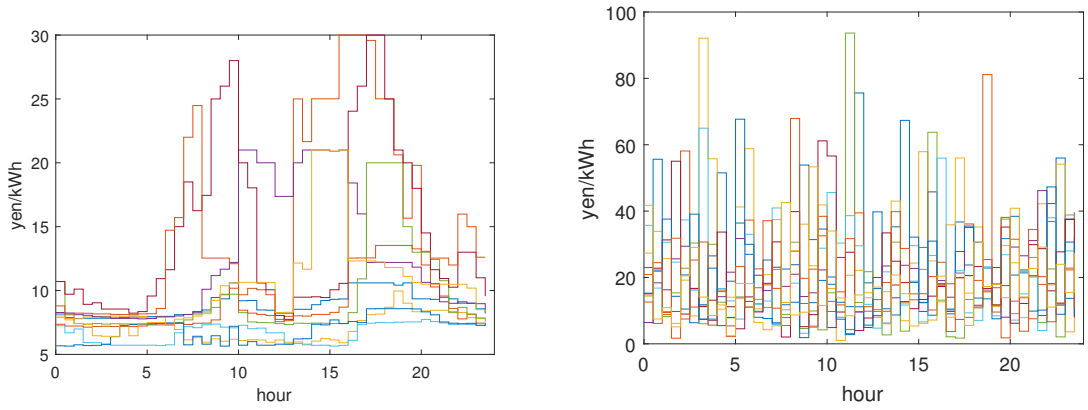

Figure 4.3: *(a) Day-ahead price profiles for the Tokyo region in the JEPX wholesale electricity market selected with scenario reduction. (b) Generated scenarios from a gamma distribution to test the model with high variability prices.*

day. In the scenario reduction approach a subset of all possible scenario (daily price profiles) is selected to represent the entire spectrum of possible scenarios, i.e., all the historical daily electricity profiles. Only the most representative scenarios are kept, and similar scenarios are discarded. The probability of the selected scenarios is updated with the sum of the probability of all the discarded scenarios most similar to the ones kept. To assess the similarity of different price profiles, the Kantorovich distance was used, which is the most common measure of distance between probability distribution used in stochastic programming [89]. All the price profiles were normalized to calculate the distance.

The forward selection algorithm described in [89] was used to select the scenarios. The day-ahead wholesale electricity market prices for the Tokyo region on the Japanese Electric Power Exchange (JEPX) in financial year 2016 (April 2016 to March 2017) were used [90]. 10 scenarios were selected (Figure 4.3a). Each scenario was associated with a weight (probability) proportional to the number of days with a profile closest to the selected one.

The Tokyo region has relatively low penetration of renewable electricity, and the wholesale market is still relatively small as the electricity market is still in the process

of being completely liberalized. In order to test the model with price profiles with higher variability, 10 more scenarios were generated from a gamma distribution with shape parameter 2 and scale parameter 10, giving an average price of 20 yen/kWh.

Figure 4.3 shows the price profiles selected in the case of JEPX historical market prices and the generated gamma distribution scenarios.

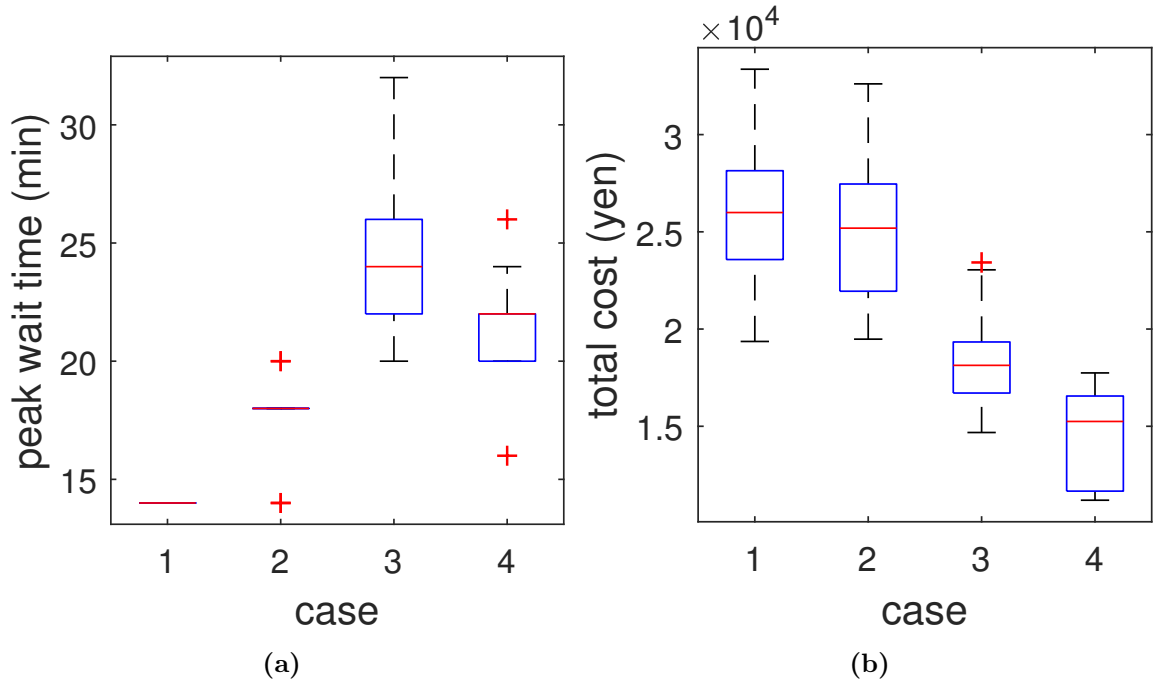

Figure 4.4: *Peak wait times and total costs for the random price profiles generated from a Gamma distribution. The 4 cases represent the unscheduled model, the 1-layer model, the 2-layer model, and the 2-layer with V2G, respectively.*

4.4 Results and discussion

The simulations were run with 30 vehicles, and an average trip rate of 1500 trips per day. The speed of vehicles was set at 20 km/h, the reported average road speed in central Tokyo at peak time [53].

Time step for the main layer is 2 minutes, with a 15 time steps horizon (30 minutes). The ratio between the two layers is $\beta = 15$, so that the higher layer has a time step of 30 minutes. The time step horizon for the higher layer is set at

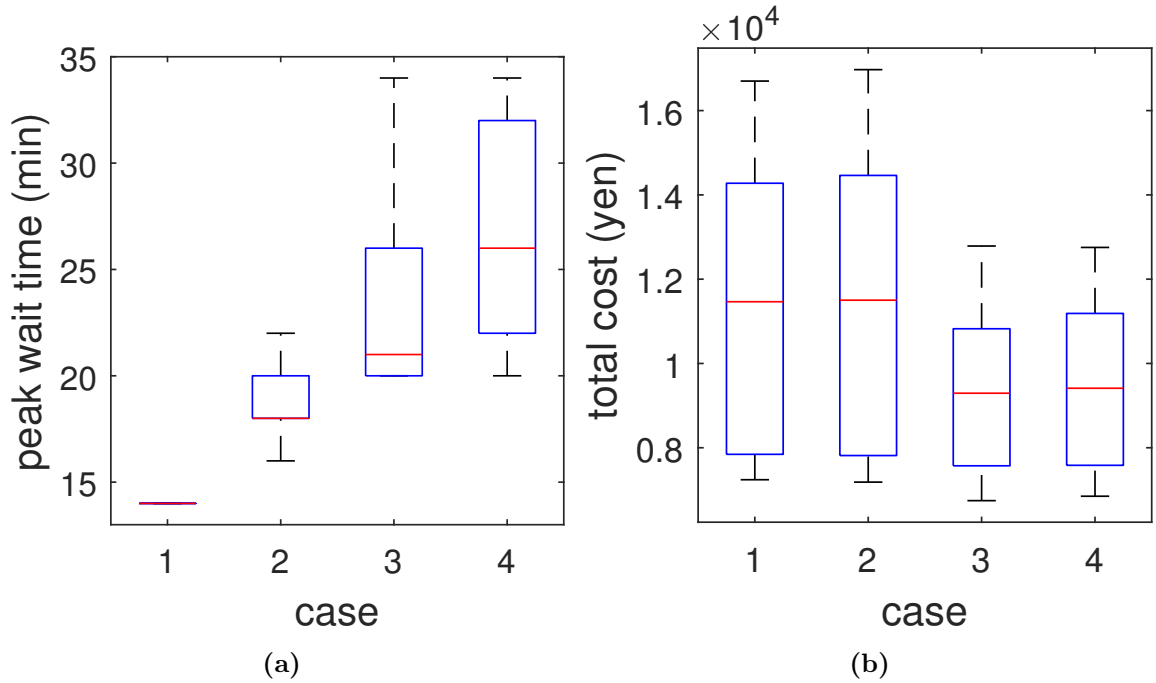

Figure 4.5: *Peak wait times and total costs for the simulation with real prices on the Japan Power exchange in 2017.*

10, giving an optimization time horizon for charging of 5 hours. Vehicles battery size was set at 50 kWh and the state of charge was limited between 0.2 and 0.9 to increase battery life.

Different models were compared to evaluate the performance of the proposed charge scheduling algorithm in terms of waiting times and charging costs:

1. no charge scheduling
2. 1-layer charge scheduling
3. 2-layer charge scheduling
4. 2-layer charge scheduling with V2G

Case 1 represent the model from the literature, where vehicles charge as much as possible as soon as they are idle. Different results may have different levels of SOC at the end of the simulation. To be able to compare different results the difference

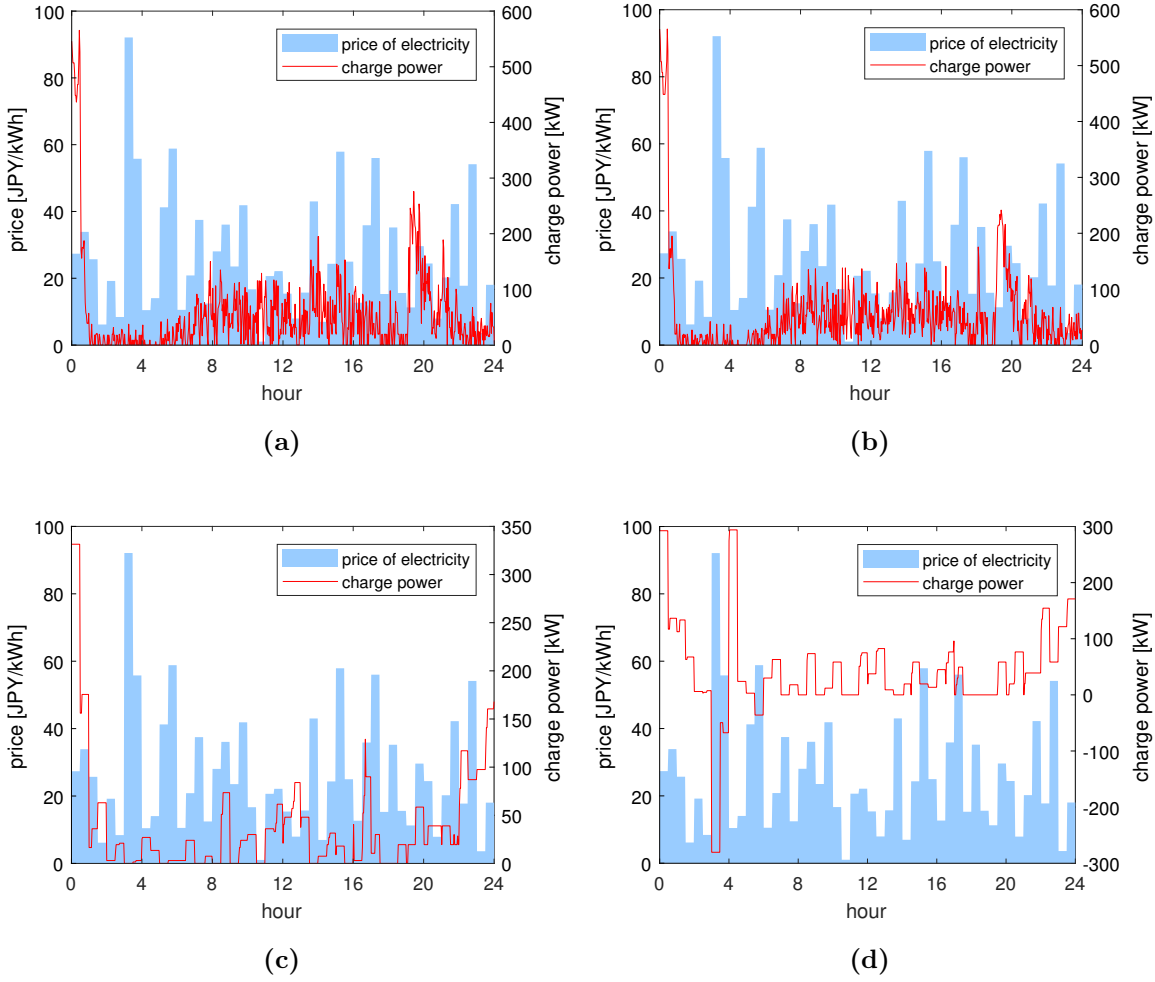

Figure 4.6: *(a) Aggregated charging power and electricity price for case 1 (unscheduled). The price profile is taken from a Gamma distribution. (b) Aggregated charging power and electricity price for case 2 (1-layer scheduling). There is almost no difference between case 1 and 2, as the charge scheduling optimization horizon is too short to be effective. (c) Aggregated charging power and electricity price for case 3 (2-layer scheduling) (d) Aggregated charging power and electricity price for case 4 (2-layer scheduling with V2G)*

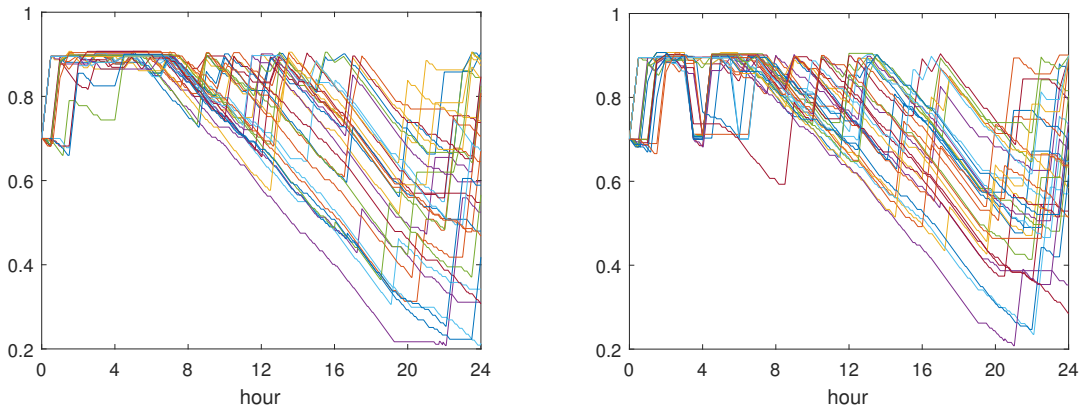

Figure 4.7: *(a) State of charge (SOC) of vehicles for case 3 (2-layer scheduling) (b) State of charge (SOC) of vehicles for the case with V2G. The steep drop in SOC around 4 am is correlated with a high electricity price and resulting V2G discharge (compare with Figure 4.6d).*

between the final SOC and the initial SOC was valued at the median price of the day.

The peak waiting times and the total costs for the simulations are presented in Figure 4.4 and Figure 4.5 for the case with random price profiles and with price profiles taken from JEPX, respectively. The model proposed with 2-layer optimization decreases total charging costs significantly when compared to the unscheduled model or the 1-layer model. The effect is much larger with the random price profile, due to the much higher variability that gives the charge optimized model a clearer advantage over the unscheduled model.

For the case with historical price profiles in Tokyo, the effect is smaller. As mentioned previously, this is due to the relatively low penetration of renewable energy sources in the Tokyo grid and the nascent state of the Japan wholesale electricity market, with both factors contributing to relatively static price profiles. Moreover, when peaks exist, they generally correspond to transport demand peaks (Figure 4.3a), rendering the model less effective since transport is always a priority in the optimization. Table 4.2 reports the results for the JEPX prices weighted

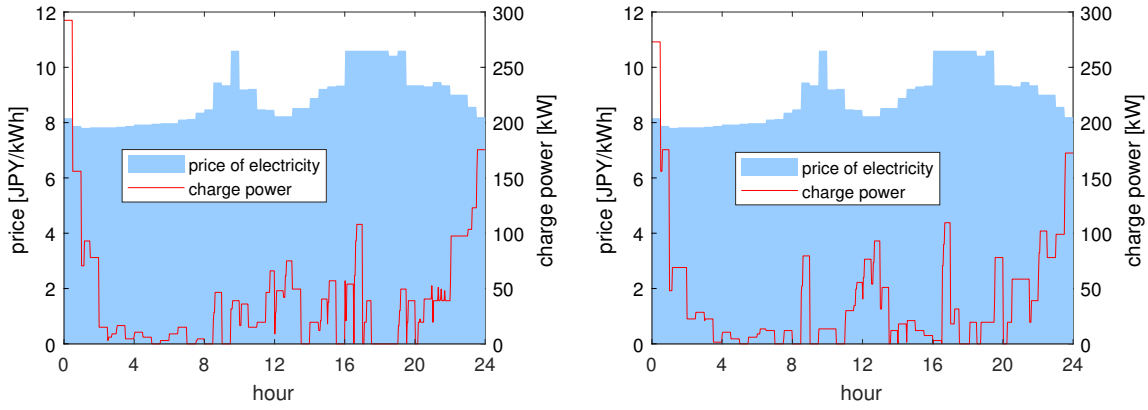

Figure 4.8: *(a) Aggregated charging power and electricity price for case 3 (2-layer scheduling) for one of the real price profiles in the Tokyo wholesale electricity market in 2017 (b) Aggregated charging power and electricity price for case 4 (2-layer scheduling with V2G) for one of the real price profiles in the Tokyo wholesale electricity market in 2017.*

with the probability of each scenario tested. Costs decrease by about 10% with the proposed model.

While the model with V2G has a significant advantage over the one without in the high variability random profiles (Figure 4.4b), the results for the two models are practically indistinguishable for the JEPX profiles (see Figure 4.5b and table 4.2). This is due to the relatively low price differentials in the JEPX profiles, which are generally not enough to overcome the costs of V2G in terms of battery degradation and opportunity cost.

It should be noted that there is not much difference between the unscheduled model and the 1-layer model in terms of costs. This shows that the 1-layer model is unable to effectively optimize charging due to the limited optimization horizon. This is evident from Figure 4.6a and Figure 4.6b, showing aggregated charging power for the 2 models. The results are almost indistinguishable. This is in contrast with Figure 4.6c and Figure 4.6d, where the charging optimization is evident as the aggregate charging peaks are correlated with lows in the electricity price profile.

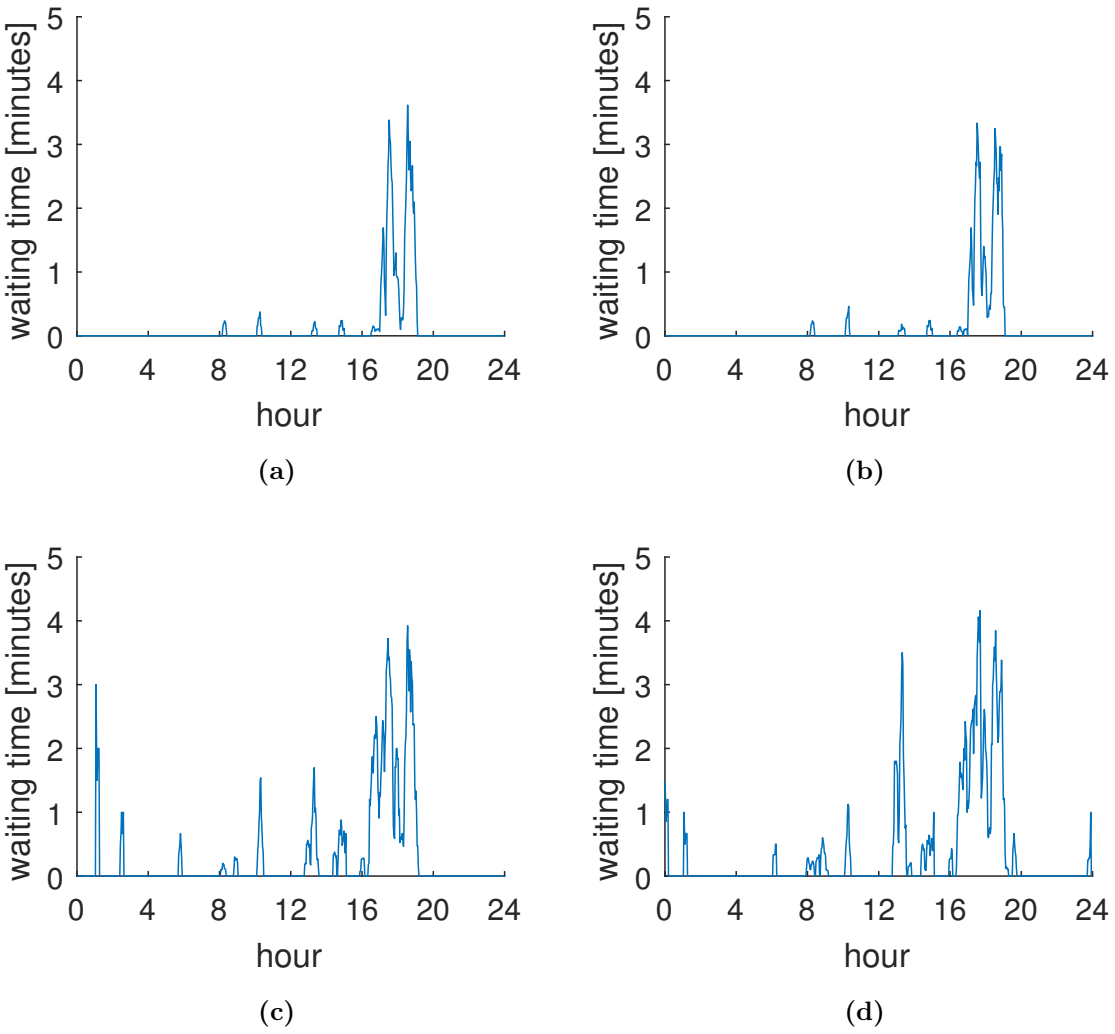

Figure 4.9: *10 minutes moving average wait times: (a) case 1; (b) case 2; (c) case 3; (d) case 4.*

Table 4.2: *Wait times and charging costs for the 4 models with the selected scenarios for the Japan Electric Power Exchange in 2017 and with the randomly generated electricity price profiles. MA is moving average.*

	1	2	3	4
JEPX price profiles				
peak wait time (minutes)	14	18	21	31
10-min MA peak wait (min.)	3:37	3:23	4:02	4:12
total electricity cost (yen)	10493	10538	9393	9282
gamma-distributed price profiles				
peak wait time (minutes)	14	18	25	21
10-min MA peak wait (min.)	3:37	3:32	4:27	4:23
total electricity cost (yen)	25868	25218	18542	14684

The state of charge of vehicles during the simulation is shown in Figure 4.7a and Figure 4.7b.

Figure 4.8a and Figure 4.8 report aggregate charging levels for a JEPX price profile. Results shown are for the most representative day of the 10 selected, representing a equivalent probability of 68%. It is evident that the price profile is extremely flat, with a maximum price differential of about 2 yen/kWh. This limits the effectiveness of the charge scheduling algorithm, especially since its priority is transport service. The 10-minutes moving average waiting times for new arrivals for the 4 models is shown in Figure 4.9 for the same price profile. The results show new peaks in waiting times corresponding to a low electricity price around noon, since some of the vehicles have been scheduled to charge and avoid the afternoon price peak.

The median computation time for a time step of the 2-layer model on a quad-core 3 GHz Intel Core i5 processor with 32GB of RAM was about 20 seconds for the upper layer and 1.5 seconds for the main layer. The average overall was 29.4 seconds per time step (5 hours 53 minutes per simulation).

4.5 Conclusions and future work

An extension of the model in [36] was developed to incorporate electricity price information for optimizing vehicle charging. A 2-layer optimization was used to optimize both charging and transport service at different time scales. The proposed model was applied to the case study of Tokyo, using transport survey data and historical electricity prices from the wholesale electricity market.

The results show that the optimization can reduce the costs of charging for the system by 10% when using historical price profiles from the Japan Electric Power Exchange. Much larger cost savings could be obtained with price profiles with higher variability. With prices sampled from a gamma distribution the savings compared to the unscheduled model are 43% and 28% for the case with and without V2G, respectively. The 2-layer model is shown to be superior to the 1-layer model, with the latter being effectively same as the unscheduled model due to the limited time horizon.

Waiting times are not excessively affected by the charging optimization, with 10-minutes moving average wait times peak increasing for the model with V2G by 16% and 21% for the real electricity prices and the generated price profiles, respectively, compared to the unscheduled model.

The work in this chapter shows the potential of SAEVs to offer effective energy storage to the grid and avoid grid congestion thanks to dynamic pricing, while effectively optimizing vehicles' rebalancing and minimizing waiting times. Several other aspects are open to investigation in future work. An important extension of the model could be the possibility of selection of which nodes are charging stations and which charging stations are available at any given time, for example due to grid constraints or vehicle congestion. In this work only wholesale electricity market participation was considered. However, other ancillary services such as operating reserve and frequency regulation could also be provided by the system. These are generally better remunerated and suitable for batteries, thus they are likely more attractive for SAEVs. The potential for the system to provide these services could be investigated by including them in the global optimization.

Chapter 5

Conclusions and future work

5.1 Conclusions

This work has addressed the problem of the integration of shared autonomous electric vehicles in the electric grid. The challenge arises from the transformation in progress in the electricity sector, with increasing penetration of renewable energy, and the transport sector, with the future shift from private transportation to transport-as-a-service models. If managed together, these transformations can offer significant synergies, making transport service cheaper and more convenient, while making available to the grid a large amount of storage and extremely flexible generation.

Simulation models and optimization algorithms were proposed for the scheduling of vehicles charge in the wholesale electricity market, the provision of ancillary services, and the optimization of renewable energy storage. The city of Tokyo was taken as a case study throughout the work, with passenger data based on the most recent transport survey.

In Chapter 2, a novel simulation model was developed to study the feasibility of a SAEV transport system and its integration with the electricity grid. A SAEV fleet serving passengers and charging at designated charging stations was simulated using a charge scheduling algorithm based on electricity prices. The model incorporated a operating reserve request model to quantitatively estimate the potential

for SAEVs to provide operating reserve to the grid. The results show that every SAEV in Tokyo could replace 7 to 10 private cars, depending on the trade-off between waiting time and cost of the system. The system's break-even price per km is much lower than the fare of traditional taxis, and comparable to the average cost of car ownership and public transport. The proposed charge scheduling algorithm can further lower the cost of transport by providing load shifting and storage for the grid. The results for the operating reserve model show that the amount of operating reserve power available depends strongly on the time of day and the allowed delay. Even at the worst time, the system can provide large amount of power without significant disruption of transport service. In a scenario of a wide implementation of this system, the model suggest that SAEVs could provide significant grid-scale storage and spinning reserves.

In Chapter 3, the possibility of integrating SAEVs with renewable energy was studied in the context of a grid-connected Virtual Power Plant (VPP) and an isolated microgrid. An optimization methodology was developed for the charge and discharge of the aggregated SAEV fleet to minimize costs for the system taking into account the necessary vehicle relocation. This is the first work that considers the integration of SAEVs with renewable energy. The fleet was sized using results from the previous part of the work. The model was tested stochastically with several scenarios in the Tokyo case study using generated weather profiles. The results show that SAEVs with the optimized charging are effective at decreasing the overall costs both in the VPP and in the isolated microgrid. In the microgrid case, SAEV can effectively replace peaker generators also significantly decreasing carbon emissions. It was also shown that the positive effects increase with increasing penetration of renewable energy in the grid, demonstrating the potential of SAEVs to promote the shift to sustainable energy.

In Chapter 4, a more systematic, detailed, and flexible multi-objective optimization framework was developed for the charging and relocation of SAEVs. An extension of the model in [36] was developed to incorporate electricity price information from the grid. This is the first multi-objective optimization framework for the

charging and relocation of SAEVs. The difference in time scales between transport and energy optimization horizons was overcome by developing a 2-layer optimization approach functioning at two different time scales. The proposed model was applied to the case study of Tokyo, showing promising results in terms of lower electricity expenditures even with low-variability price profiles and with acceptable marginal increases in wait times.

This thesis has shown the potential of SAEVs to contribute to a changing electricity sector by offering effective energy storage services, ancillary services, and avoiding grid congestion thanks to responsive charging without compromising transport service. This work represents one of the first investigation of the charge scheduling potential of SAEV, and presents one of the first algorithms that take into account vehicles' relocation and time-varying electricity price-based multi-objective optimization. While the current work has used Tokyo as a case study, the methodology presented is completely general and can be applied to any case for which enough data is available.

5.2 Additional findings

Additional findings of this work are summarized as follows. The simulation results show that service quality, fleet size, and cost of SAEVs are highly dependent on the area served (distance of trips and density of passenger requests). This was also confirmed by recently published literature. The performance of the system would be therefore highly dependent on the system boundary.

Another key finding of this study is that transport service is much higher value than electricity in the current markets. Simulations with data from the wholesale day-ahead electricity market show that current prices are too low and not variable enough to justify V2G. Higher prices would be needed to have meaningful incentives for demand response and storage. This reflects the fact that the electricity system is still far from the level of renewable energy penetration when the storage availability becomes a constraint. The Japanese electricity system is still dominated by fossil

fuels, especially gas, that keep prices relatively low at all times thanks to their dispatchability. However, in order to phase out fossil fuels and avoid the worst outcomes of climate change, the penetration of renewable energy and less dispatchable sources such as nuclear power will need to increase up to 100% of electricity generation. The current plans for decarbonization of the electricity sector up to mid-century by the Japanese government and by other countries seem overly conservative, and the shift to renewable energy will need to happen orders of magnitude faster to keep Japan and most countries from becoming deserts due to changing climate.

The cost analysis showed that SAEVs have very low cost even with conservative estimates of uncertainty in future technology. Because of this, SAEVs have the potential to disrupt today's transport system, and in the near future this technology could potentially replace car ownership in densely populated areas. Perhaps, one day private cars may become illegal to drive in cities and lighter, lower speed and more efficient SAEVs could offer taxi services within these areas.

5.3 Future work

The work presented here is a first approach to the problem of SAEVs and grid integration. Much work is still needed to address many aspects that were not subject of the present work or found in the literature.

One of the main simplifying assumption that this work and most of the rest of the literature use is that of static transport patterns. This may be sufficient for an initial investigation, but is highly likely that transport patterns would change with the introduction of this new transport mode. Some work (reviewed in Section 1.3.1) addressed this problem. However, a comprehensive model that takes into account both dynamic transport patterns and electricity is still needed. This is especially important in the context of ancillary services, which are highly sensitive to the availability of vehicles.

Another simplification found in this work and in most of the literature is that of uniform vehicles fleets. Vehicles are generally assumed to be all of the same

size and characteristics. However, one of the important advantages of SAEVs is the possibility of selecting the most appropriate vehicle for the specific task. For example, a single passenger would be assigned a one-person vehicle instead of a full-size car, while a larger group would use a larger vehicle. This is expected to be the main driver of decreased energy consumption of SAEVs compared to private vehicles or taxis [9]. The non-uniformity of vehicle fleets (and presumably battery sizes) add a further level of complexity in the optimization of the relocation, trip assignment, and charging of vehicles, which would need to be addressed in future work.

Another possible future subject of investigation is the integration of a realistic model of the electricity transmission network to account for transmission constraints. Although this point is probably less critical for SAEVs than for private EVs (thanks to the fact that charging stations can be easily controlled and connected to high voltage transmission), this has not been quantitatively verified yet.

An interesting future direction of research could be focused on the transport-side demand response aspect of the system. Using a dynamic transport demand model, dynamic pricing of vehicles could be introduced not only to account for varying level of congestion in the transport network, but also depending on the price of electricity. Analysis done during this work however show that the effect of electricity pricing on the transport costs is likely extremely low, unless there is a significant increase in electricity prices and price variability. This however cannot be completely discarded due to the changing electricity system with ever increasing penetration of non-controllable energy sources.

Appendix A

Data

A.1 Transport survey data

The case study used throughout this work is based on the Tokyo Person Trip Survey 2008 [1], a survey of around 2 million trips in the Tokyo metropolitan area. The 2008 survey is the latest available survey released for Tokyo. Although somewhat old, the demographics and infrastructure of Tokyo has remained stable and it is expected that this importantly implies a relatively stable demand pattern when compared to 2008. Infrastructure and ridership of all major railways are shown to be mostly unchanged between 2008 and 2015, and in the same period, the length of roads in Tokyo city changed by less than 1% [91].

Most of the trips in the survey are by public transport. However, for the purpose of this study, only trips by car or taxi were considered. These are the trips with characteristics more likely to be similar to trips done with the SAEV system. These trips represent about 20% of the total trips in the survey. Trips by car or taxi in the selected area are a total of 73,000, or 3.8% of the total trips in the survey. Of these, only about 70,000 are found to have a reported trip starting time. These are the trips that were used in this work. Although this is a small proportion of the total trips, it should be noted that the aim of the system is not to cover 100% of trips, but rather enough of them for the system to be sustainable. Further work could consider the migration of bus or train-based trips onto the SAEV service, but that

is not the focus of the current study.

Each trip in the survey also has a starting time and a weight. The weight is used to indicate the relative significance of that specific trip and to normalize the survey results over the total demographics of Tokyo. Although trip starting time is specified by hour and minute, it was found that most trips start at minute 0 of each hour. The minute information was therefore judged to be unreliable and was not considered in this work.

Each selected trip k is then defined with four values $[rw_k, rt_k, ro_k, rd_k]$ to indicate respectively associated weight, hour of departure (0-23), origin node, and destination node. The probability $p_{i,j}(t)$ was found as:

$$p_{i,j}(t) = \frac{\sum_{k'} rw_{k'}}{\sum_k rw_k}, \quad k : rt_k = t', k' : rt_{k'} = t', ro_{k'} = i, rd_{k'} = j \tag{A.1}$$

where $t' = \lfloor ((t \cdot \ell - 1) \mod 1440)/60 \rfloor$ is the hour of the day corresponding to time step t.

The relative number of trips departing at hour h from the survey is:

$$f(h) = \frac{\sum_{k'} rw_{k'}}{\sum_k rw_k}, \quad k' : rt_{k'} = h \tag{A.2}$$

At each time step t (at hour of the day h), the rate of the Poisson process in (2.2) is then:

$$\lambda(t) = TPH \cdot 24 \cdot f(t') \cdot \ell/60 \tag{A.3}$$

where TPH is the average rate of trips per hour.

A.1.1 Geocoding

The survey associates the origins and destinations of trips to zones, corresponding to specific addresses in Tokyo. These geographical zones were used in the model as the reference nodes. The geographic coordinates of the zones were found from the addresses reported in the survey using the Google Maps Geocoding API [92]. The

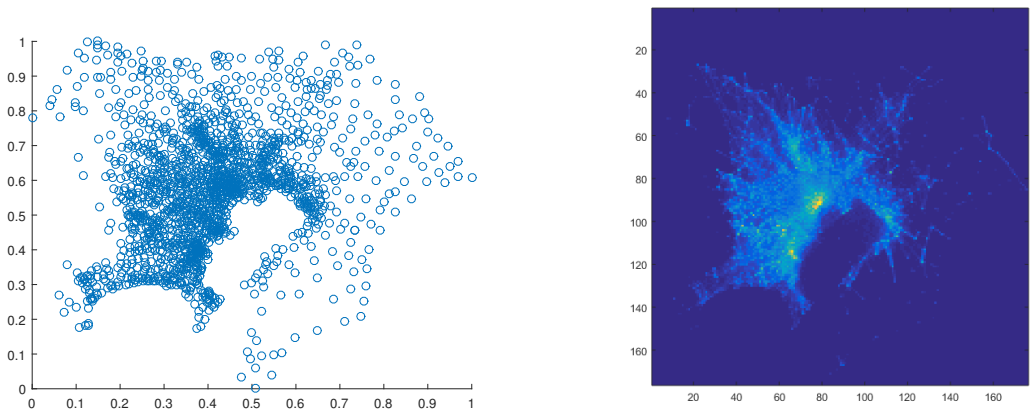

(a) **(b)**

Figure A.1: *(a) A figure representing all the nodes found in the survey (b) Map of Tokyo created by tracing lines for each origin/destination pair for trips done by car in the survey. Brighter colors correspond to more vehicles passing in that point.*

approximate area of the zones was also found and was used as the area associated with the node.

Figure A.1a shows the map of all the nodes found in the survey by associating coordinates to reported addresses in Tokyo and neighbouring areas with the method detailed in Section A.1. Relative normalized coordinates are used. Tokyo Bay is clearly visible in the figure. Figure A.1b shows a map of Tokyo created by tracing lines for each origin/destination pair for trips done by car in the survey. This is roughly equivalent to a pollution map of Tokyo, since necessarily vehicles need to pass through the locations between origin and destination.

A.1.2 Tortuosity factor of roads

The ratio of trip distance to Euclidean distance (tortuosity factor) was determined by testing random trips within the selected area and averaging the value of effective distance to Euclidean distance between the coordinates. Only coordinates associated with an address in the immediate vicinity were considered, thus excluding unoccupied areas. The associated addresses and the actual travel distance was found with

the Google Maps Geocoding API [92]. 1298 origin-destination pairs were tested, with a resulting average $\beta = 1.48$, which was used in the simulations. It was also confirmed that the value of β is not significantly correlated with any trip characteristic, such as travel distance or geographic area, so that the use of a single average value can be considered acceptable.

References

[1] Ministry of Land, Infrastructure, Transport and Tourism, Japan (MLIT), "Tokyo Metropolitan Area Person trip survey," 2008.

[2] B. Boyacı, K. G. Zografos, and N. Geroliminis, "An optimization framework for the development of efficient one-way car-sharing systems," *European Journal of Operational Research*, vol. 240, no. 3, pp. 718–733, Feb. 2015.

[3] J. B. Greenblatt and S. Shaheen, "Automated Vehicles, On-Demand Mobility, and Environmental Impacts," *Current Sustainable/Renewable Energy Reports*, vol. 2, no. 3, pp. 74–81, Sep. 2015.

[4] D. J. Fagnant and K. M. Kockelman, "The travel and environmental implications of shared autonomous vehicles, using agent-based model scenarios," *Transportation Research Part C: Emerging Technologies*, vol. 40, pp. 1–13, Mar. 2014.

[5] S. Rand Transportation, and Technology (Program), *Autonomous Vehicle Technology: a Guide for Policymakers*, 2014.

[6] S. Hörl, F. Ciari, and K. W. Axhausen, "Recent perspectives on the impact of autonomous vehicles," 2016. [Online]. Available: https://www.ethz.ch/content/dam/ethz/special-interest/baug/ivt/ivt-dam/vpl/reports/2016/ab1216.pdf

[7] Waymo, "On the Road." [Online]. Available: https://waymo.com/ontheroad/

[8] A. Barr, "Waymo Gets the O.K. for a Commercial Driverless Ride-Hailing Service - Bloomberg," Feb. 2018. [Online]. Available: https://www.bloomberg.com/news/articles/2018-02-16/waymo-gets-o-k-for-commercial-driverless-ride-hailing-service

[9] J. B. Greenblatt and S. Saxena, "Autonomous taxis could greatly reduce greenhouse-gas emissions of US light-duty vehicles," *Nature Climate Change*, vol. 5, no. 9, pp. 860–863, Jul. 2015.

[10] T. D. Chen, K. M. Kockelman, and J. P. Hanna, "Operations of a shared, autonomous, electric vehicle fleet: Implications of vehicle & charging infrastructure decisions," *Transportation Research Part A: Policy and Practice*, vol. 94, pp. 243–254, Dec. 2016.

[11] J. Weiss, R. Hledik, R. Lueken, T. Lee, and W. Gorman, "The electrification accelerator: Understanding the implications of autonomous vehicles for electric utilities," *The Electricity Journal*, vol. 30, no. 10, pp. 50–57, Dec. 2017.

[12] Timothy Sweda and Diego Klabjan, "An Agent-Based Decision Support System for Electric Vehicle Charging Infrastructure Deployment," Institute of Electrical and Electronics Engineers, Power Electronics Society, and Vehicular Technology Society, Eds. Piscataway, NJ: IEEE, 2011.

[13] Z. Wadud, D. MacKenzie, and P. Leiby, "Help or hindrance? The travel, energy and carbon impacts of highly automated vehicles," *Transportation Research Part A: Policy and Practice*, vol. 86, pp. 1–18, Apr. 2016.

[14] D. B. Richardson, "Electric vehicles and the electric grid: A review of modeling approaches, Impacts, and renewable energy integration," *Renewable and Sustainable Energy Reviews*, vol. 19, pp. 247–254, Mar. 2013.

[15] D. Dallinger and M. Wietschel, "Grid integration of intermittent renewable energy sources using price-responsive plug-in electric vehicles," *Renewable and Sustainable Energy Reviews*, vol. 16, no. 5, pp. 3370–3382, 2012. [Online].

Available: https://econpapers.repec.org/article/eeerensus/v_3a16_3ay_3a2012_3ai_3a5_3ap_3a3370-3382.htm

[16] W. Kempton and J. Tomić, "Vehicle-to-grid power implementation: From stabilizing the grid to supporting large-scale renewable energy," *Journal of Power Sources*, vol. 144, no. 1, pp. 280–294, Jun. 2005.

[17] M. Yilmaz and P. T. Krein, "Review of the Impact of Vehicle-to-Grid Technologies on Distribution Systems and Utility Interfaces," *IEEE Transactions on Power Electronics*, vol. 28, no. 12, pp. 5673–5689, Dec. 2013.

[18] K. Clement-Nyns, E. Haesen, and J. Driesen, "The Impact of Charging Plug-In Hybrid Electric Vehicles on a Residential Distribution Grid," *IEEE Transactions on Power Systems*, vol. 25, no. 1, pp. 371–380, Feb. 2010.

[19] C. Fernandes, P. Frías, and J. M. Latorre, "Impact of vehicle-to-grid on power system operation costs: The Spanish case study," *Applied Energy*, vol. 96, pp. 194–202, Aug. 2012.

[20] B. Tarroja, B. Shaffer, and S. Samuelsen, "The importance of grid integration for achievable greenhouse gas emissions reductions from alternative vehicle technologies," *Energy*, vol. 87, pp. 504–519, Jul. 2015.

[21] J. D. K. Bishop, C. J. Axon, D. Bonilla, and D. Banister, "Estimating the grid payments necessary to compensate additional costs to prospective electric vehicle owners who provide vehicle-to-grid ancillary services," *Energy*, vol. 94, pp. 715–727, Jan. 2016.

[22] Burns, Jordan, and Scarborough, "Transforming Personal Mobility," Tech. Rep., 2013.

[23] S. Hörl, "Implementation of an autonomous taxi service in a multimodal traffic simulation using MATSim," 2016. [Online]. Available: http://studentarbeten.chalmers.se

[24] J. Liu, K. M. Kockelman, P. M. Boesch, and F. Ciari, "Tracking a system of shared autonomous vehicles across the Austin, Texas network using agent-based simulation," *Transportation*, vol. 44, no. 6, pp. 1261–1278, Nov. 2017.

[25] W. Zhang, S. Guhathakurta, J. Fang, and G. Zhang, "Exploring the impact of shared autonomous vehicles on urban parking demand: An agent-based simulation approach," *Sustainable Cities and Society*, vol. 19, pp. 34–45, Dec. 2015.

[26] K. Spieser, K. Treleaven, R. Zhang, E. Frazzoli, D. Morton, and M. Pavone, "Toward a Systematic Approach to the Design and Evaluation of Automated Mobility-on-Demand Systems: A Case Study in Singapore," in *Road Vehicle Automation*, G. Meyer and S. Beiker, Eds. Cham: Springer International Publishing, 2014, pp. 229–245.

[27] M. W. Levin, K. M. Kockelman, S. D. Boyles, and T. Li, "A general framework for modeling shared autonomous vehicles with dynamic network-loading and dynamic ride-sharing application," *Computers, Environment and Urban Systems*, vol. 64, pp. 373–383, Jul. 2017.

[28] M. Pavone, S. L. Smith, E. Frazzoli, and D. Rus, "Robotic load balancing for mobility-on-demand systems," *The International Journal of Robotics Research*, vol. 31, no. 7, pp. 839–854, Jun. 2012.

[29] M. Volkov, J. Aslam, and D. Rus, "Markov-based redistribution policy model for future urban mobility networks," in *Intelligent Transportation Systems (ITSC), 2012 15th International IEEE Conference on*. IEEE, 2012, pp. 1906–1911.

[30] F. Acquaviva, D. D. Paola, and A. Rizzo, "A novel formulation for the distributed solution of load balancing problems in mobility on-demand systems," in *2014 International Conference on Connected Vehicles and Expo (ICCVE)*, Nov. 2014, pp. 906–911.

[31] E. S. Rigas, S. D. Ramchurn, and N. Bassiliades, "Algorithms for Electric Vehicle Scheduling in Mobility-on-Demand Schemes," in *2015 IEEE 18th In-*

ternational Conference on Intelligent Transportation Systems, Sep. 2015, pp. 1339–1344.

[32] E. Biondi, C. Boldrini, and R. Bruno, "The impact of regulated electric fleets on the power grid: The car sharing case," in *2016 IEEE 2nd International Forum on Research and Technologies for Society and Industry Leveraging a better tomorrow (RTSI)*, Sep. 2016, pp. 1–6.

[33] S. Pourazarm, C. G. Cassandras, and T. Wang, "Optimal routing and charging of energy-limited vehicles in traffic networks: Optimal routing and charging of energy-limited vehicles in traffic networks," *International Journal of Robust and Nonlinear Control*, vol. 26, no. 6, pp. 1325–1350, Apr. 2016.

[34] T. Chen, B. Zhang, H. Pourbabak, A. Kavousi-Fard, and W. Su, "Optimal Routing and Charging of an Electric Vehicle Fleet for High-Efficiency Dynamic Transit Systems," *IEEE Transactions on Smart Grid*, vol. 9, no. 4, pp. 3563–3572, Jul. 2018.

[35] G. S. Bauer, J. B. Greenblatt, and B. F. Gerke, "Cost, Energy, and Environmental Impact of Automated Electric Taxi Fleets in Manhattan," *Environmental Science & Technology*, vol. 52, no. 8, pp. 4920–4928, Apr. 2018.

[36] R. Zhang, F. Rossi, and M. Pavone, "Model predictive control of autonomous mobility-on-demand systems," in *2016 IEEE International Conference on Robotics and Automation (ICRA)*, May 2016, pp. 1382–1389.

[37] Z. Yi and M. Shirk, "Data-driven optimal charging decision making for connected and automated electric vehicles: A personal usage scenario," *Transportation Research Part C: Emerging Technologies*, vol. 86, pp. 37–58, Jan. 2018.

[38] D. Freund, A. F. Raab, T. Küster, S. Albayrak, and K. Strunz, "Agent-based integration of an electric car sharing fleet into a smart distribution feeder," in *Innovative Smart Grid Technologies (ISGT Europe), 2012 3rd IEEE PES International Conference and Exhibition on*. IEEE, 2012, pp. 1–8.

[39] J. Bischoff and M. Maciejewski, "Agent-based Simulation of Electric Taxicab Fleets," *Transportation Research Procedia*, vol. 4, pp. 191–198, Jan. 2014.

[40] H. Wang and R. Cheu, "Operations of a taxi fleet for advance reservations using electric vehicles and charging stations," *Transportation Research Record: Journal of the Transportation Research Board*, no. 2352, pp. 1–10, 2013.

[41] N. Kang, F. M. Feinberg, and P. Y. Papalambros, "Autonomous Electric Vehicle Sharing System Design," *Journal of Mechanical Design*, vol. 139, no. 1, p. 011402, Oct. 2016.

[42] J. Tomić and W. Kempton, "Using fleets of electric-drive vehicles for grid support," *Journal of Power Sources*, vol. 168, no. 2, pp. 459–468, Jun. 2007.

[43] M. Kahlen and W. Ketter, "Aggregating Electric Cars to Sustainable Virtual Power Plants: The Value of Flexibility in Future Electricity Markets." in *AAAI*, 2015, pp. 665–671.

[44] F. Mwasilu, J. J. Justo, E.-K. Kim, T. D. Do, and J.-W. Jung, "Electric vehicles and smart grid interaction: A review on vehicle to grid and renewable energy sources integration," *Renewable and Sustainable Energy Reviews*, vol. 34, pp. 501–516, Jun. 2014.

[45] P. Nunes and M. C. Brito, "Displacing natural gas with electric vehicles for grid stabilization," *Energy*, vol. 141, pp. 87–96, Dec. 2017.

[46] J. Hu, H. Morais, T. Sousa, and M. Lind, "Electric vehicle fleet management in smart grids: A review of services, optimization and control aspects," *Renewable and Sustainable Energy Reviews*, vol. 56, pp. 1207–1226, Apr. 2016.

[47] S. M. Nosratabadi, R.-A. Hooshmand, and E. Gholipour, "A comprehensive review on microgrid and virtual power plant concepts employed for distributed energy resources scheduling in power systems," *Renewable and Sustainable Energy Reviews*, vol. 67, pp. 341–363, Jan. 2017.

[48] E. Ela, M. Milligan, and B. Kirby, "Operating reserves and variable generation," *National Renewable Energy Laboratory*, vol. 303, pp. 275–3000, 2011.

[49] H. W. Kuhn, "The Hungarian method for the assignment problem," *Naval Research Logistics Quarterly*, vol. 2, no. 1-2, pp. 83–97, Mar. 1955.

[50] W. J. Mitchell, C. Borroni-Bird, and L. D. Burns, *Reinventing the automobile personal urban mobility for the 21st century.* Cambridge, Mass.: Massachusetts Institute of Technology, 2010.

[51] Q. Wang, C. Zhang, Y. Ding, G. Xydis, J. Wang, and J. Østergaard, "Review of real-time electricity markets for integrating Distributed Energy Resources and Demand Response," *Applied Energy*, vol. 138, pp. 695–706, Jan. 2015.

[52] Japan Electric Power Information Center, Inc. (JEPIC), "Operating and Financial Data," 2015. [Online]. Available: https://www.jepic.or.jp/en/data/japan_data.pdf

[53] Tokyo Metropolitan Government Environment Bureau, "Traffic volume and traffic speed in Tokyo." [Online]. Available: http://www.kankyo.metro.tokyo.jp/en/attachement/c-3_data.pdf

[54] National Research Council, *Transitions to Alternative Vehicles and Fuels.* Washington, D.C.: National Academies Press, Mar. 2013.

[55] U.S. Department of Energy, "2013 Nissan Leaf Advanced Vehicle Testing – Baseline Testing Results," 2013. [Online]. Available: https://energy.gov/sites/prod/files/2015/01/f19/fact2013nissanleaf.pdf

[56] X. Han, M. Ouyang, L. Lu, and J. Li, "A comparative study of commercial lithium ion battery cycle life in electric vehicle: Capacity loss estimation," *Journal of Power Sources*, vol. 268, pp. 658–669, Dec. 2014.

[57] "MaxRange Tesla Battery Survey." [Online]. Available: goo.gl/JCLJOE

[58] Tesla Inc., "Tesla Powerwall Limited Warranty (USA)," Jun. 2016.

[59] K. Uddin, T. Jackson, W. D. Widanage, G. Chouchelamane, P. A. Jennings, and J. Marco, "On the possibility of extending the lifetime of lithium-ion batteries through optimal V2g facilitated by an integrated vehicle and smart-grid system," *Energy*, vol. 133, pp. 710–722, Aug. 2017.

[60] IHS Automotive, "Emerging technologies: autonomous cars— not if, but when," 2014.

[61] D. J. Fagnant and K. Kockelman, "Preparing a nation for autonomous vehicles: opportunities, barriers and policy recommendations," *Transportation Research Part A: Policy and Practice*, vol. 77, pp. 167–181, Jul. 2015.

[62] B. Nykvist and M. Nilsson, "Rapidly falling costs of battery packs for electric vehicles," *Nature Climate Change*, vol. 5, no. 4, pp. 329–332, Mar. 2015.

[63] I. J. Fernández, C. F. Calvillo, A. Sánchez-Miralles, and J. Boal, "Capacity fade and aging models for electric batteries and optimal charging strategy for electric vehicles," *Energy*, vol. 60, pp. 35–43, Oct. 2013.

[64] S. Han, S. Han, and H. Aki, "A practical battery wear model for electric vehicle charging applications," *Applied Energy*, vol. 113, pp. 1100–1108, Jan. 2014.

[65] TEPCO, "Customer Communication | Rate Calculation." [Online]. Available: http://www.tepco.co.jp/en/customer/guide/ratecalc-e.html

[66] "Order a Cab (Rates Table) ? Tokyo Taxi [Tokyo Hire-Taxi Association(THTA)]." [Online]. Available: http://www.taxi-tokyo.or.jp/english/call/pricelist.html

[67] J. C. Mukherjee and A. Gupta, "A Review of Charge Scheduling of Electric Vehicles in Smart Grid," *IEEE Systems Journal*, vol. 9, no. 4, pp. 1541–1553, Dec. 2015.

[68] L. Liu, F. Kong, X. Liu, Y. Peng, and Q. Wang, "A review on electric vehicles interacting with renewable energy in smart grid," *Renewable and Sustainable Energy Reviews*, vol. 51, pp. 648–661, Nov. 2015.

[69] "Code for the Earth Movers Distance (EMD)." [Online]. Available: http://ai.stanford.edu/~rubner/emd/default.htm

[70] M. H. K. Tushar, C. Assi, M. Maier, and M. F. Uddin, "Smart Microgrids: Optimal Joint Scheduling for Electric Vehicles and Home Appliances," *IEEE Transactions on Smart Grid*, vol. 5, no. 1, pp. 239–250, Jan. 2014. [Online]. Available: http://ieeexplore.ieee.org/document/6693776/

[71] HOMER, "HOMER® Pro Version 3.7 User Manual," 2016. [Online]. Available: https://www.homerenergy.com/pdf/HOMERHelpManual.pdf

[72] TEPCO, "Electricity Forecast | Download past electricity demand data." [Online]. Available: http://www.tepco.co.jp/en/forecast/html/download-e.html

[73] Statistics Bureau, Ministry of Internal Affairs and Communications, "Japan Statistical Yearbook - Chapter 11 Energy and Water," 2018. [Online]. Available: http://www.stat.go.jp/english/data/nenkan/67nenkan/1431-11.htm

[74] "Japan Meteorological Agency|Data of Solar and Infrared Radiation." [Online]. Available: http://www.data.jma.go.jp/gmd/env/radiation/en/data_rad_e.html

[75] NOAA, "Climate Data Online." [Online]. Available: https://www7.ncdc.noaa.gov/CDO/cdo

[76] E. Hahn, "The Japanese Solar PV Market and Industry," Nov. 2014. [Online]. Available: https://www.eu-japan.eu/sites/default/files/publications/docs/pvinjapan.pdf

[77] IRENA, "Renewable Power Generation Costs in 2017," 2017. [Online]. Available: /publications/2018/Jan/Renewable-power-generation-costs-in-2017

[78] Intergovernmental Panel on Climate Change, *Climate Change 2014 Mitigation of Climate Change: Working Group III Contribution to the Fifth Assessment*

Report of the Intergovernmental Panel on Climate Change. Cambridge: Cambridge University Press, 2014.

[79] H. Hao, Z. Mu, S. Jiang, Z. Liu, and F. Zhao, "GHG Emissions from the Production of Lithium-Ion Batteries for Electric Vehicles in China," *Sustainability*, vol. 9, no. 4, p. 504, Apr. 2017.

[80] U.S. Department of Energy (DOE), "Compare Side-by-Side 2016 Toyota Prius." [Online]. Available: https://www.fueleconomy.gov/feg/Find.do?action=sbs&id=37163

[81] JAMA, "The motor industry of Japan 2017," May 2017. [Online]. Available: http://www.jama-english.jp/publications/MIJ2017.pdf

[82] FEPC, "Electricity Review Japan," 2017. [Online]. Available: https://www.fepc.or.jp/library/pamphlet/pdf/04_electricity.pdf

[83] Ministry of Economy, Trade and Industry (METI). [Online]. Available: http://www.enecho.meti.go.jp/category/saving_and_new/saiene/kaitori/index.html

[84] Y. Iwafune, T. Ikegami, J. G. d. S. Fonseca, T. Oozeki, and K. Ogimoto, "Cooperative home energy management using batteries for a photovoltaic system considering the diversity of households," *Energy Conversion and Management*, vol. 96, pp. 322–329, May 2015. [Online]. Available: http://linkinghub.elsevier.com/retrieve/pii/S0196890415002046

[85] T. Adefarati, N. B. Papy, M. Thopil, and H. Tazvinga, "Non-renewable Distributed Generation Technologies: A Review," in *Handbook of Distributed Generation*. Springer, Cham, 2017, pp. 69–105. [Online]. Available: https://link.springer.com/chapter/10.1007/978-3-319-51343-0_2

[86] Mark Chediak, "The Latest Bull Case for Electric Cars: the Cheapest Batteries Ever," *Bloomberg.com*, Dec. 2017. [Online]. Available: https://www.bloomberg.com/news/articles/2017-12-05/latest-bull-case-for-electric-cars-the-cheapest-batteries-ever

[87] Japan Automobile Manufacturers Association, "The motor industry of Japan," 2015. [Online]. Available: http://www.jama-english.jp/publications/MIJ2015.pdf

[88] M. Yilmaz and P. T. Krein, "Review of Battery Charger Topologies, Charging Power Levels, and Infrastructure for Plug-In Electric and Hybrid Vehicles," *IEEE Transactions on Power Electronics*, vol. 28, no. 5, pp. 2151–2169, May 2013.

[89] A. J. Conejo, M. Carrión, and J. M. Morales, *Decision making under uncertainty in electricity markets*. Springer, 2010, vol. 1.

[90] JEPX, "Trading Information: Spot Market / Intraday Market," 2017. [Online]. Available: http://www.jepx.org/english/market/index.html

[91] Tokyo Metropolitan Government, "Tokyo Statistical Yearbook 2009-2015," 2016. [Online]. Available: http://www.toukei.metro.tokyo.jp/tnenkan/tn-eindex.htm

[92] "Developer's Guide | Google Maps Geocoding API." [Online]. Available: https://developers.google.com/maps/documentation/geocoding/intro

List of publications

Journal papers

1. R.Iacobucci, B.McLellan, T.Tezuka, "Modeling Shared Autonomous Electric Vehicles: potential for transport and power grid integration", *Energy*, Volume 158, Pages 148-163, September 2018. DOI: 10.1016/j.energy.2018.06.024

2. R.Iacobucci, B.McLellan, T.Tezuka, "The Synergies of Shared Autonomous Electric Vehicles with Renewable Energy in a Virtual Power Plant and Microgrid", *Energies*, vol. 11, no. 8, p. 2016, August 2018. DOI: 10.3390/en11082016

3. R.Iacobucci, B.McLellan, T.Tezuka, "Optimization of Shared Autonomous Electric Vehicles operations with charge scheduling and vehicle-to-grid", *Transportation Research Part C* (in review), 2018

Conferences

1. R. Iacobucci, W. Kusumaningdyah, N. Kaerkitcha, H. Lin, N. Luangchosiri, R. Motoori, K. Olaniyan, T. Sagawa, N. K. Ishihara, "Technology options towards a clean and sustainable road transport system in Japan by 2030", *Poster presented at the 7th International Symposium of Advanced Energy Science*, Kyoto, September 2016

2. R.Iacobucci, B.McLellan, T.Tezuka, "Shared Autonomous Electric Vehicles as operating reserve", *Kyoto-Ajou-Zhejiang Joint Symposium on Energy Science*, Kyoto, January 2017

3. R.Iacobucci, B.McLellan, T.Tezuka, "Shared Autonomous Electric Vehicles as operating reserve: A case study in Tokyo", *Japan Society for Energy and Resources 33rd Conference*, Tokyo, February 2017

4. R.Iacobucci, B.McLellan, T.Tezuka, "New method for evaluating Shared Autonomous Electric Vehicles Storage Performance in the power network with Intermittent Renewable Energy", *Japan Society for Energy and Resources 34th Conference*, Tokyo, January 2018

5. R.Iacobucci, B.McLellan, T.Tezuka, "Model Predictive Control of a Shared Autonomous Electric Vehicles system with charge scheduling and electricity price response", in 3rd International Conference on Intelligent Transportation Engineering (Singapore, September 2018), *ICITE 2018 conference Proceedings* (accepted)

6. R.Iacobucci, B.McLellan, T.Tezuka, "Costs and carbon emissions of shared autonomous electric vehicles in a Virtual Power Plant and Microgrid with renewable energy", in 5th International Conference on Power and Energy Systems Engineering (Nagoya, September 2018), *Energy Procedia* (accepted)